The Institute of Paper Chemistry

Appleton, Wisconsin

Doctor's Dissertation

Methods for the Evaluation of the Physical Structure of Clay-Starch Coating Films

David John Kraske

June, 1959

METHODS FOR THE EVALUATION OF THE PHYSICAL STRUCTURE OF CLAY-STARCH COATING FILMS

A thesis submitted by

David John Kraske

B.S. 1953, Western Michigan College
M.S. 1956, Lawrence College

in partial fulfillment of the requirements
of The Institute of Paper Chemistry
for the degree of Doctor of Philosophy
from Lawrence College,
Appleton, Wisconsin

June, 1959

TABLE OF CONTENTS

INTRODUCTION

Pigment-coated papers have found widespread acceptance in the printing industry because of their superior appearance and performance characteristics. In general, coated papers present a smoother printing surface than do uncoated papers. The coating also serves to increase the gloss and opacity of the sheet and to improve its ink receptivity. Because of its importance to the paper industry the pigment coating process has been the subject of rather intensive research effort.

In the past, research work in the coating field has been limited to the evaluation of properties of the coated sheet such as smoothness, gloss, opacity, strength and ink receptivity which are thought to be related to the performance of the coated paper in the printing operation. Such characteristics are hereafter referred to as end-use properties. Although the evaluation of end-use properties of coated papers is important from a quality control standpoint, information obtained from such tests is necessarily restricted in its interpretation. It has become increasingly evident that a more fundamental research approach is required for a complete understanding of the complex processes involved in the coating of paper. A fundamental approach has been employed more frequently in recent years, particularly with regard to pigment dispersion and coating color rheology problems.

All of the end-use properties commonly used to evaluate coated papers are related to the physical structure of pigment coatings. Earlier work has been restricted to the development of relationships

between such end-use properties and such coating variables as pigment particle size, adhesive content, rawstock properties, coat weight and so on. Little attention has been directed to the relationships between such variables and the more fundamental property of coating film structure. Coating structure, however, provides a basis for a greater understanding of variations in the performance of coated papers. Further, the structural analysis of pigment coatings could shed light upon such phenomena as vehicle and adhesive migration during coating application and gloss development during the supercalendering operation.

Much information of a qualitative nature is available in the literature which pertains to the appearance and performance characteristics of coated papers. Such information permits speculation about the influence of coating structure on the end-use behavior of coating films. Certain effects of coating process variables upon coating film structure are indirectly suggested. However, with the exception of certain measurements of the permeability of coated papers to air and organic liquids, no quantitative information describing coating structure is available.

It is obvious that an investigation of the previously neglected field of coating structure would be both fruitful and interesting. However, such an investigation is contingent upon the development of valid methods capable of describing coating structure.

Accordingly, the first objective of this thesis is the development and verification of experimental techniques which assist in the

characterization of certain prominent structural features of clay coating films. The criteria useful for study are:

1. Clay particle orientation with respect to the plane of the coating,
2. the unbonded surface area of the coating,
3. the pore distribution of the coating, and
4. the void volume of the coating.

The second objective of this study is the demonstration of the ability of the methods developed and adapted in the first phase to detect variations in coating structure. The development of relationships between coating variables and the structural forms of coating films is beyond the scope of this work although it is expected that a certain insight into some of the structural variations possible will be obtained.

SUMMARY

This investigation was directed at the development and adaptation of methods useful for the evaluation of the physical structure of clay coating films. The coatings examined in this work were prepared by the application of aqueous clay-starch coating colors to a porous rawstock, Millipore filter, which was easily soluble in an organic solvent.

During this work a method was developed for the isolation of clay-starch coatings from Millipore filter in pieces of convenient size. The rawstock was dissolved in baths of ethyl acetate leaving the coating unchanged in its structural properties. Coatings as light as 4 lb./ream were isolated by this method. Removal of the Millipore filter was shown to be essentially complete.

It was shown in this investigation that low temperature nitrogen adsorption measurements were sufficiently flexible to describe the surface area, the internal void volume and the pore distribution of isolated coating. Particular care was required in the determination of the nitrogen desorption isotherm since the useful data were obtained at values of relative pressure greater than 0.96. Certain qualifications were imposed upon the pore distributions determined by this method due to the size and possible shapes of the pores in the coatings.

An established x-ray diffraction method was modified to measure the extent of preferred orientation, with respect to the plane of the

coating surface, of pigment particles in coatings. The original method was modified to allow its use with sheet materials which were not infinitely thick to the x-rays used. Experimental confirmation of derived absorption correction factors was obtained. It was shown that the results presented in this report contain a constant error that resulted from defocusing of the diffracted x-ray beam. The magnitude of this error was established and a suggestion was presented for avoiding it in systems where fine resolution of the diffracted beam is not required.

With certain selected experiments it was shown that this system for the analysis of coating structure adequately detects differences in coating structure arising from changes in coating component and process variables. The scope of this work did not permit conclusions based on the results of these experiments. However, the following observations were recorded.

1. The pore size of the clay coatings analyzed in this work was considerably smaller than was indicated by previous work in this field. Carson (1) found average pore radii of 0.2 and 0.3 mu for double- and single-coated book paper, respectively. In the present work, the majority of coating pores were less than 0.1 mu in radius. The difference in these values is attributed primarily to basic differences in the techniques employed to obtain these values.
2. The pore structure of three coatings examined varied significantly

with the particle size of the clay used in the coating. The pore structure became finer and encompassed a narrower range as the clay particle size was decreased.

3. The pore structure of the clay coatings was essentially uniform through their thickness when small particle size clays were used. A coating containing the large particle size clay fraction had a pore structure indicative of non-uniform transverse pore structure.

4. The degree of pigment orientation in coatings was found to be dependent upon the average particle size of the clay fraction used in the coating. The 1.0 - 2.0 mu clay fraction coating had the least orientation; the 0.0 - 0.5 mu clay fraction yielded a coating whose orientation values were only slightly lower than that of the 0.5 - 1.0 mu clay fraction coating. Reasons for this behavior pattern were not developed.

5. Coat weight differences (10-20-30 lb./ream) did not appear to have large scale effects upon coating structure in the case of a coating which contained the 0.5 - 1.0 mu clay fraction.

6. Supercalendering of coated Millipore filter sheets produced a realignment of clay particles, some rupture of pigment-adhesive and/or adhesive-adhesive bonds, and an interesting shift in the pore distribution of the coating. The internal void volume of the coating was not altered by supercalendering.

7. Mechanical treatment (passage through a dispersion mill) of the coating color increased the amount of bonding occurring in a

coating but had no effect upon the extent of clay particle orientation. The clay used in this experiment had been chemically dispersed.

8. Roughening of the rawstock surface produced a large change in the pigment particle orientation of a coating but had no effect upon the free or unbonded surface area of the coating.

As a general conclusion it may be stated that this work has established and demonstrated the utility of a system for the analysis of the structure of clay-starch coatings.

BACKGROUND OF THE PROBLEM

The literature in the coating field contains a great deal of information on the properties of coatings and coating components. Much of this information is concerned with the end-use properties of coatings and certain rather nebulous characteristics of the coating components. This type of information allows speculation about the various forms in which coating structure may exist. Variations in film structure resulting from changes in coating composition and subsequent treatment are also implied. Nowhere is information available on the actual measurement and definition of coating structure as such.

It is not the intent of this review to prove that specific forms of coating structure exist. Rather, this survey is intended to show that factors contributing to a variable structure are present in the pigment coating process and to suggest ways in which these factors may operate.

PREVIOUS WORK ON COATING STRUCTURE

The complexities involved in the measurement and analysis of pigment coating structure are indicated by the few attempts made in the past to characterize this property. Carson (1) used an air permeability method to arrive at the conclusion that coated book papers have continuous pores with a radius of 0.2 to 0.3 mu. In more recent work Tollenaar (2) described a method which measures continuously the air displaced from pores by a nonswelling fluid penetrating the sheet from one side. This method does not differentiate between the number of pores and pore

radius. This fact limits the usefulness of the method and restricts somewhat the interpretation of the information obtained. Both the air and fluid permeability methods are sensitive to the presence of pinholes in the sheet.

Certain authors (3, 4) have published electron micrographs of the surface of clay-coated papers which show the exposed clay particles to be in the plane of the raw stock. No coating cross-section electron micrographs have been published.

It is obvious that published information dealing with coating film structure is lacking and that which does exist has limited usefulness. Essentially, the work by Carson (1) and Tollenaar (2) only verifies the assumption that coated papers have a pore structure. Other structural characteristics have been neglected completely in so far as direct measurement is concerned.

Many of the end-use properties of coated papers are evaluated in such a way that the test results may reflect changes in the physical structure of the coating. For example, the opacity of coating reflects variations in the surface areas and pore distributions (5). Bonding strength may logically be related to the apparent density of a coating if other conditions are held constant. Ink receptivity may be a function of the pore size distribution and the total pore volume of a coating (6). Naturally, the relationships between these end-use properties and structure characteristics are not clear-cut or quantitative. Assuming that these relationships do exist, regardless of how obscure they may be, it

is possible to evaluate additional literature. The ensuing discussion is to be regarded as a speculative interpretation of the literature in terms of factors which may affect coating structure.

EFFECTS OF COATING RAW MATERIALS ON STRUCTURE

Pigment

Roderick and Hughes (7) have shown that the addition of kaolin clays (which have a hexagonal platelet shape) to coating colors containing irregularly shaped calcium carbonate particles increases the gloss and smoothness of the coating but decreases the opacity and the ink receptivity. Others (8 - 11) have shown that the gloss of clay coatings increases as the particle size of the clay used is decreased. An additional effect of small particle size is decreased strength in the coating (9, 10, 12). This may indicate a relationship between pigment surface area and adhesive demand although certain investigators (13, 14) have evidence which indicates that such a relationship does not exist.

The foregoing seems to indicate that the pigment exerts an effect upon coating structure which may be related to its size, shape and surface area. These, in turn, may control the ability of the pigment particles to pack or align. There is some disagreement in the literature over whether a wide (15) or narrow (12) pigment particle size range represents the best compromise of the various effects of particle size.

In addition to the rather direct effects of pigment particle size and shape, it is possible that the chemical nature of the pigment

has an indirect effect upon coating structure. This effect may be exerted through the ability of the pigment to hold a shell of vehicle and adhesive around itself, thereby reducing the amount of free vehicle and adhesive available for migration into the rawstock (8, 16, 17).

Adhesive

It has been shown (7, 18) that the opacity and ink receptivity of clay coatings decrease as the adhesive content is increased to maintain strength standards. This effect is, of course directly related to the amount of adhesive in the coating. The information available implies that the pore system of the coating decreases in total volume and/or becomes considerably finer with respect to pore radii as the adhesive content is increased.

Adhesives may have an indirect effect upon coating structure which is exerted through rheological and migration phenomena. This type of interaction is discussed in a later section.

Vehicle

The vehicle should not affect coating structure directly since it is not present to any significant extent in the finished coating. It does, however, affect the rheological characteristics of the coating color (19) and migration phenomena (20). These do have effects upon coating structure as will be discussed in a later section.

Dispersant

As in the case of the vehicle, dispersants probably do not affect coating structure directly. However, their action of pigment particle dispersion does affect the rheological characteristics of the coating color (21) and, through this, vehicle and adhesive migration (20). It is conceivable that the charge imparted to the pigment by the dispersant may interact with the charge on the rawstock in such a manner that the final structure of the coating is affected (22).

Rawstock

Perhaps one of the most important factors determining coating structure is the rawstock or substrate upon which the coating is deposited (23, 24). Among the ways in which the rawstock can affect coating structure are:

1. Vehicle, adhesive and pigment migration as controlled by the rawstock pore size and volume (20, 24); migration phenomena will be discussed in another section.
2. The intimacy of contact between the rawstock surface and the coating color during application as determined, in part, by rawstock surface roughness (20, 25, 26).
3. The wettability of the rawstock by the vehicle (20).

Except for a possible effect of surface roughness, it is evident that the rawstock acts upon coating film structure primarily through vehicle migration.

Throughout this discussion it has been evident that few of the components of coatings, in themselves, exert strong influence upon coating structure. To a large extent, interaction between the components is responsible for structural variations. The complexity of the problem of coating structure analysis is further increased when additional variables such as coat weight, coating color solids content, method of coating application, drying rate and subsequent treatment such as supercalendering are considered.

VEHICLE, ADHESIVE AND PIGMENT MIGRATION

The phenomenon of vehicle migration into the coating rawstock has been evident since aqueous coatings were first applied to paper. Consideration of Washburn's equation (27) for the flow of free liquid into an idealized pore system shows that the rate of flow, at the instant of contact, is infinite.

$$\frac{dZ}{d\theta} = 1/2 \sqrt{\frac{R\gamma}{2\eta}} \sqrt{\frac{1}{\theta}}$$

where Z = distance penetrated,

R = capillary radius,

θ = time,

γ = surface tension, and

η = viscosity.

Although the application of this equation to a coating color-rawstock system would be extremely complex, this point remains pertinent:

the flow of vehicle from the color at the instant of contact with the porous rawstock must be very rapid, even though the presence of the adhesive increases the viscosity of the system. This rapid flow of the vehicle into the rawstock may create viscous drag forces in the coating color which then should tend to align the pigment particles (particularly platelike particles such as those in kaolin clays) in conformity with the surface of the rawstock. The effect of these aligning forces should be transmitted into the coating over the entire region from which the rawstock draws vehicle. The magnitude of these drag forces is probably chiefly controlled by rawstock pore size and color viscosity, as indicated in Washburn's equation.

The flow of vehicle from the coating color should continue, at a diminishing rate, until the pigment particles touch. At this point the particles may become immobilized (14, 28). When the pigment particles come into contact with each other, the basis of a capillary system is established in the coating which then may compete with the rawstock pore system for the available vehicle (29, 30). Cobb (30) also suggests that the pigment particles can serve to plug the pores of the rawstock and reduce the rate of flow of the vehicle into the rawstock. This concept has been substantiated experimentally (20, 31).

If it is assumed that the penetration of the vehicle into the rawstock reaches an equilibrium point, then the removal of the vehicle by evaporation during the drying operation must involve further movement of the vehicle through both the rawstock and the coating toward a free surface. According to Dappen (32), this evaporation takes place at the

surface as long as the capillary system is capable of supplying the vehicle to the surface. The vehicle surface gradually recedes into the coating as its supply rate is diminished. At this point menisci form in the capillary system of the coating.

When menisci form in the coating capillary system the surface tension forces first discussed by Campbell (33) begin to have an effect upon coating structure. These effects have recently been reviewed by Cobb (34). The menisci in the coating exert a contracting force on the particles bounding them. The contracting force is due to the surface tension of the liquid forming the menisci and its magnitude is a function of the radius of curvature. These contracting forces reach values of several hundred atmospheres of pressure in menisci with radii of curvature in the range of 0.1 to 0.01 mu. As the vehicle menisci retreat into the coating, the contracting force of the menisci is replaced, at least to some extent, by bonds formed between pigment particles and adhesive molecules. The net result is a highly compacted, open capillary system in the coating.

Associated with movements of the vehicle may be a redistribution of the adhesive. Cobb and Lowe (29) first demonstrated that the flow of vehicle into the rawstock is accompanied by movement of the adhesive in the same direction. Davidson (35) has shown that the vehicle actually penetrates farther into the rawstock than the adhesive. Other workers have discussed factors affecting adhesive migration (22, 23). McCready (36) and, indirectly, Schoch (37) suggest that only the low molecular weight

fraction of adhesives migrates with the vehicle. Others (38, 39) relate the "water retentivity" of starch adhesive coating colors to their ability to lose starch to the rawstock. Lyons (8) and Rowland (40) feel that the chemical nature of the pigment controls, to some extent, the adhesive migration which occurs.

Casey and Libby (23) have qualitatively examined certain factors affecting adhesive migration and its effects upon coating properties. These investigators found that increased rawstock density and sizing decreased starch penetration. Increased starch penetration into the rawstock increased the ink receptivity of a coating. Singleterry (41) attributes a "zone of weakness" in the coating to depletion of the adhesive in this zone. A more informative study was performed by Dappen (32) who examined both vehicle and adhesive redistribution in starch-clay coatings. This author found that as much as 30-40% of the vehicle originally in the coating color migrated into the rawstock but only 3-4% of the starch was transferred. In addition, it was determined that starch migration toward the air-coating interface occurred when the coating was rapidly dried. Presumably the starch was carried to this interface by the vehicle during the evaporative stage of the drying operation. Air-dried coatings do not show excessive starch redistribution during this stage of drying.

Although Dappen did not study the rheological characteristics of the coating colors used, it is possible that they exert an influence on vehicle and adhesive migration. In this sense, the relation between

vehicle and adhesive, the physical and chemical properties of the adhesive and pigment, the solids content of the coating color, etc., all exert effects upon migration phenomena and indirectly upon coating structure (42).

Cobb (14, 34) has applied certain concepts of the soil technology field to the adhesive-pigment relationship in the coating matrix. This investigator found that 21-24% of the dry pigment voids (as determined by the addition of water to the dry pigment to a point where the pigment-water mass becomes cohesive) must be filled with adhesive before the coating achieved a strength greater than the bonding strength in a rawstock. She concluded that most of the adhesive was deposited at the points of contact between pigment particles. Although the experimental work presented in this study has some limitations, the concept advanced seems to be of some value.

Whether or not pigment particle penetration accompanies vehicle and adhesive migration into the rawstock is not clear. Certain investigators (11, 23) mention the "absorption" of coating by the rawstock. The predominant opinion appears to be that the pigment particles plug, rather than penetrate, the pores in the rawstock (20, 30, 31). Both situations are conceivable and, in either case, an effect upon coating structure seems possible.

The foregoing establishes the fact that vehicle and adhesive migration occur in the coating-rawstock system and implies that this migration can affect coating structure. The following statements attest to this:

1. Rowland (40) states that excessive adhesive penetration leaves the coating in a rough and porous condition.
2. Davidson (35) found that inadequate adhesive penetration reduces coating ink receptivity.
3. Casey and Libby (23) found a relationship between the depth of starch penetration into the rawstock and the ink receptivity of the coating film.

This information leads to the assumption that the removal of adhesive by the rawstock leaves the coating with a different pore system than would otherwise be the case. Unfortunately, the effects of adhesive and vehicle migration have not been separated. The structural effects do, however, appear to be real and significant.

Summarizing, the effects on coating structure resulting from vehicle and adhesive migration are probably the result of:

1. Alignment or packing of pigment particles due to friction forces generated by the rapid flow of vehicle into the rawstock during the initial stages of the coating process.
2. The immobilization of pigment particles due to the removal of the vehicle from the coating.
3. Adhesive redistribution occurring during all stages of vehicle removal from the coating.

MECHANICAL FACTORS

Coating Color Dispersion

The most obvious objectives of mechanical coating color dispersion operations are twofold (5, 43). First, soft agglomerates in the coating color are broken up. Secondly, intimate mixing of the vehicle, adhesive and pigment are desired. Thus, the effect of mechanical dispersion upon coating structure is probably related to the ability of the pigment particles to pack and to the rheological characteristics of the coating color.

The Application of the Coating Color to the Rawstock

Many methods of applying fluid coating colors to a rawstock are available. The differences of concern here are:

1. The pressure applied during the coating operation.
2. The rates of shear operative during coating deposition.
3. The manner in which the color supply and the coated rawstock are separated from each other.

Probably none of these characteristics influences coating structure in itself but acts through or with adhesive migration and the rheological properties of the color which have a more direct effect upon coating structure.

The pressure applied during the coating operation may serve to accelerate the instantaneous phase of vehicle and adhesive migration (5, 20); conversely, the release of coating pressure may suspend these processes. The shearing forces created in the color by the coating process should tend to rotate platelike pigment particles toward the direction in which they offer the greatest resistance to rotation in a shear field.

The method of separation of the color supply and the coating film dictates, to some extent, the direction in which the final shearing forces will operate. For example, the filaments formed in the separation of the paper from the roll surface in a roll printing operation indicate that the final shearing forces in the ink are directed normal to the plane of the paper surface (44). It is conceivable that these filaments also form a roll coating operation. The rheological characteristics of the color with respect to the presence of thixotropy or dilatant tendencies would be of considerable importance here.

Supercalendering

The objective of the supercalendering operation is to produce a smooth printing surface on both coated and uncoated papers. This is accomplished with pressure, shearing forces and heat. Van den Akker (45) and Thomas (46) have discussed the creation of shear forces in this operation and have commented upon their magnitude. The effects of these forces on coated papers are an increase in gloss, sheet density and surface smoothness and a simultaneous decrease in opacity, brightness and strength. From this information it can be assumed that the surface of the sheet is made more planar, the pore size is decreased and some rupture of bonds occurs (47). There is little evidence available which indicates whether these effects occur in the coating film or the rawstock.

Rowland (40) assumed, from the behavior of hydrous and calcined clays in the supercalendering operation, that crystal plane slippage occurs in the kaolin particles when they are subjected to these great

shearing forces. Tollenaar (2) found evidence that some inner layer of the coated paper was compressed during the calendering operation. Little else, excepting end-use property values, is known about what actually happens to coating structure during this operation.

SUMMARY

This brief survey of the pertinent literature in the field of pigment coatings reveals that the majority of the work is concerned with the effects of certain variables upon the end-use properties of coated papers. The basic reasons for the effects of these variables are not clearly understood. It has been pointed out that a great many of these end-use properties may be related to the physical structure of coatings. No satisfactory methods have been described in the literature for the analysis of coating structure.

GLOSSARY

e.s.d. - equivalent spherical diameter; a measure of particle size determination by the rate of fall of the particle in a viscous medium and expressed as the size of a sphere which falls at the same rate.

lb./ream - a term used in paper technology to express the weight per unit area of paper. In this work the ream size is 25 inches x 38 inches x 500 sheets: 475,000 $in.^2$

IPC Bonding strength test - a test which measures the resistance of a coating or paper to "picking" or rupture under the influence of complex applied stresses.

Starch:clay ratio - a term common in the coating field; the ratio of starch to clay, by weight, in the coating formulation.

Unbonded area - used interchangeably with free surface area and surface area in this discussion of coating properties. These terms are intended to describe the area of a coating which is accessible to nitrogen molecules.

Void volume - this term is used to describe the internal pore volume of coatings. It does not include the very large surface pores which result from projections from the coating surface.

MATERIALS AND COATING PREPARATION

CLAY

Three particle size fractions of "Lustra" coating clay were supplied by Southern Clays Inc. The whole clay had been dispersed with tetra-sodium pyrophosphate, fractionated, flocculated with H_2SO_4 and oven dried (48).

The particle size distributions of these clay fractions were determined by repeated fractionation in a basket-type centrifuge. Stoke's equation (49) was used to calculate the centrifugal forces and times required. The particle size distributions obtained in this manner are presented in Figure 1. This confirms the excellent separation of clay particle size achieved by the supplier. For the remainder of this work, the various clay fractions will be described by the nominal particle size range listed with each curve in Figure 1. These particle size distributions are described in terms of the equivalent spherical diameter (e.s.d.) rather than any true dimension of the particles.

Table I lists the surface area of the clay fractions as obtained by the Brunauer, Emmett and Teller method (see page 42). The experimental data for the surface area determinations are listed in Table X, Appendix. From a knowledge of the surface area and the average equivalent spherical diameter of the clay fractions, approximate length-to-thickness ratios of the clay particles may be calculated through the use of the Müller equation (50, 84). These calculated ratios have also been listed in

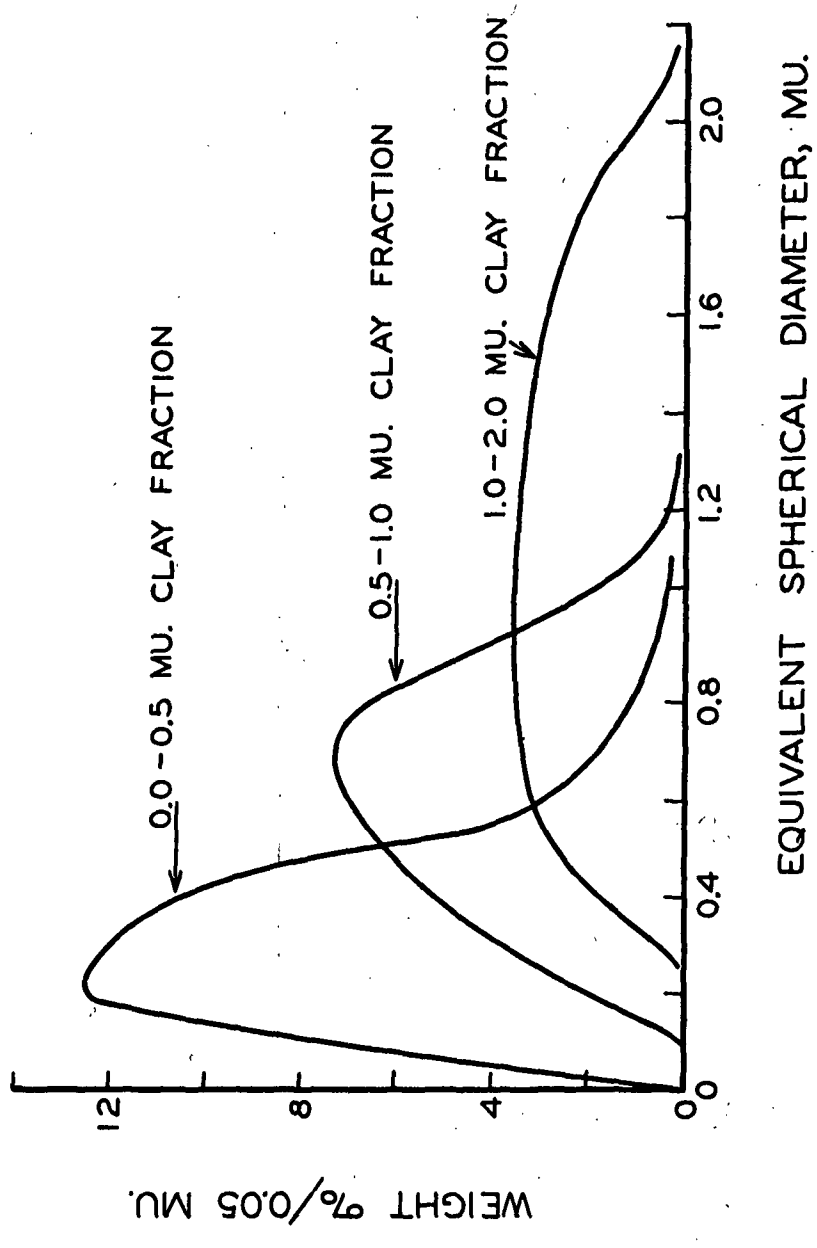

Figure 1. Particle Size Distributions

Table I. The values indicate that the clay particles tend to become thicker, with respect to their largest diameter, as the equivalent spherical diameter is decreased. The length-to-thickness ratios listed can be considered only as approximations since the Müller equation is correctly used only with essentially mono-disperse particle size fractions.

TABLE I

PHYSICAL CHARACTERISTICS-CLAY FRACTIONS

Nominal Particle Size, mu.	B.E.T. Surface Area, M^2/g.	Length/Thickness Ratio
0.0 - 0.5	20.15	6.0
0.5 - 1.0	14.04	7.7
1.0 - 2.0	10.30	10.0

The electron micrographs shown in Figures 2 and 3 show that the two largest particle size clays are composed of well-defined hexagonal platelets. The electron micrograph of the smallest clay fraction, Figure 4, does not show sharp definition; this indicates that the form of the particles in this fraction is less well-defined. X-ray examination of this fraction gave no evidence of nonkaolin impurities.

Figure 5 represents the viscosity of a 64% solids slurry of the 0.0 - 0.5 mu clay fraction as influenced by the addition of a dispersant (Quadrafos). The slurry was adjusted to a pH of 8.0 with 1.0N NaOH prior to the determination of the viscosity. The clay slip viscosity was measured with a Brookfield viscometer. The graph indicates that 2-3

Figure 2

1.0 - 2.0 mu Clay
8000 X

Figure 3

0.5 - 1.0 mu Clay
8000 X

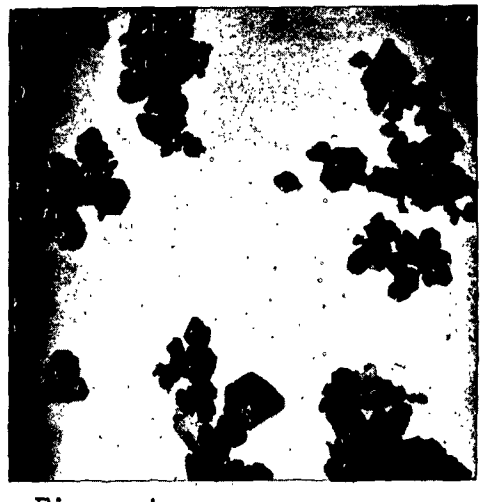

Figure 4

0.0 - 0.5 mu Clay
8000 X

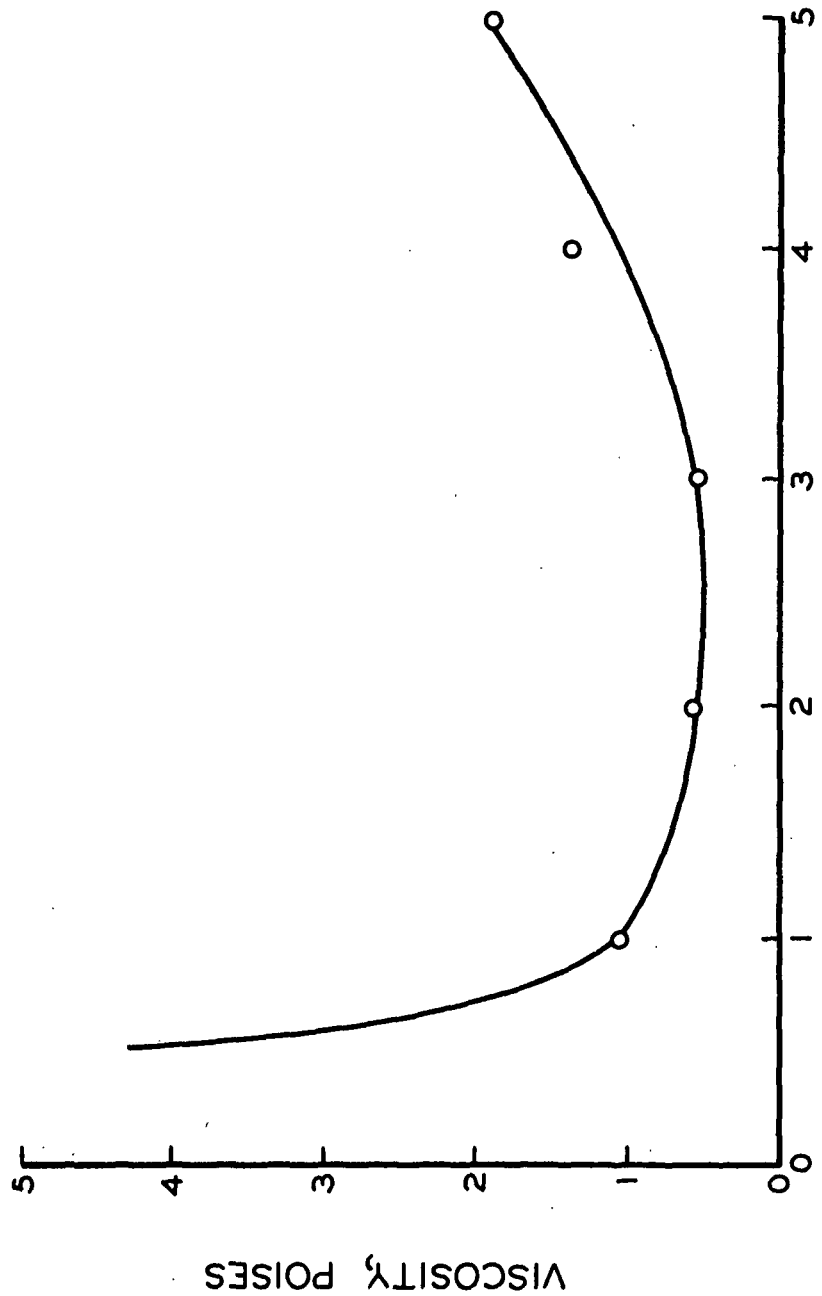

Figure 5. Dispersing Agent Requirement, 0.0 - 0.5 Clay Fraction

milliequivalents of Quadrafos for each 100 grams of clay adequately dispersed the clay slip to its minimum viscosity at this pH level.

ADHESIVES

Much coated paper contains a modified starch as the adhesive. For this reason, and for reproducibility of preparation, an oxidized cornstarch, Stayco M supplied by A. E. Staley Co., was selected for use in this work. This starch began to swell at 62°C. and reached its maximum viscosity at 70°C. The maximum torque generated by the starch slurry on the stirring device of the Corn Industries Viscometer was 270-320 g.-cm. Retrogradation upon cooling the starch slurry to 50°C. is slight.

DISPERSANTS

The clay slips were dispersed with 3 meq. of Quadrafos/100 g. of clay. The pH of the slip was adjusted to 8.0 with 1.0N NaOH. Quadrafos ($Na_6P_4O_{13}$ - sodium tetraphosphate) is a product of the Rumford Chemical Works.

RAWSTOCK

For reasons which are discussed on page 33, Millipore filter, a product of the Millipore Filter Corp., was selected as the rawstock used in this work. This material is a nitrocellulose sheet of controlled porosity. The physical characteristics of this material are presented in Table II.

This material is unique in that its pores are very nearly perpendicular

TABLE II

PHYSICAL CHARACTERISTICS OF MILLIPORE FILTERS

	Filter Designation		
	VC	HA	AA
Pore diameter, mu	0.10 ± .008	0.45 ± .02	0.80 ± .05
Basis weight, lb./ream	33.6	28.4	21.3
Caliper, mils.	4.3	4.9	4.2
Apparent density, g./ml.	0.45	0.34	0.29
Chapman smoothness, % contact, 354 p.s.i.	-	29	20
Dry indicator size, sec. (TAPPI std., T 433 m-44)	10	6	2

to the plane of the sheet rather than randomly oriented and interconnected as in matted fiber sheets. The surface of the filter is very smooth, as good or better than most supercalendered coated papers. The structure of the filter is not destroyed by water. The filter is soluble in several slightly polar organic solvents. Careful handling of the material is necessary since both the folding endurance and the tearing resistance are very low.

The selection of type HA Millipore filter for use throughout much of this work with coatings was arbitrary. The pore diameter of this filter stock, 0.45 mu, appears to be smaller than normally encountered in papers although there is no truly reliable data available on the pore distributions of papers. Corte (57) has shown that, in many cases, the pore distribution obtained for a paper depends upon the method of determination. Depending

upon the method used and the paper examined, Corte gave values for pore radii ranging from 0.25 mu to 3-4 mu. Most of the papers showed a maximum in the pore distribution at about 1. mu.

In view of the pore type, the pore size, the surface smoothness and the reaction of this filter material to water, Millipore filter is best considered as an idealized rawstock. Direct comparisons between coatings analyzed in this work and coatings laid on paper rawstocks should be made only with the qualifications mentioned above.

STARCH SLURRY PREPARATION

The oxidized starch, Stayco M, was cooked in the Corn Industries Viscometer following the cooking schedule recommended by the starch supplier. Two hundred and twenty-five grams (o.d.) of starch were dispersed in sufficient distilled water to yield a total weight of 900 g. (25% solids). The dispersed starch was then placed in the Corn Industries Viscometer; the temperature was raised to 96°C. and was held at this point for 30 minutes. After this cooking period the slurry was cooled to 50°C. and kept at this temperature until used (not longer than 3-4 hours). The Corn Industries Viscometer recorded the viscosity changes throughout the cooking cycle and held evaporation losses to a minimum.

THE PREPARATION OF COATING COLORS

Clay slips of the desired solids content were prepared by dispersing the clays in distilled water containing 3 meq. Quadrafos/100 g. of clay and approximately 3 meq. NaOH/100 g. clay. The clay slip was then agitated.

for 30 minutes with a Hamilton-Beach stirrer. The required amount of warm starch suspension was weighed into the slip and the agitation was continued for an additional 30 minutes. The pH of the color was adjusted to 8.0 with 1.0N NaOH. The solids content of the color was measured and sufficient water added to bring the solids content to 55%. The color was then passed through a hand-operated dispersion mill (Chicago Apparatus Co., no. 22950) followed by screening through a 325-mesh sieve.

Hercules Viscometer rheograms of colors prepared in this fashion showed them all to be pseudoplastic in nature. The viscosity calculated from these rheograms (at 1150 r.p.m. using bob A) was quite low; 0.66 poise for a color containing the 1.0 - 2.0 mu clay fraction, 0.43 poise for a color containing the 0.5 - 1.0 mu clay fraction, and 0.43 poise for a color containing the 0.0 - 0.5 mu clay fraction. The latter color had a yield value of approximately 60,000 dyne cm.

COATING METHOD

The coating colors were spread on Millipore filter with a Bird applicator bar coating device which had a clearance of 0.0015 inches and a coating width of 6 inches. The filter rawstock was fastened to a piece of level plate glass with a single strip of Scotch tape. The coating color was laid upon the tape strip with an eye-dropper. The Bird applicator bar was then brought up behind the color and pulled the length of the rawstock at a uniform speed. The coating weight was varied by adjusting the clearance between the coating bar and the rawstock

surface. This clearance was increased by allowing the bar to run on strips of Scotch tape which were fastened to the plate glass next to the rawstock. The clearance was decreased by shimming the rawstock with full size pieces of one-mil cigarette paper.

All coatings were air dried at 73°F. and 50% R.H.

METHODS FOR THE EVALUATION OF COATING STRUCTURE

COATING ISOLATION

Coated papers consist of a porous pigment-adhesive layer over a porous rawstock system. As has been discussed, some intermingling of the components of the two pore systems does occur. Of primary importance in this investigation is the pigment coating layer. The rawstock pore system, although of importance during the deposition of the coating, does not affect the structural characteristics of the coating after it has been dried. The presence of the rawstock does seriously complicate the analysis of coating structure.

It is necessary to separate the rawstock and coating systems either experimentally or mathematically in the determination of the pore volume and distribution, the surface area and the clay particle orientation of coatings. In all of these cases, the presence of the rawstock adds nothing to the information obtained but does make the experimental work more difficult.

The solution to this problem is the use of a rawstock from which the coating can be removed, in pieces large enough to be useful, without altering the coating structure. To this end, attempts were made to form handsheets from chloroform-soluble, fibrous cellulose acetate. Although the fibrous acetate could be slightly swollen in acetone-water mixtures, considerable difficulty was encountered in forming satisfactory handsheets. This approach was abandoned.

Millipore filter (hereafter referred to as MF rawstock) was used in succeeding trials and was found to perform in a satisfactory manner. This material is soluble in ethyl acetate which, according to Cushing (51), does not swell starch. It should be possible then to dissolve the MF rawstock in this solvent, leaving the coating as a coherent sheet unchanged in its important properties.

The following coating isolation procedure was adopted as the most efficient. It consisted of a seven-stage, countercurrent washing of the coated sheets in ethyl acetate. The washing was accomplished in 15-cm. culture dishes which had been filled with ethyl acetate. A 10-mesh screen was placed in the bottom of each dish to facilitate the transfer of coating pieces from one bath to the next. The coating pieces, about one-inch square, were placed in the first bath coating side down. After 10 minutes the screen was lifted from the first bath and transferred to the next. A second coating sample was then placed in the first bath. After these first two steps, the baths were moved countercurrently to the coating so that clean ethyl acetate was entering the system continually. The MF rawstock was largely removed in the first two baths.

In the fourth or fifth bath a thin film or mat was observed to break loose from that surface of the coating which had been in the rawstock-coating interface. (This surface is hereafter referred to as the "bottom" surface of the isolated coating.) This material stained blue with iodine solution and was assumed to be that portion of the starch which had migrated into the rawstock. If portions of this starch mat

adhered to the coating in the seventh bath, they were brushed loose with a small brush.

After the coating was removed from the last bath it was allowed to air dry. Work with this method showed that coatings as light as 4 lb./ream could be isolated in a coherent form although 8-10 lb./ream appeared to be the practical limit.

In order to demonstrate that the MF rawstock had been completely dissolved in this process without significant effects on the coating structure, the following experiments were performed.

Dissolution of MF Rawstock

A sample of isolated coating (1 gram) was allowed to soak in 50 ml. of ethyl acetate for twelve hours. Examination of the solvent with the Rayleigh Interferometer showed that no further quantity of the MF rawstock was dissolved from the coating.

In a second experiment, a sample of isolated coating (0.50 g.) was macerated in 5 ml. of warm concentrated H_2SO_4. The mixture was filtered through a thin layer of Celite filter-aid on a fritted glass funnel. The "brown ring" test for nitrates was performed on the filtrate with negative results. Since a control experiment showed that 0.2 mg. of the MF rawstock per ml. of H_2SO_4 are detectable by this method, it was evident that less than 0.2%, by weight, of the MF rawstock remained on the coating.

The Effect Of Ethyl Acetate Treatment on Coating Structure

A 50% solids coating color containing HT coating clay (Minerals and Chemicals Corp. of America) and Stayco M starch in a 14:100 ratio was spread upon a paper rawstock and allowed to air dry. Thirty strips of the coated paper were cut to the dimensions 1 x 13 inches. Fifteen of these strips were soaked in ethyl acetate for two hours and then air-dried. IPC bonding strength tests were run on all samples using the I.G.T. device (13). The results showed that the averages of both sets of strips came from the same statistical population. The test data are recorded in Table XI, Appendix.

In a second experiment, a 55% solids color consisting of the 0.0-0.5 mu clay fraction and 10.7% starch was deposited upon lightly scrubbed aluminum foil with an 0.006-inch Bird applicator bar. The coatings were air dried and the coat weight was determined to be approximately 100 lb./ream. It was possible to isolate this heavyweight coating from aluminum foil simply by cutting the coated foil into 1-inch wide strips and twisting these slightly from the ends. The coating flaked off the foil in large pieces. A very thin film of the coating adhered to the surface of the foil.

One sample of the coating which was isolated in this manner was examined for clay particle orientation by means of the x-ray technique which is described on page 57. This sample of the coating was then soaked in ethyl acetate for thirty minutes, air dried and then re-examined. No difference in the two orientation profiles so obtained was detectable.

The two orientation profiles are presented in Figure 6 and the experimental data are listed in Table XII, Appendix.

In a second set of experiments with this heavyweight coating, the surface area and pore distribution were determined (see page 42) in duplicate. The sample was then removed from the adsorption apparatus and allowed to equilibrate with the moisture in the air. The sample was then soaked in ethyl acetate for thirty minutes after which it was allowed to air dry. The surface area and pore distribution of this ethyl acetate-treated sample were determined in the same manner as before. The surface area was determined in duplicate, but only one pore distribution was run.

The surface areas obtained were 8.16 and 8.12 M^2/g. for the control and the ethyl acetate-treated sample, respectively. The difference between these two values is not significant. The adsorption-desorption isotherms for these two samples are presented in Figures 7a and 7b. It is clearly evident that the control sample and the ethyl acetate-treated sample have identical isotherms and, therefore, identical pore distributions. The experimental data are recorded in Tables XIII and XIV, Appendix.

On the basis of the evidence presented, it is reasonable to conclude that the method described for the isolation of pigment coatings from Millipore filter accomplishes essentially complete solution of the raw-stock without detectable effects upon the strength, the clay particle orientation, the surface area and the pore distribution of coatings.

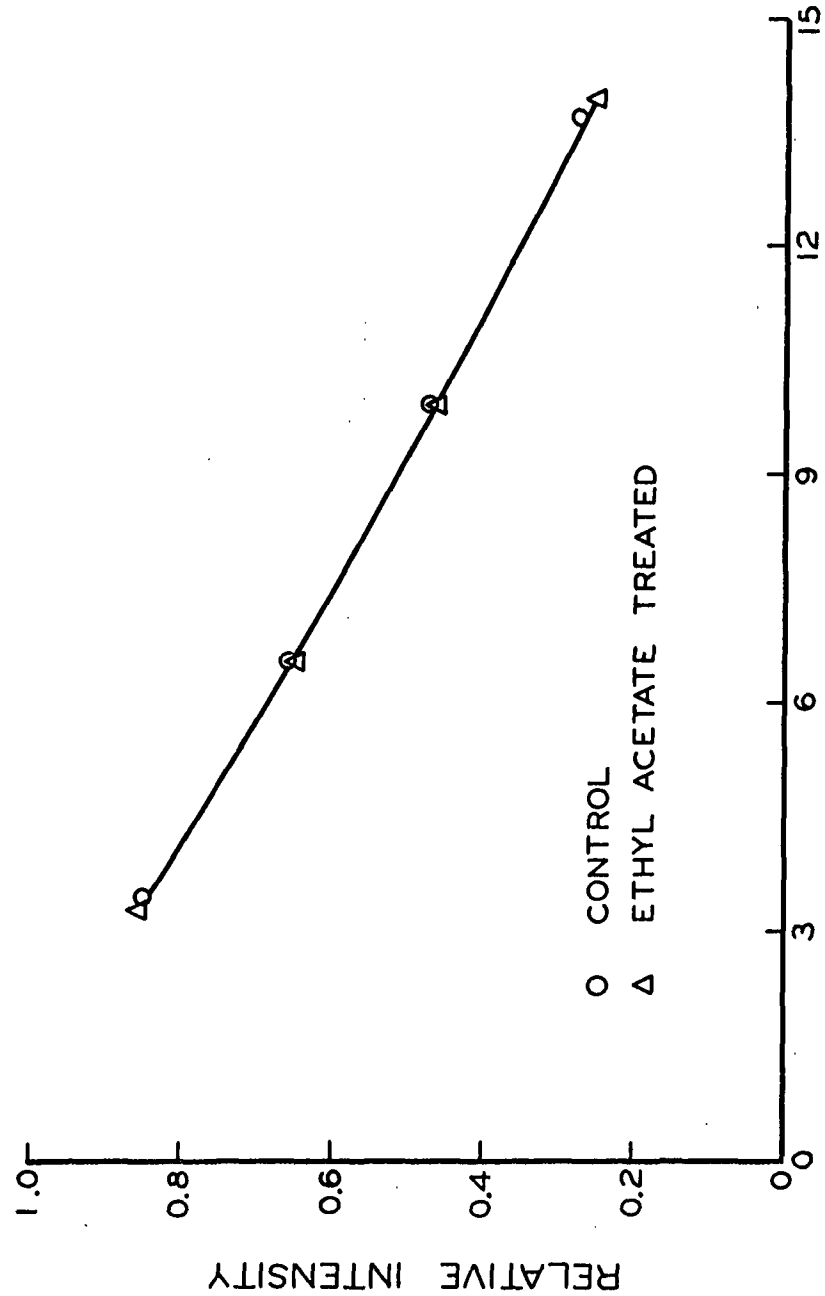

Figure 6. The Effect of Ethyl Acetate on Clay Particle Orientation

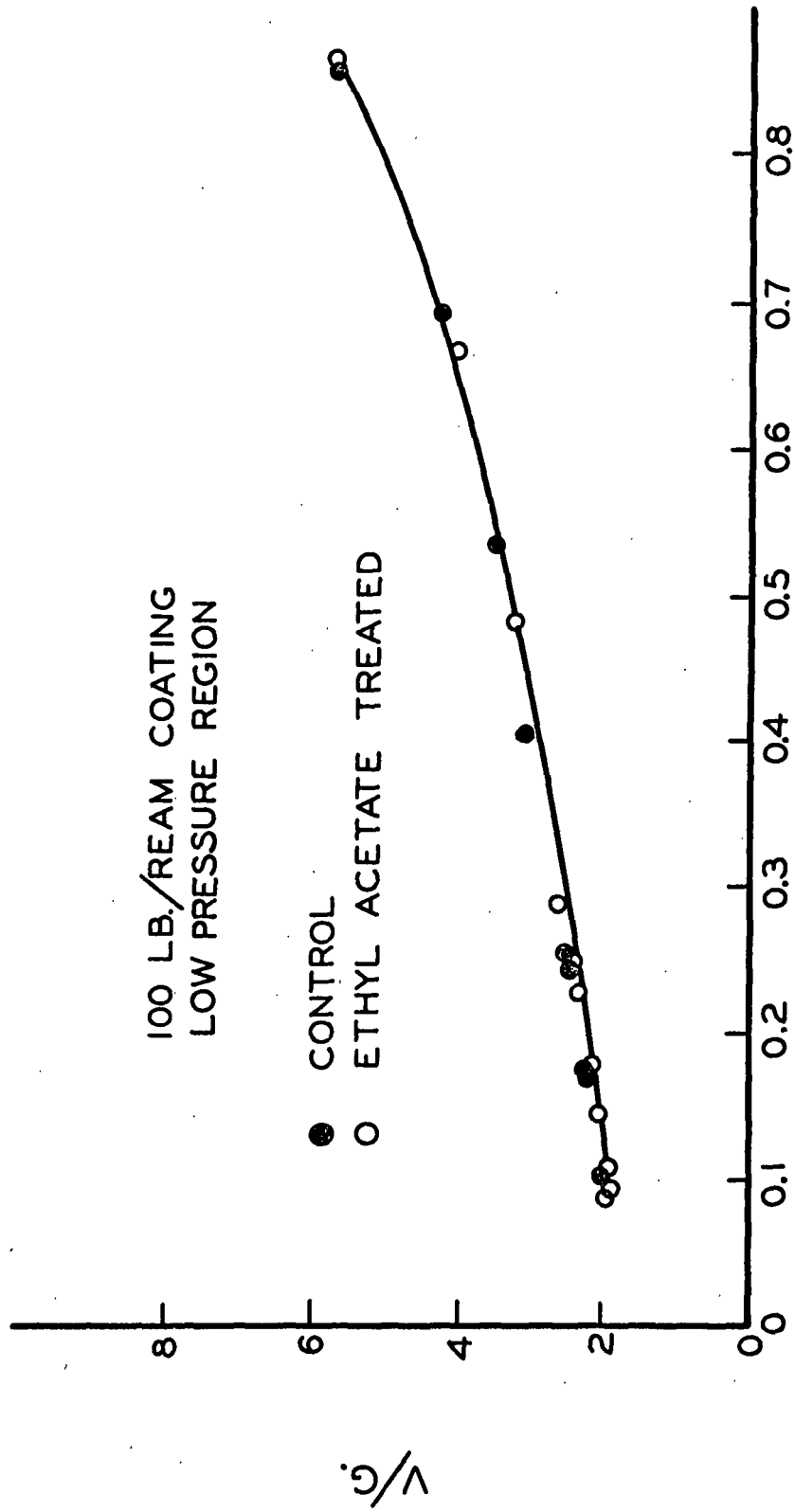

Figure 7a. Nitrogen Adsorption Isotherm

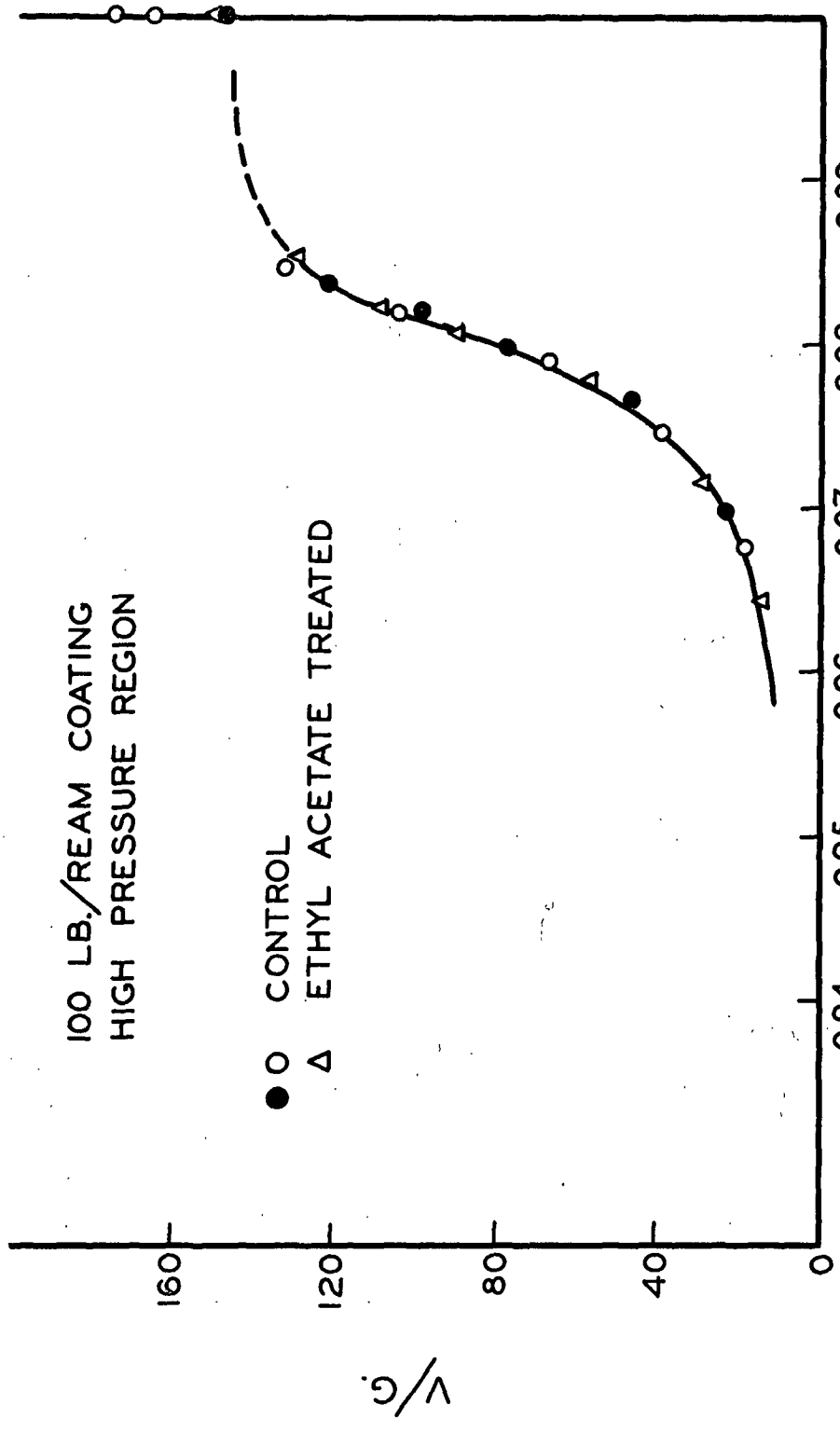

Fibure 7b. Nitrogen Desorption Isotherm

Residual Solvent

It has been shown (52) that the solvent-exchange drying of cellulose results in the retention of small amounts of the solvent in the pores of the cellulose. This solvent is trapped in such a manner that it is not readily released even under high vacuum. It can be removed by wetting the cellulose with water and then oven drying the material.

The process of coating isolation by dissolution of the MF rawstock on ethyl acetate is analogous to solvent-exchange drying only in so far as that small percentage of water retained in an air-dried coating is concerned (about 2% on the weight of the coating). In order to examine the possibility that a small amount of the ethyl acetate may have been trapped in the coating, samples of isolated coating were oven dried and weighed. The samples were then soaked in water for 4 hours, after which the water was evaporated. The samples were oven dried and reweighed. The weight loss in this process varied from 0.03 to 0.20% for the five samples. According to Merchant (52), this weight loss results from the release of solvent when the coating structure was destroyed by water. A control sample of coating showed no weight loss. The quantity of residual ethyl acetate retained in isolated coatings is small and is assumed to have only insignificant effects upon coating structure as measured by the techniques to be described.

SURFACE AREA MEASUREMENT

The surface area of a pigment coating which is accessible to small

molecules may be construed to be a measure of the potential light-scattering surface and the unbonded area. As such, the surface area is conceivably related to the optical and strength properties of coatings.

Low temperature gas adsorption measurements represent the most reliable and convenient method for the measurement of surface area. An excellent review of various gas adsorption methods has been presented by Haselton (53). The first reliable method is that of Brunauer, Emmett and Teller (54). These authors have derived expressions, based on a multilayer gas-adsorption theory, which are capable of describing most adsorption isotherms over a wide range of relative pressures. The Brunauer, Emmett and Teller (B. E.T.) equation for the isothermal adsorption of an infinite number of molecular layers of a gas on a free surface may be expressed in the form

$$\frac{P}{V(P_o - P)} = \frac{(c - 1)}{V_m c} \frac{P}{P_o} + \frac{1}{V_m c}$$

where

P = the equilibrium gas pressure,

P_o = the saturation vapor pressure of the adsorbate,

V = the volume of adsorbed gas (ml. S.T.P.) per gram of absorbent,

V_m = the volume of gas required to form a monolayer on the adsorbent surface, and

c = a dimensionless constant.

This equation is of the form, $y = mx + b$. Therefore, a plot of $P/V(P_o - P)$ versus P/P_o should yield a straight line of slope $(c - 1)/V_m c$

and intercept $1/V_m c$. This is actually the case for relative pressures ranging from 0.05 to 0.30 (54). The volume of gas corresponding to monolayer formation (V_m) can be obtained from the slope and intercept of the straight-line plot. Then, since the cross-section area of the absorbate molecule is known, 16.2 $A^2_\circ$ (53), the area corresponding to (V_m) may be calculated.

The apparatus used in the determination of low-temperature gas-adsorption measurements is that built and described by Haselton (53) and later slightly modified by Merchant (52). No useful purpose would be served by further description of this equipment.

It is worthy of mention that the "deadspace" in the sample bulb (the volume of the bulb not occupied by the sample) was kept as small as practical. This was done in order to reduce the effect of errors in the deadspace determination on measured surface areas. It should also be noted that all coating samples were dried for 48 hours at 60°C. and 28 inches (Hg) vacuum in order to shorten the outgassing time on the adsorption apparatus.

THE DETERMINATION OF PORE DISTRIBUTION

Perhaps the most important single structural characteristic of coating films is their pore structure. It is reasonable to assume that the rate and extent to which inks are absorbed by coatings are strongly related to pore size and volume. Also, the light-scattering coefficient must be at least partially dependent upon pore size, volume and area.

Among the methods which are available for the determination of this characteristic are high pressure mercury intrusion (55), electron microscopy (56), gas permeation (57) and low-temperature gas adsorption. The mercury intrusion method is objectionable in work with fragile materials due to the possibility of pore collapse. The measurement of pore distribution with the electron microscope is tedious and is subject to uncertain coating sectioning effects. The gas permeation method measures only continuous pores and is sensitive to pinholes in the sheet. Low-temperature gas-adsorption measurements are tedious but yield results of proven validity. Pore distributions obtained by this method have been checked by means of the electron microscope (56, 58) and by the mercury intrusion method (59, 60). The gas-adsorption method yields total pore volume and pore area data in addition to the pore distribution. For these reasons, this method was used throughout this work.

The interpretation of gas-adsorption isotherms to yield pore-distribution data is dependent upon the mechanism by which it is assumed that adsorption takes place. Cohen (61, 62) reasoned that monolayer gas adsorption was followed by capillary condensation of the absorbate and based his calculations on this premise. After the publication of the B.E.T. multilayer theory of adsorption (54), the popularly accepted mechanism was multilayer adsorption in combination with capillary condensation at higher values of relative pressure. Carman (63) has published experimental confirmation of this mechanism which is now accepted as the basis for most isotherm interpretation methods.

In one of the earliest methods for isotherm interpretation, Shull (64) developed Wheeler's theories (65) based on the assumption that the pore distribution of the absorbent is Gaussian or Maxwellian in nature. Barrett, Joyner and Halenda (66) developed a treatment which does not require this assumption but contains an arbitrary constant. Pierce (67) has published a simplified version of the Barrett, Joyner and Halenda procedure. Since Pierce's treatment is quite simple and direct, it will be used throughout this work.

Pierce's method is based upon the assumption that some form of the Kelvin equation,

$$\ln \frac{P}{P_o} = - \frac{2\gamma M_v}{RT\, r}$$

where

P = gas pressure at equilibrium,

P_o = saturation vapor pressure of adsorbate,

γ = surface tension,

M_v = molar volume,

r = pore radius,

R = gas constant, and

T = absolute temperature,

is valid over the range of pore sizes in the sample. It is also somewhat dependent upon the assumption that the pores in the absorbent are uniformly cylindrical over their length. The first assumption is valid since the Kelvin equation has been shown to apply to pores with a radius

close to 20 A. (67). The second assumption is made for the purpose of standardizing the computation. It cannot be strictly valid.

A third opportunity for error in this treatment is the use of an arbitrary adsorbed gas layer thickness at various values of relative pressure. The values for the thickness of this layer are based upon the average of the gas layers adsorbed on a large number of nonporous adsorbents. In systems containing large pores, the error due to this source is small.

The pores in pigment coatings are quite large, and this fact causes several difficulties in the determination of the isotherm and, consequently, in the determination of the pore distribution. Figure 8 shows the high relative pressure region of an isotherm obtained with an isolated coating which contained 10.7% starch and the 0.0-0.5 mu clay fraction. In order to detect the hysteresis loop in this isotherm, it was necessary to expand the relative pressure scale as shown.

The adsorption isotherm was determined according to the method described by Haselton (53) and Merchant (52). Saturation of the sample, as determined by an approach from the adsorption side, evidently occurred at V/g = 130 ml. Now, desorption of the sample was begun from this point and curve A was obtained. If an excess of nitrogen is admitted to the sample chamber after apparent saturation is achieved and eight hours are allowed for the attainment of equilibrium, desorption curve B is obtained. The location of curve B is not changed if 5 or 10 hours are allowed for equilibrium at this saturation point. It is evident that curve B differs

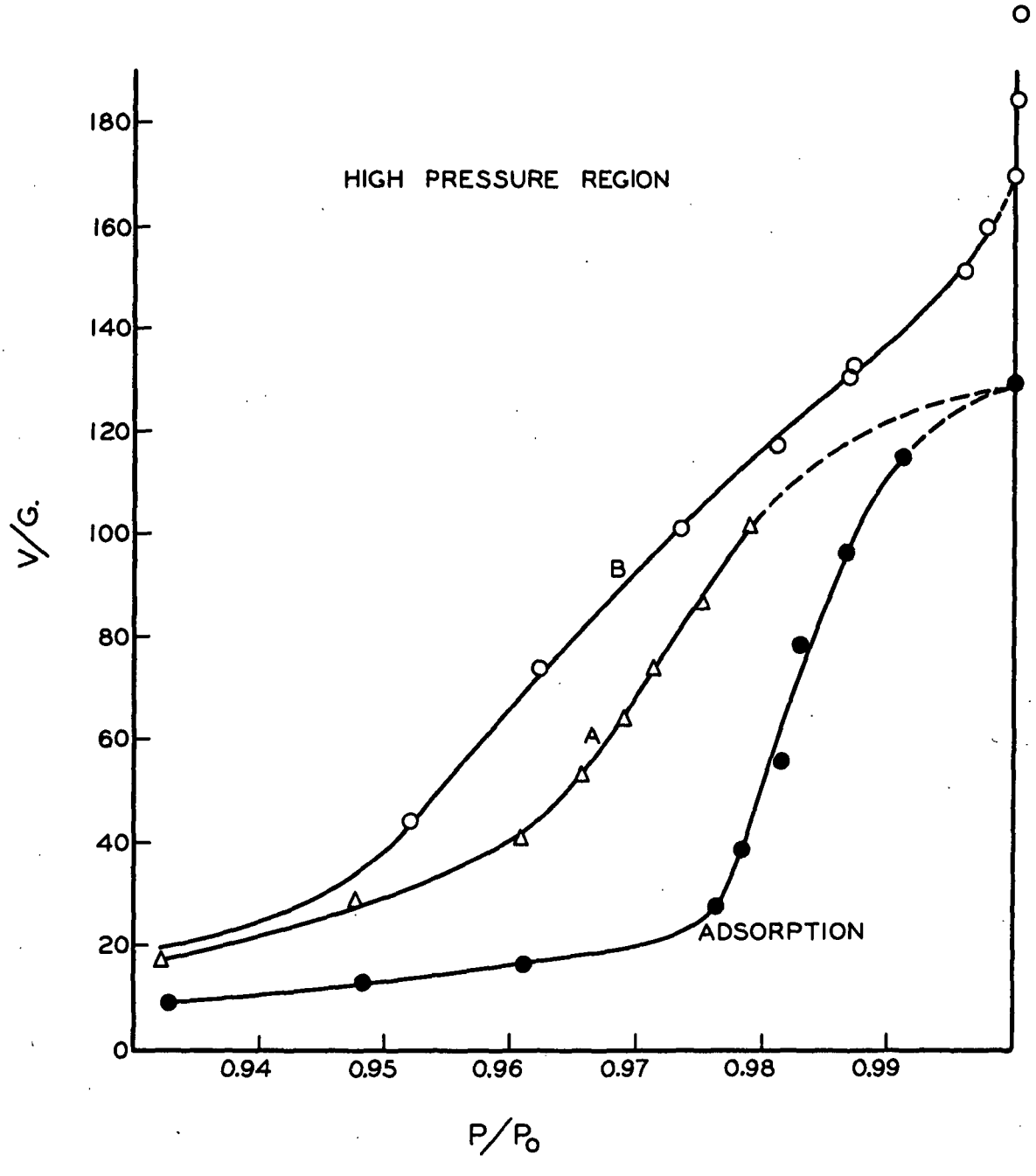

Figure 8. Nitrogen Sorption Isotherms

significantly from curve A, confirming the phenomenon noted by Barrett and Joyner (68). The saturation point approached from the adsorption side is too low and is probably caused by "raining" of condensed nitrogen on the sample coupled with insufficient time allowance for equilibrium. The result, of course, is that the pores are not completely filled at this apparent saturation value. It is doubtful that a true saturation value can be obtained for this type of isotherm by an approach from the adsorption side with a reasonable time expenditure.

Barrett and Joyner (68) recommend the procedure used to obtain curve B (Figure 8). This procedure is used throughout the course of this study. Ries and co-workers (69, 70) advocate a similar method which they claim yields a valid saturation value. In many of their isotherms, they were able to show the existence of a break in the asymptotic approach of the desorption isotherm to the saturation axis. (This same phenomenon can be noted in curve B if the relative pressure scale is compressed.) They found that saturation values taken at this "break" showed good agreement with the adsorbent void volume as measured by mercury displacement. This indicates that extrapolation of the desorption curve to the saturation axis yields a true saturation value from which the internal void volume of the isolated coatings can be calculated.

It is interesting that the P/P_o values greater than 0.995 in curve B again appear to approach the saturation axis asymptotically. This is probably due to the filling of interparticle voids and, possibly, surface aberrations in the sample begin to act as pores in this relative pressure range.

The pore distributions of isolated coatings determined by the nitrogen adsorption method cannot be considered absolute. The following qualifications should be recalled when the pore data presented herein are evaluated.

1. The pore distributions are based upon computations for effective circular pore cross sections. It is likely that the pores in coatings have cross sections of all possible shapes.
2. The pore distributions should be considered as pore volumes controlled by pore openings of the size indicated. In other words, the pore body may be slightly larger or of different shape than the pore opening. These openings are not necessarily in the surface of the coatings.
3. The precision of the pore data at a pore radius of 0.10 mu is estimated to be ± 6%; at 0.03 mu the estimated precision is ± 3%. These estimates are based upon the possible greatest error in the physical measurements involved in the determination plus an allowance for error in the attainment of equilibrium. At values of pore radii greater than 0.1 mu the precision is poor.

The reproducibility of the nitrogen adsorption techniques is well illustrated in Figure 7b. The points plotted in this Figure represent, in essence, three desorption determinations on one sample. Some scatter of points is evident but in general the reproducibility appears to be excellent.

VOID VOLUME BY MERCURY DISPLACEMENT

The determination of the void volume of isolated coatings by mercury displacement was intended primarily as an independent check of void volume values determined by the nitrogen adsorption technique.

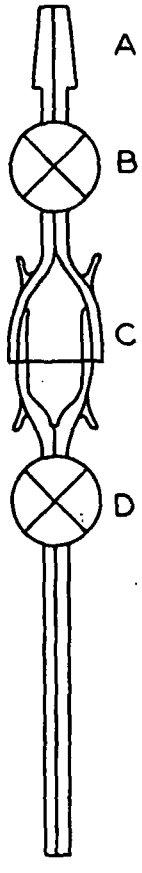

Figure 9.
Mercury Pycnometer

Assuming a contact angle between mercury and coating surfaces of 130° (59), it can be shown, through the use of a capillary rise equation (59), that mercury at atmospheric pressure will penetrate all pores and surface aberrations with an effective circular radius greater than 6 mu. The void volume determined by this method includes all pores and surface aberrations smaller than this value.

The apparatus used in this determination is shown in Figure 9. The equipment was designed to provide easy access to and convenient evacuation of the sample chamber. In order to improve the reproducibility with which the 15/20 ground-glass joint (C) was sealed, this joint was lapped with 600-mesh carborundum

followed by jeweler's rouge. This treatment reduces the quantity of grease required to provide a vacuum-tight seal of the joint.

The apparatus is assembled with all joints lightly greased. A vacuum connection is made at the 10/30 ground-glass joint (A) and the sample chamber (C) is partially evacuated. The lower end of the apparatus is inserted into a mercury reservoir which is maintained at 25° ± 0.1°C. The mercury is allowed to rise to a point just above stopcock (D). The apparatus is then evacuated to 1 mm. Hg or less. Mercury is allowed to fill the sample chamber and rise above stopcock (B). Both stopcocks are closed and the vacuum connection is broken. With the apparatus in an upright position, stopcock (B) is opened for a few seconds to allow the pressure in the apparatus to equilibrate with atmospheric pressure. Stopcock (B) is then closed and joint (A) is wiped free of grease. Excess mercury is cleaned from the tubing above stopcock (B) and below stopcock (D). The entire assembly is weighed on an analytical balance.

After this weighing, the mercury is run out of the apparatus and joint (C) is opened and closed. The procedure described above is repeated until three successive weighings agreeing within 0.03 g. are obtained. After these blank measurements have been obtained, a carefully weighed sample (0.20 g.) of isolated coating is placed into the sample chamber. The apparatus is assembled and three determinations made as above. The apparent density is calculated from the following equation:

$$\text{apparent density} = \text{weight of sample/volume of sample}$$

$$= \frac{(\text{wt. of sample}) \times (\text{density of Hg})}{(\text{blank wt.} - \text{wt. with sample}) + (\text{wt. of sample})}$$

Four determinations of the apparent density of a 27-lb. coating were made with the following results: 1.35, 1.36, 1.345, 1.343 g./ml. The standard error for each determination ranged from 0.75 to 2.14%. The average error was 1.5%. Therefore, for the average of four determinations a precision of 0.75% may be expected; for two determinations, the precision is 1.0%.

To check the accuracy of this method, the density of a sample of glass beads was measured with a water pycnometer and found to be 2.36 g./ml. The density by mercury displacement was 2.37 g./ml. Since the beads were not porous, the two density measurements should agree, as they do. In a second experiment, the apparent density of type VC Millipore Filter (0.1 mu pore radius) was measured by the caliper and weight method and was found to be 0.450 g./ml. The mercury displacement value was 0.449 g./ml. Good agreement between the two values was expected since the Millipore filter had a very smooth surface and was uniform in caliper.

It can be shown by calculation that normal fluctuations in room temperature do not affect the results of this test method to a significant degree. Since the apparatus holds approximately 4.9 ml. of mercury, a temperature variation of one degree Centigrade occasions a weight variation of only 0.012 g. This is one-third of the weight variation acceptable in the method.

In order to calculate the void volume, it is necessary to ascertain the density of the coating. This was done using the buoyancy principle. Various mixtures of bromoform and carbon tetrachloride were

admitted to an evacuated chamber which contained a sample of isolated coating. It was found that the coating floated on a mixture of density 2.38 g./ml. and sank in a mixture of density 2.35 g./ml. This range shows good agreement with the value calculated for a coating having a 12:100 starch:clay ratio containing 2% moisture. The calculated specific gravity was 2.37 g./ml. based on a clay specific gravity of 2.6 g./ml. and a starch specific gravity of 1.5 g./ml. (71).

The void volume of the 100-lb. coating described on page 36 was determined by this mercury displacement method and was found to be 0.230 ml./g. The desorption isotherm for this coating (Figure 7b) may be extrapolated to yield a saturation gas volume of 145 ml. (S.T.P.). This volume of gas corresponds to a void volume of 0.226 ml./g. The agreement between the two values is excellent. This evidence indicates that the nitrogen adsorption method for the determination of pore distribution does include all the pores found in this coating and does yield valid void volume information.

Further work with this mercury displacement method showed that it was sensitive to the surface conditions of coatings to the extent that it had only restricted usefulness as a void volume measurement. Figure 10 compares the void volumes, as determined by nitrogen adsorption and mercury displacement, of coatings which differ only in coat weight. The divergence of the two curves increases as coat weight is decreased as would be expected if the surface aberrations of the coatings were behaving as void volume in the mercury displacement method. It

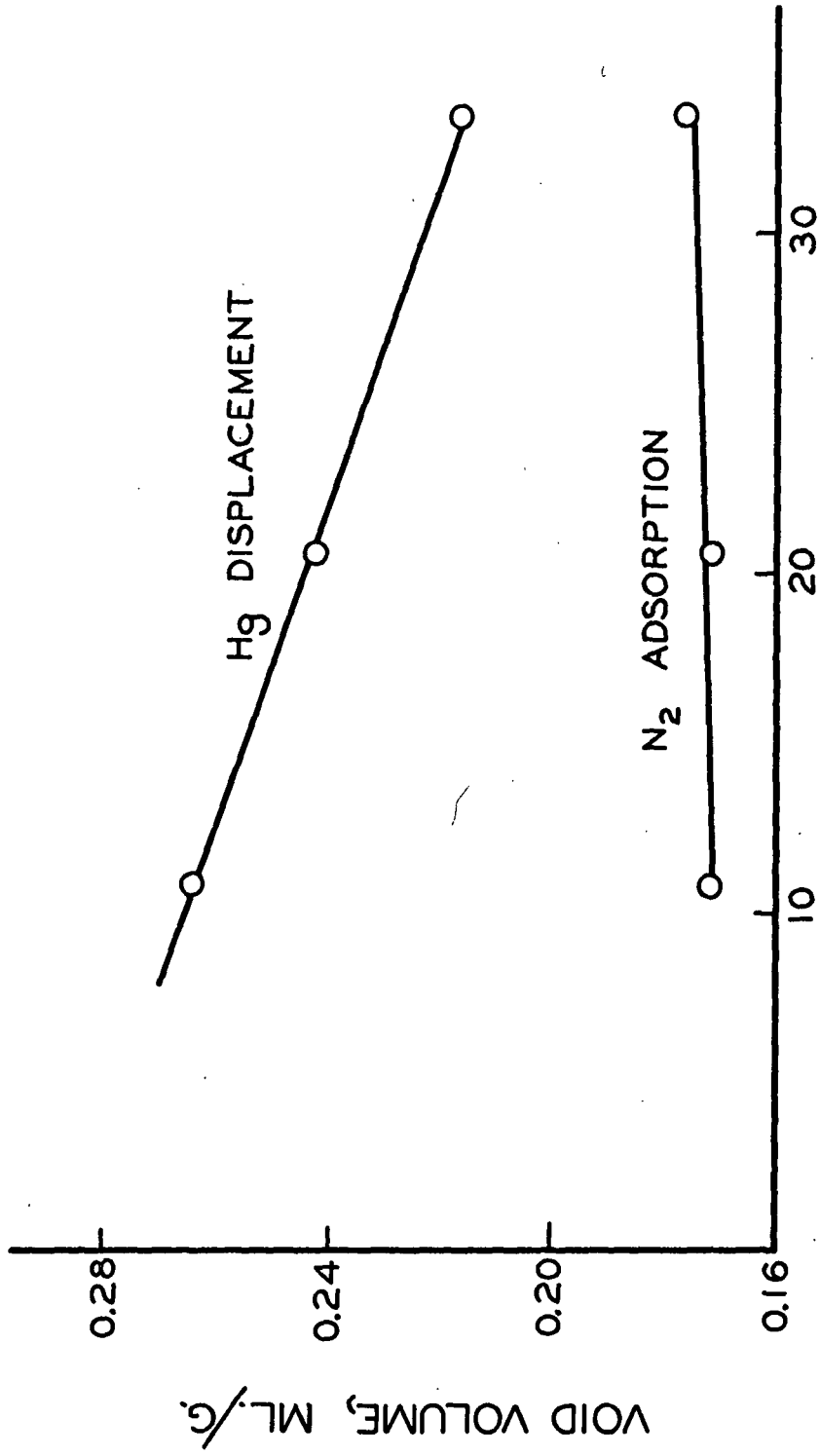

Figure 10. Void Volume Comparison

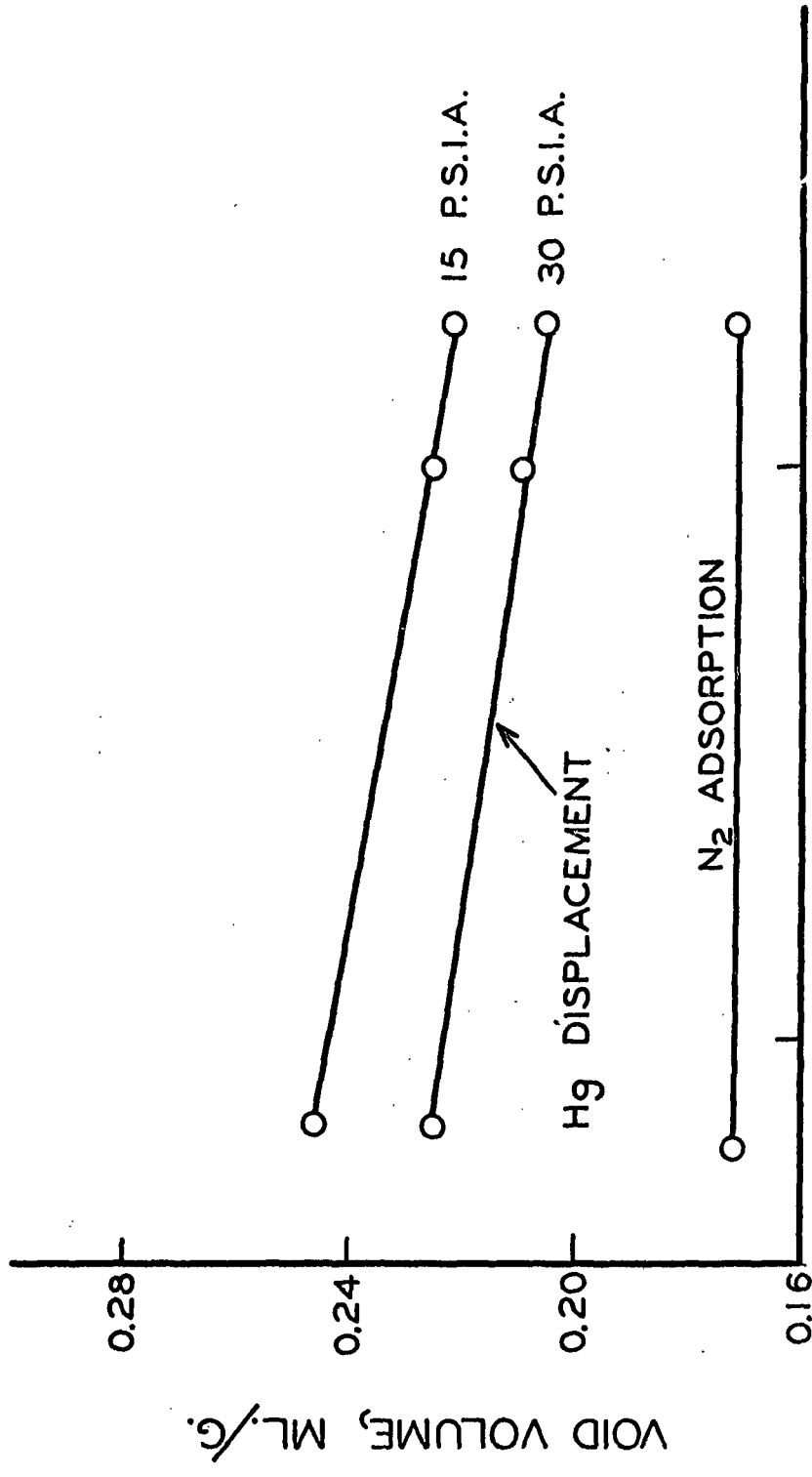

Figure 11. Void Volume Comparison

should be recalled that the two methods showed good agreement on a heavy-weight coating.

As additional evidence of the effect of surface conditions upon mercury displacement void volume, Figure 11 presents a comparison of values obtained by both nitrogen adsorption and mercury displacement on supercalendered coatings. Again, the curves diverge as the smoothness of the coating surface is decreased. In an effort to bring the mercury displacement and the nitrogen adsorption method into closer agreement, a positive pressure (30 p.s.i.a.) was applied to the mercury in the sample cell. (It was necessary to attach springs to the hooks shown in the sketch of the apparatus in Figure 9.) At 30 p.s.i.a., mercury penetrates pores with an effective circular radius as small as 3 mu. The values obtained with this procedure are also plotted in Figure 11. The agreement found is significantly better but it is evident that pressures considerably higher than 30 p.s.i.a. would be required to establish agreement between the two methods.

As a result of this information, further use of the mercury displacement method for the determination of internal void volumes was abandoned in favor of the nitrogen adsorption method. The data plotted in Figures 10 and 11 are recorded in Table XVI, Appendix.

CLAY PARTICLE ORIENTATION

Theory

It was shown in Figures 2, 3, and 4 that the kaolin clays used in

this study have a hexagonal platelet shape. It was also shown that the greatest diameter of these clay particles ranged from 6 to 10 times their thickness. Particles of this general shape should have a tendency to orient with their larger surfaces parallel to the plane of the surface of the body on which they are supported. This can occur with clays in the dry powder form and does occur to a significant degree when the particles are deposited upon a smooth surface from a dilute suspension (72-75). Conceivably this tendency to assume a preferred orientation can be accentuated by shear and friction forces operating in appropriate directions. The extent to which this does occur in coatings possibly influences such coating properties as gloss, strength, and pore size and shape.

The kaolin crystal, Figure 12, is so constructed that the (001) crystal plane is parallel to the large surface of the clay particle (76). This makes the measurement of preferred orientation in films containing these particles basically simple.

Any regularly, minutely spaced planes (or more correctly, atoms) are capable of diffracting an x-ray beam incident upon them at certain angles, much in the manner that light is diffracted.[1] The angle at which diffraction occurs is related to the spacing of the crystal planes through Bragg's law (77).

$$n\lambda = 2d \sin\theta$$

[1] For an excellent review of the production, absorption, and diffraction of x-rays, the reader is referred to "X-Ray Diffraction Procedures" by Klug and Alexander (77).

where

θ = incident angle,

$\underline{d}$ = plane spacing,

λ = x-ray wave length, and

$\underline{n}$ = diffraction order.

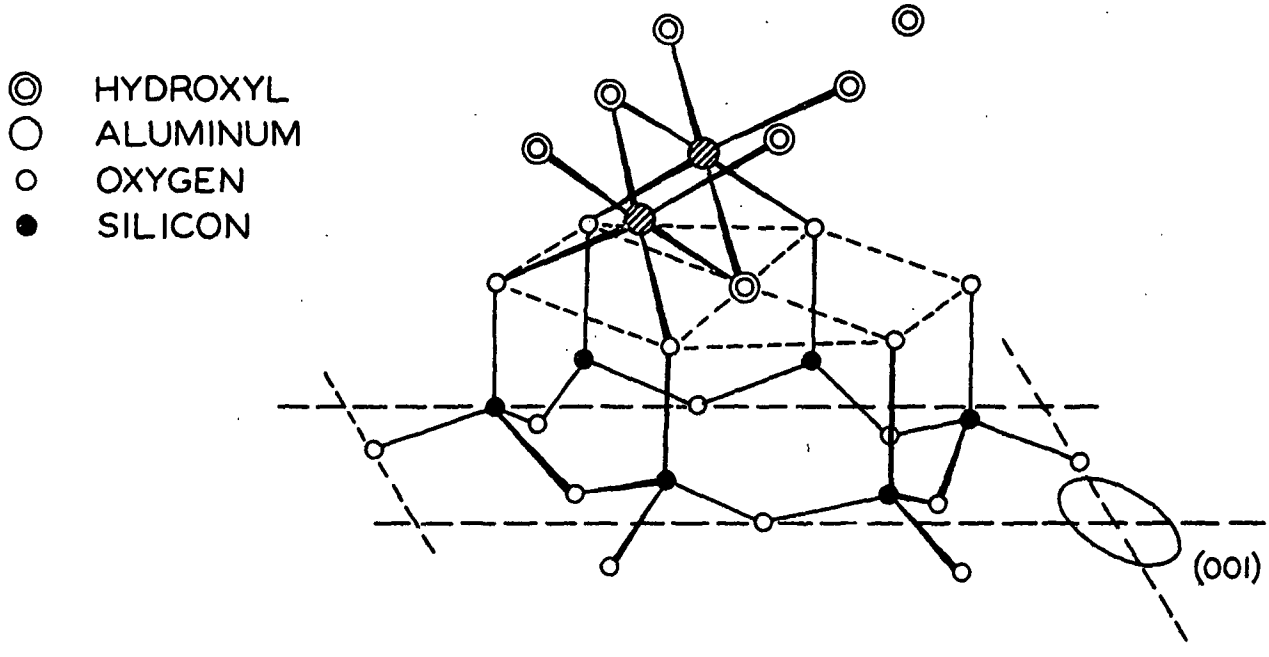

Figure 12. Kaolinite Crystal Structure

The intensity of the diffracted x-ray beam is proportional to the mass of material properly oriented for diffraction (77). The diffracted intensity measured in the Bragg position can be considered a crude measure of crystal plane of orientation provided the incident x-ray intensity, the perfection of crystallinity, the weight of the sample, machine alignment, and the nature of the supporting material can be held constant. Adherence to these restrictions renders this direct method difficult to use for the measurement of preferred orientation.

Another possibility for the measurement of preferred orientation exists. If the x-ray source and the diffracted beam are held in the correct position for diffraction from a given crystal plane and the sample is rotated about an axis perpendicular to the plane of the x-ray beams to an angle α, the diffracted intensity measured under these condition is due to the number of crystal planes oriented at the angle α to the surface of the specimen. Depending upon the geometry of the system, certain corrections for x-ray absorption in the sample are required. This general type of method is internally standardized and, therefore, does not have the disadvantages listed for the direct method in which the diffracted intensity at $\alpha = 0$ is considered a measure of orientation.

Decker, Asp, and Harker (78) have used this principle with a transmission method for the measurement of orientation. Their method requires the construction of rather expensive apparatus and has the added disadvantage of not being suited to the study of crystal planes oriented at small angles to the surface of the specimen. Schulz (79) has developed

a "reflection" method for use with samples that are infinitely thick to x-rays. This method can be adapted for use with thin films but, again, this technique requires rather expensive alteration to the x-ray equipment available. Field and Merchant (80) have developed a reflection method for use with thick films that can be adapted for use with thin films. This method has the advantage of not requiring construction of special attachments for the x-ray equipment. For this reason, the Field and Merchant method has been modified for use with thin films of pigment coatings.

The photograph in Figure 13 shows the arrangement of the x-ray tube (A), the divergence slit (B), the specimen holder (C), the receiving slit (D), the scatter slit (E), and the Geiger tube (F) of the Norelco X-Ray Diffractometer. In the Field and Merchant method, a thick sample is positioned in the diffractometer and the x-ray intensity diffracted from a convenient crystal plane is measured. Then, the incident x-ray beam and the diffracted beam are held at the value of θ corresponding to this crystal plane and the sample is tilted away from its original position by an angle α. The intensity diffracted from the sample in this new position is recorded. This intensity arises from diffraction from crystals oriented at the angle α to the surface of the sample. Now, since the diffracted intensity is proportional to the number of crystal planes in position for diffraction, these measurements are related to the number of crystal planes oriented at the angle α and those oriented in the plane of the sample surface.

However, as the sample is tilted away from the normal position,

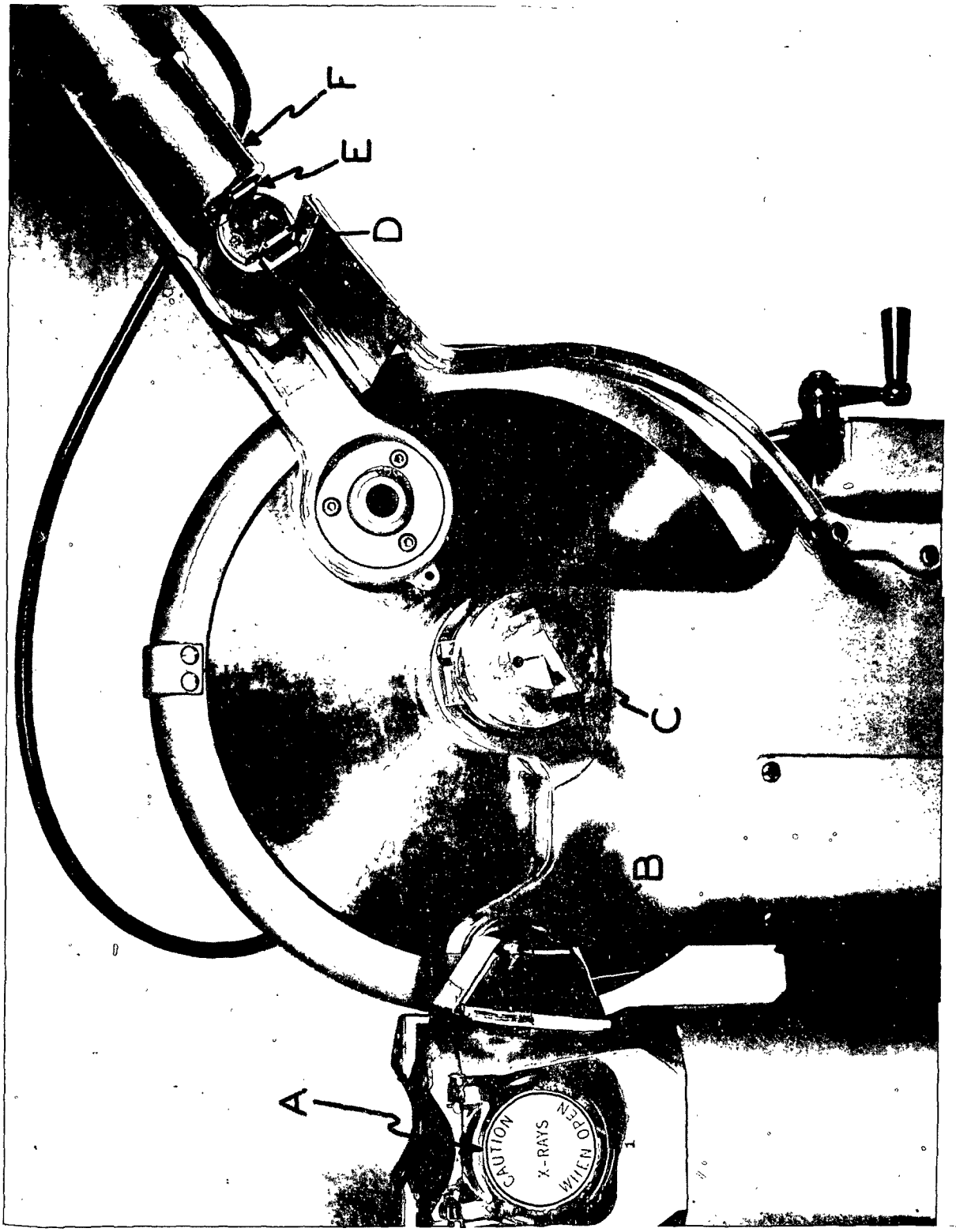

Figure 13. Norelco X-ray Diffractometer

the path length of the x-rays in the specimen changes as seen in Figure 14. It is necessary to correct for differences in absorption of the diffracted beam caused by these changes in path length before the measured intensities at various values of α can be compared with one another and with the value obtained at $\alpha = 0$.

Considering the samples shown in Figure 14 to be infinitely thick to x-rays, Field and Merchant have presented the following derivation of the required absorption correction factor.

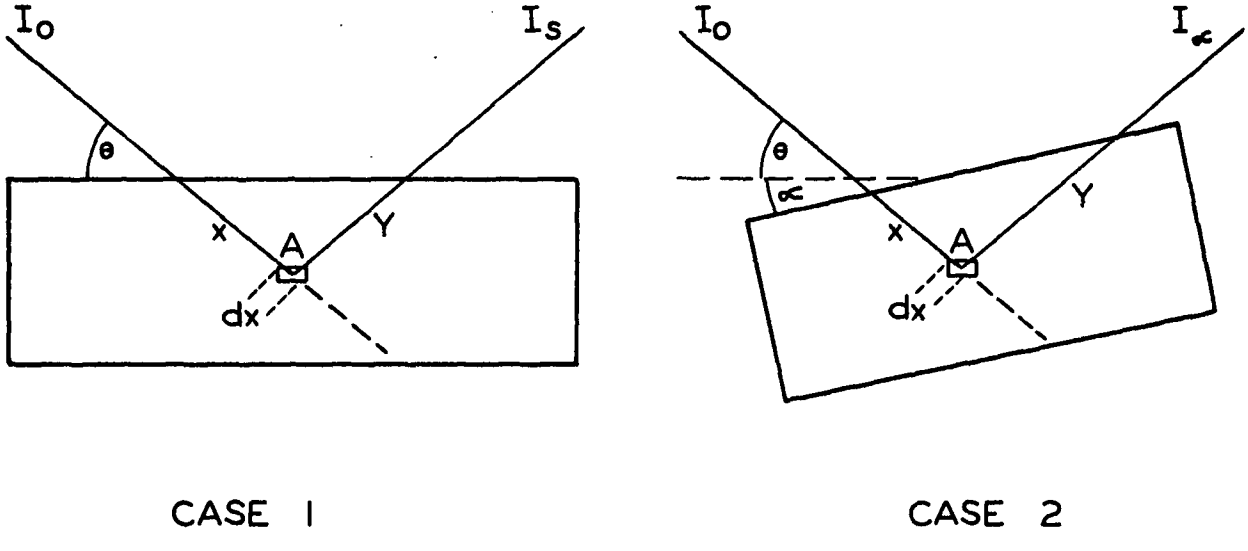

Figure 14. X-ray Path in Infinitely Thick Samples

$\underline{I_o}$ = incident x-ray intensity

$\underline{x}$ = the distance along the incident x-ray path from the surface to an increment of thickness ($\underline{dx}$) at point $\underline{A}$

$\underline{I_a}$ = the x-ray intensity at point $\underline{A}$

$\underline{dx}$ = an increment of thickness along path $\underline{x}$

$\underline{D}$ = the fraction of x-rays scattered per unit thickness of the sample

$\underline{y}$ = the path length of the diffracted beam in the sample

$\underline{I_s}$ = the intensity of the diffracted beam leaving the specimen in the normal (or $\alpha = 0$) position

$\underline{I_\alpha}$ = the intensity of the diffracted beam leaving the sample in the general case

μ = the linear absorption coefficient of the specimen

e = the base of natural logarithms

θ = a convenient Bragg angle for the specimen

Working with the general situation, case II, Figure 14, the x-ray intensity reaching point $\underline{A}$ is

$$\underline{I_a} = \underline{I_o}\, e^{-\mu \underline{x}} \qquad (1)$$

The incident beam, in passing through the increment of thickness ($\underline{dx}$) along the path $\underline{x}$ at point $\underline{A}$, contributes a minute fraction ($\underline{D}$) of its energy to the diffracted beam.

$$\text{At point } \underline{A},\ \underline{dI_\alpha} = \underline{I_a D dx} = \underline{I_o}\, e^{-\mu \underline{x}}\, \underline{D}\, \underline{dx} \qquad (2)$$

This portion of the beam which is diffracted at point $\underline{A}$ loses some of its energy in traversing the path $\underline{y}$ from point $\underline{A}$ to the surface of the specimen.

$$\underline{dI_\alpha} \text{ (at surface)} = (\underline{I_o}\, e^{-\mu \underline{x}}\, \underline{D}\, \underline{dx})\, e^{-\mu \underline{y}} \qquad (3)$$

This equation may be simplified by recognizing that $\underline{x}$ and $\underline{y}$ are related through θ and α.

$$\underline{y} = \underline{x} \sin (\theta + \alpha)/\sin (\theta - \alpha)$$

so that $\underline{y} = \underline{xM}$, where $\underline{M} = \sin (\theta + \alpha)/\sin (\theta - \alpha)$. Then,

$$\underline{dI_\alpha} \text{ (at surface)} = \underline{I_o}\, \underline{D} e^{-\mu \underline{x}}\, e^{-\mu \underline{xM}}\, \underline{dx} \qquad (4)$$

Now, if it is assumed that $\underline{dx}$ is essentially zero in thickness, it is possible to collect terms and integrate Equation (4). Since the specimen is infinitely thick to x-rays, the integration is from $\underline{x} = 0$ to $\underline{x} = \infty$.

$$\underline{I_\alpha} \text{ (at surface)} = \underline{I_o}\, \underline{D} \int_0^\infty e^{-(1 + \underline{M})\mu \underline{x}}\, \underline{dx} \qquad (5)$$

and

$$\underline{I_\alpha} = \underline{I_o D}/\mu(1 + \underline{M}). \qquad (6)$$

At $\alpha = 0$ (case I), $\underline{M} = 1$, so that

$$\underline{I_{\alpha = 0}} = \underline{I_s} = \underline{I_o D}/2\mu. \qquad (7)$$

From Equations (6) and (7), the following ratio may be formed:

$$\frac{\underline{I_\alpha}}{\underline{I_s}} = \frac{2}{(1 + \underline{M})}. \qquad (8)$$

Equation (8) represents the ratio of intensities that may be expected in this method due to absorption differences alone; that is, the ratio

of the diffracted intensity at $\alpha = \alpha$ to the diffracted intensity at $\alpha = 0$ if the sample is perfectly randomly oriented. The measured intensities at finite values of α for a partially oriented sample are divided by the factor $2/(1 + \underline{M})$. This yields an intensity value which has been corrected for absorption differences and is directly comparable to diffracted intensities measured at $\alpha = 0$.

This absorption correction factor was derived for use with specimens which are infinitely thick to x-rays. Paper coating films, except in rare instances, are not sufficiently thick (approximately 300-lb./ream for $\theta = 18.8°$) to fulfill this requirement. It was necessary, therefore, to modify this correction factor to accommodate thin films such as those normally used in paper coatings. Schulz (79) recognized that such a modification is proper but did not carry through experimental verification of the equation derived. Field and Merchant did not derive the thin film expression since their method was designed originally for work with metal sheets which are opaque to x-rays.

The derivation of the thin film absorption correction factor differs from the Field and Merchant derivation in two respects. First, it is necessary to integrate Equation (5) from $\underline{x} = 0$ to $\underline{x} = \underline{x}$.

$$\underline{I}_\alpha \text{ (at surface)} = \underline{I}_o \, \underline{D} \int_0^{\underline{x}} e^{-(1 + \underline{M})\mu \underline{x}} \, \underline{dx} \qquad (9)$$

and

$$\underline{I}_\alpha = \frac{\underline{I}_o \, \underline{D}}{\mu(1 + \underline{M})} \left[1 - e^{-(1 + \underline{M})\mu \underline{x}}\right] \qquad (10)$$

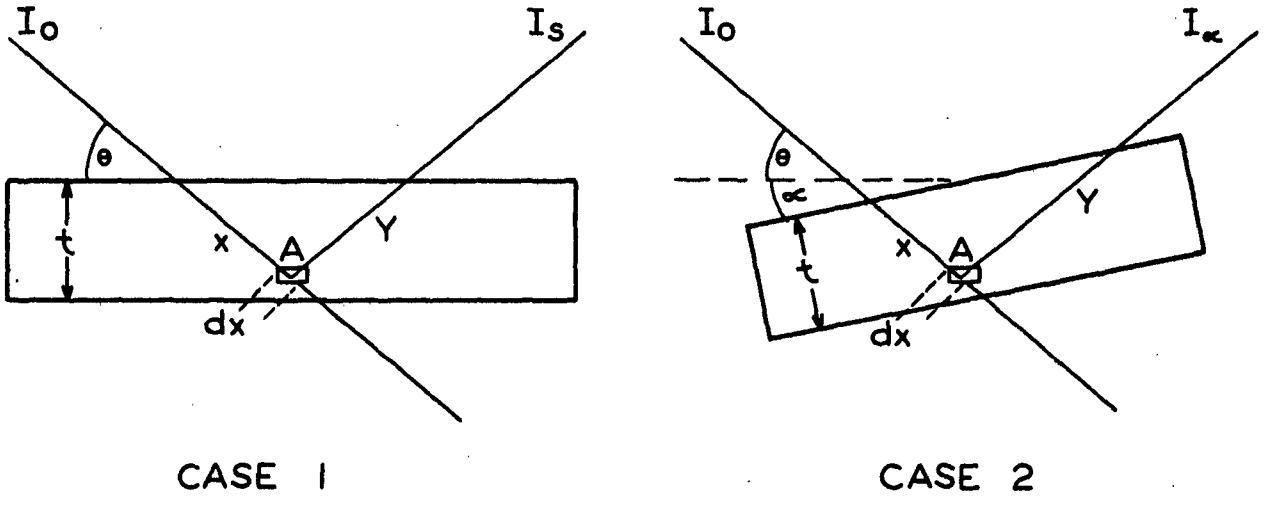

Figure 15. X-ray Path in Thin Samples

The second difference between the thin and thick film equations arises from the fact that in the case of a thick film, the incident x-ray beam path length is constant regardless of the value of α. For thin films, however, the incident x-ray path length decreases as α is increased (Figure 15). The value of the path length (x) varies as indicated in the following equation

$$x = t/\sin(\theta + \alpha) \qquad (11)$$

Where (t) is the thickness of the sample in centimeters.

Then Equation (10) may be written

$$\underline{I}_{\alpha} = \frac{I_o D}{(1 + \underline{M})\mu}\left[1 - e^{-(1 + \underline{M})\mu\, \underline{t}/\sin(\theta + \alpha)}\right] \quad (10a)$$

Again, at $\alpha = 0$, $\underline{M} = 1$ and $\sin(\theta + \alpha) = \sin\theta$, so that

$$\underline{I}_{\alpha = 0} = \underline{I}_s = \frac{I_o D}{2\mu}\left[1 - e^{-2\mu \underline{t}/\sin\theta}\right] \quad (12)$$

and

$$\frac{\underline{I}_{\alpha}}{\underline{I}_s} = \frac{2}{1 + \underline{M}}\left[\frac{1 - e^{-(1 + \underline{M})\mu\, \underline{t}/\sin(\theta + \alpha)}}{1 - e^{-2\mu\, \underline{t}/\sin\theta}}\right] \quad (13)$$

Equation (13) is used in exactly the same way as Equation (8) of the Field and Merchant method. It should be noted that as ($\underline{t}$) becomes large, Equation (13) reduces to Equation (8).

It is obvious from consideration of Figures 14 and 15 that this method for the evaluation of preferred orientation is limited to values of α less than θ. At the tilting angle $\alpha = \theta$, the sample cuts off the diffracted x-ray beam entirely. In the case of kaolin clay coatings this limitation of tilting angle has no serious consequences.

The Measurement Of Preferred Orientation

Specimen Holder

Figure 16 shows the specimen holder that is used in this method. The holder was cut from brass; the dimensions are easily adjusted to fit individual machines. The top surface of the specimen holder was machined flat so that the diffractometer geometry is not disturbed.

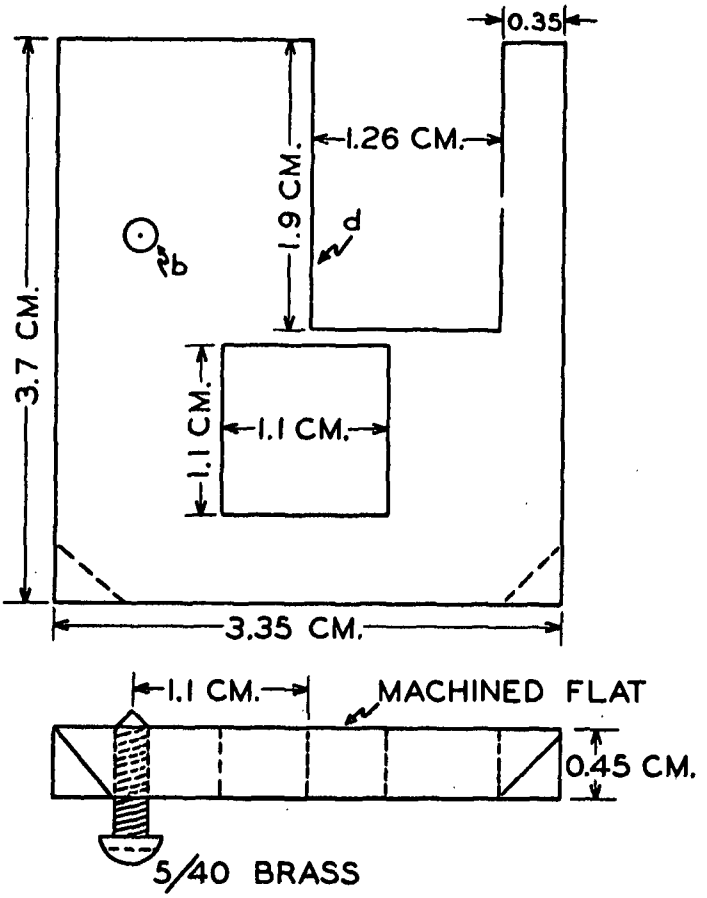

Figure 16. Specimen Holder

Specimen Mounting

The first sample of isolated coating to be mounted on the specimen holder was cut to 1.3 x 1.5 cm. This sample was laid, "top" surface down, on a flat, smooth surface. A thin film of Duco cement was spread around the opening of the specimen holder which was then

pressed down on the coating sample. The piece of coating should be centered over the opening of the specimen holder. If any bows or wrinkles were visible in the mounted coating, the specimen was discarded. Additional pieces of coating were cut to the size of the opening of the specimen holder and placed against the first coating from the under side. Small drops of Duco cement applied to the corners of the opening served to hold these additional samples in position. The cement was most easily applied with a hypodermic syringe.

In the preliminary evaluation of this method, it was determined that differences in the mounting of the coating samples, with respect to the drawdown direction, had no effect upon the orientation data obtained. This point should receive considerable attention in future studies with this method if coatings are prepared by a method which involves large rates of shear.

Position in the Diffractometer

The specimen holder was placed in the Norelco goniometer sample clamp as shown in Figure 13. The screw (b), in Figure 16, was turned down so that the top surface of the specimen holder was flush with the bottom surface of the sample clamp. The inner edge (d) of the cut-out portion of the specimen holder was aligned with the reference mark on the goniometer sample clamp. It was important that this alignment be made carefully since misalignment resulted in serious defocusing effects at finite values of α (81).

Measurement of the Angle

The goniometer was set manually to the value of θ required and the difference in elevation of the two corners of the specimen holder was measured with a cathetometer. Since the width of the specimen holder was known, the angle at which the holder was set may be calculated. To set the specimen holder at some value of α, the screw (b) was turned up slightly. The elevations of the corners of the specimen holder were measured and the new angle was calculated. The difference between this angle and the angle first measured was, of course, α.

The Measurement of Diffracted Intensity

After the specimen was positioned, the goniometer was set to an angle several degrees lower than the Bragg angle selected for examination. The strip chart on the Brown Recorder unit was synchronized with the goniometer and both units were started. The goniometer was allowed to traverse the diffraction peak area twice, both times including a sufficient angular range so that the background radiation may be traced. An example of a strip chart obtained in this manner is shown in Figure 17.

The dotted lines across the bottom of the peaks in Figure 17 represent the operator's estimate of the contribution of background radiation to the peak area. The peak area was determined by counting squares and, by use of machine constants, was converted to total counts received by the Geiger tube. Ideally, the diffracted intensity is best

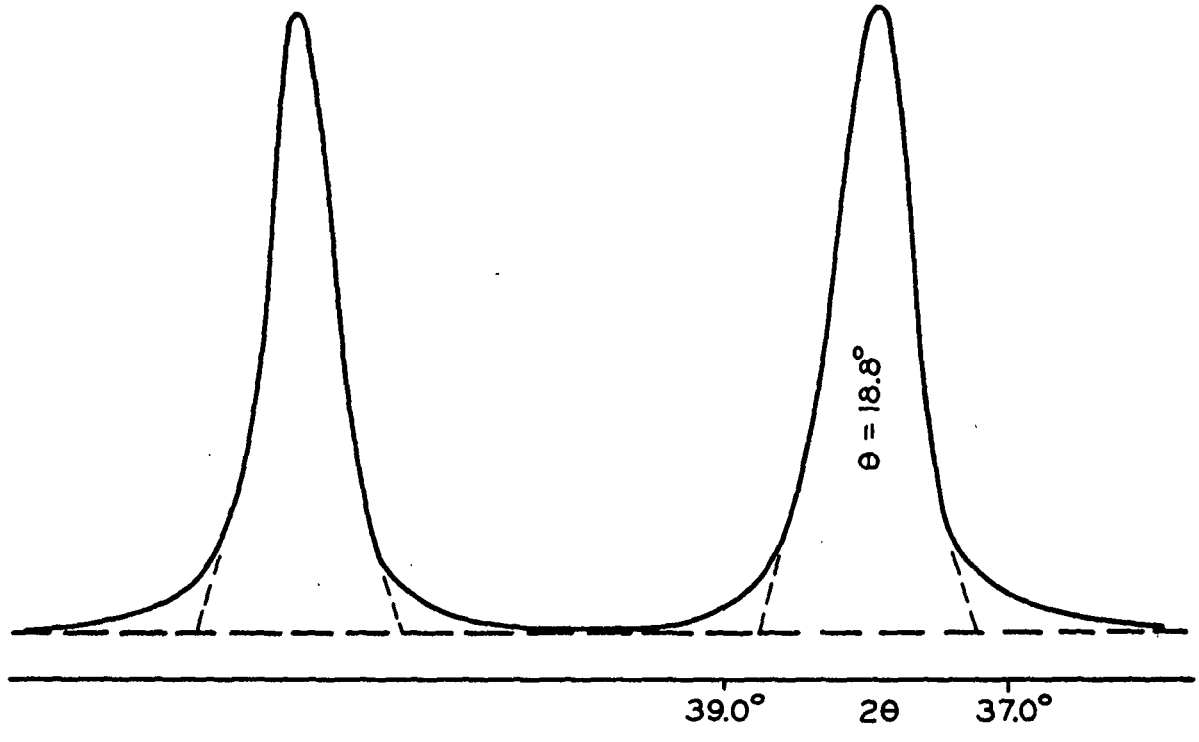

Figure 17. X-ray Diffraction Strip Chart

represented by the height of the diffraction peak above the background. However, due to machine variables, the peak area yields a more reliable value (82).

Data Presentation

From the raw datum (i.e., the area under the diffraction peaks, the sample weight per unit area, and the angles θ and α) the corrected diffraction intensities were calculated using Equation (8) or (13) depending on sample thickness. The linear absorption coefficient (μ) for

x-rays was obtained from tables of mass absorption coefficients (μ/ρ) of the elements (77). The approximate chemical composition of the coatings was necessary. The data in Table III shows the contribution of the various components of a typical coating film to the total absorption coefficient. The calculation was made for Cu-K_α radiation which was used throughout this work. The wavelength of this radiation is 1.542 A.

TABLE III

LINEAR ABSORPTION COEFFICIENT CALCULATION
KAOLIN CLAY COATING; 12 PARTS STARCH

Components	μ/ρ [Cu-K]	ρ	Wt. %	Fractional μ/ρ
$Al_4(Si_4O_{10})(OH)_8$	30.37	2.6	87.5	26.6
$C_6H_{10}O_5$	8.71	1.5	10.7	0.9
H_2O	11.3	1.0	2.0	0.2
				27.7

$\mu/\rho = 27.7$; and $\rho = 2.37$

since $[\mu/\rho]\rho = \mu$; $\mu = 65.5$

The linear absorption coefficient for all computations in this work was assumed to be 65.5. Some error can be expected due to variations in chemical composition of the clays and minor variations in coating composition. Measurements of (μ) for various coatings were made by inserting coating samples between the scatter slit and the Geiger tube. A collimated, low intensity x-ray beam was employed. From a knowledge of the weight of the coating per unit area and the decrease in intensity of the x-ray beam entering the Geiger tube, it was possible to calculate (μ) from the following equation:

$$\underline{I} = \underline{I}_o \, e^{-\mu \underline{x}}$$

where

$\underline{x}$ = sample thickness in centimeters,

$\underline{I}_o$ = x-ray intensity without the coating in place,

$\underline{I}$ = x-ray intensity with coating sample in place, and

e = the base of natural logarithms.

The measured values of (μ) ranged from 63.8 to 71.6 with most values grouped around 65-67. The experimental data are recorded in Table XV, Appendix. These measured values are subject to experimental error, particularly in the measurement of ($\underline{x}$). The results do show that the measured values of (μ) agree well with the calculated value.

After the measured intensities have been corrected for absorption losses, the corrected intensity at various values of α was divided by the standard intensity measured at $\alpha = 0$. This yields a Relative Intensity, a figure which represents the ratio of the number of crystal planes oriented at various values of α to the number oriented in the plane of the coating surface. For graphic presentation, the values of Relative Intensity are plotted against α as shown in Figure 18. Generally, the orientation values reported in this study represent the slope of the best straight line drawn through data points from three composite samples.

It is to be expected that these "orientation profiles" should have the form of a distribution curve. That is, the straight line presented

in Figure 18 probably represents the greatest slope of a curve which approaches the ordinate abruptly and the abscissa asymptotically. Accuracy limitations preclude work at values of α less than one degree and the diffracted radiation beyond $\alpha = 15°$ is too low for satisfactory work in this range so that definition of an actual distribution curve is impractical under present conditions.

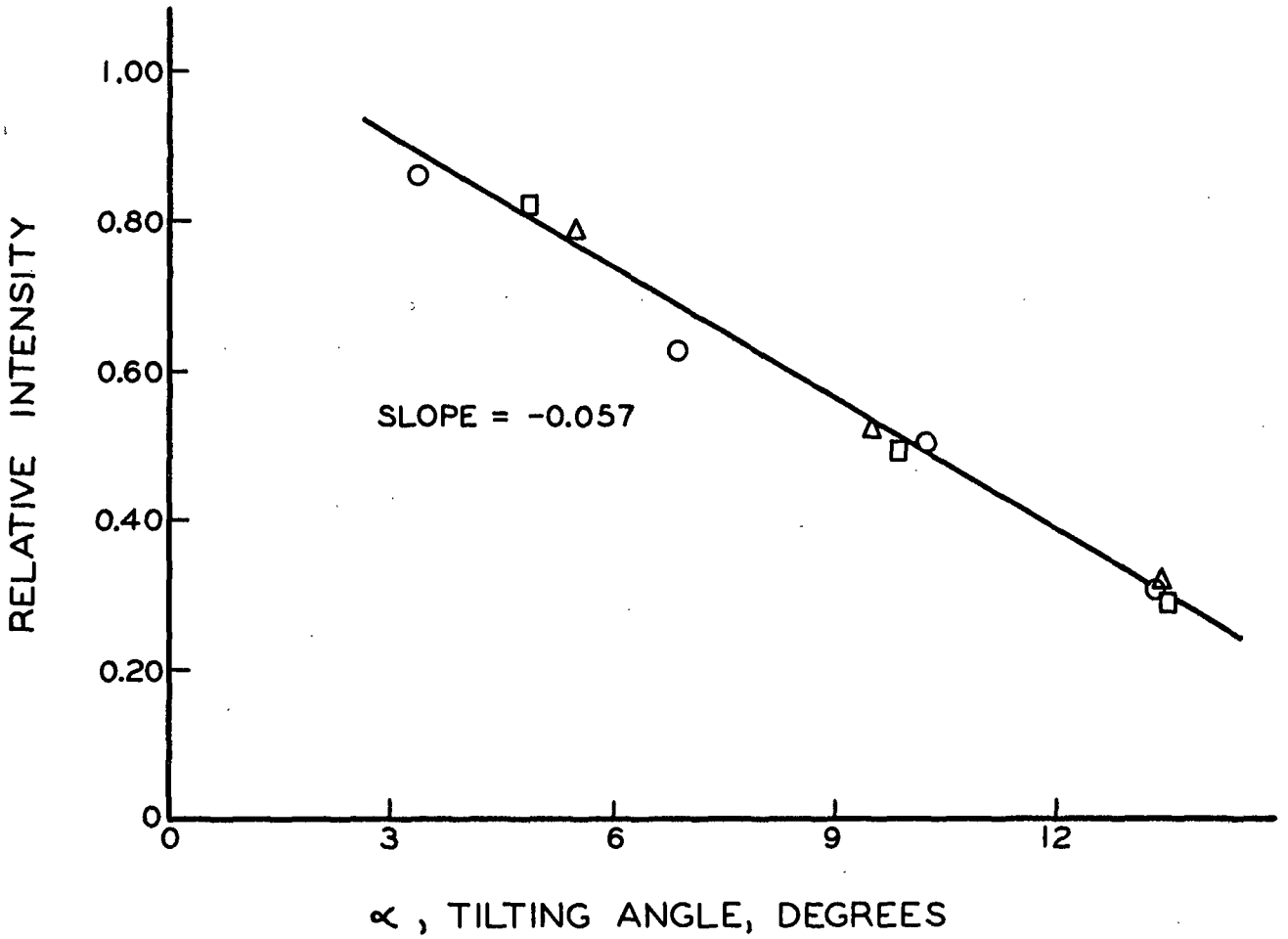

Figure 18. Graphic Presentation of Orientation Data

Equation Validity

Equation (13) may be proven valid as a correction factor for x-ray absorption in thin films simply by the examination of a randomly oriented thin film. Some difficulty was encountered in the preparation of such a film. Several attempts were made to form a thin film of ground NaCl suspended in collodion. In all cases, visibly nonuniform films were obtained. Annealed aluminum foil was also used but was found to wrinkle when slightly heated by the x-ray beam. Attempts to deposit a thin film of MgO upon a very thin collodion film were also unsuccessful.

Decker, Asp, and Harker (78) used exposed x-ray film to prove the validity of the absorption correction factor for a "transmission" orientation method. These workers found that the silver halide crystals in such film were randomly oriented. The possible effects of the supporting material (usually cellulose acetate) were neglected.

In the present work, the gelatin emulsions, containing the silver halide crystals, were stripped from two exposed photographic films and examined by the method described. The emulsion portion of the exposed films was freed from the cellulose acetate support by soaking the films in chloroform for six hours. The photographic films used were Cronar ortho A litho (Du Pont) and Royal Pan (Eastman Kodak).

The absorption coefficient (μ) appears in Equation (13) only as the product μt, where (t) is the thickness of the material to be examined. The value of μt for each film was measured by inserting pieces of the

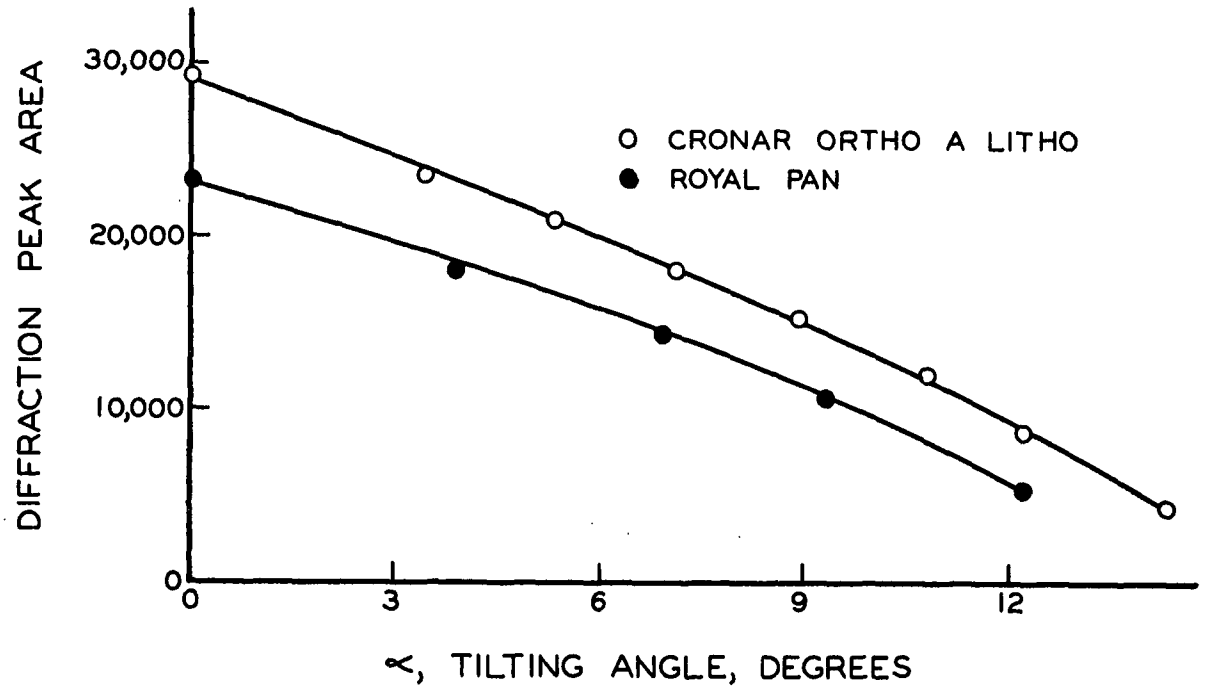

Figure 19. X-ray Diffraction From Photographic Emulsions

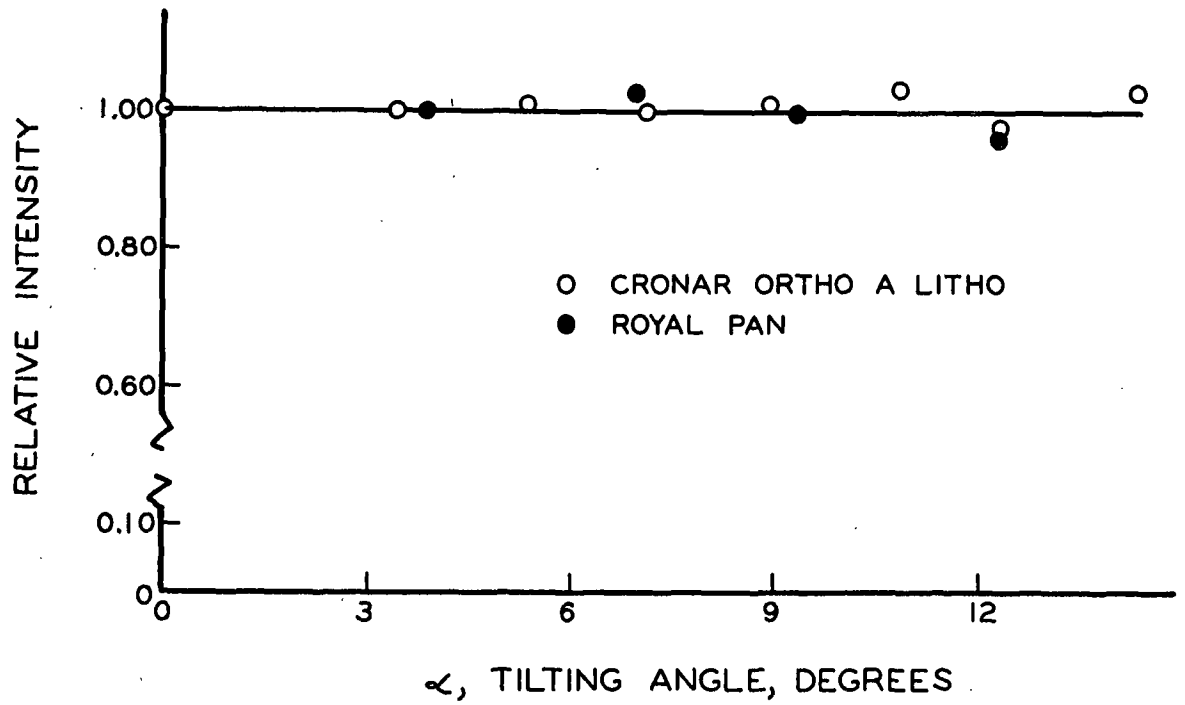

Figure 20. Orientation Profiles for Photographic Emulsions

emulsion layer into a collimated x-ray beam and recording the decrease in intensity received by the Geiger tube. The value of μt was then obtained from the following equation:

$$I = I_o e^{-\mu t}$$

The emulsion films were then mounted on the specimen holders and examined for particle orientation. The slit system of the diffractometer was modified to avoid defocusing errors (see pages 81 to 88). Absorption losses were corrected by Equation (13). The measured intensities for both films are plotted in Figure 19. The orientation profiles are shown in Figure 20. The data are recorded in Table XVII, Appendix.

The experimental points in Figure 20 form a straight line of zero slope, an orientation profile which is characteristic of a randomly oriented film. The points for both films fell on the same line even though the μt values for these films were quite different. On the basis of these two experiments, it may be concluded that Equation (13) is valid.

Reproducibility

Machine, Angle, and Data Calculation Variables

Figure 21 shows the extent to which variables inherent in the Norelco X-Ray Diffractometer, the variables in angle measurement, and the variables in the measurement and correction of intensity affect the reproducibility of this method for the evaluation of orientation in thin films. A 22.6-lb. coating was mounted on the specimen holder and placed

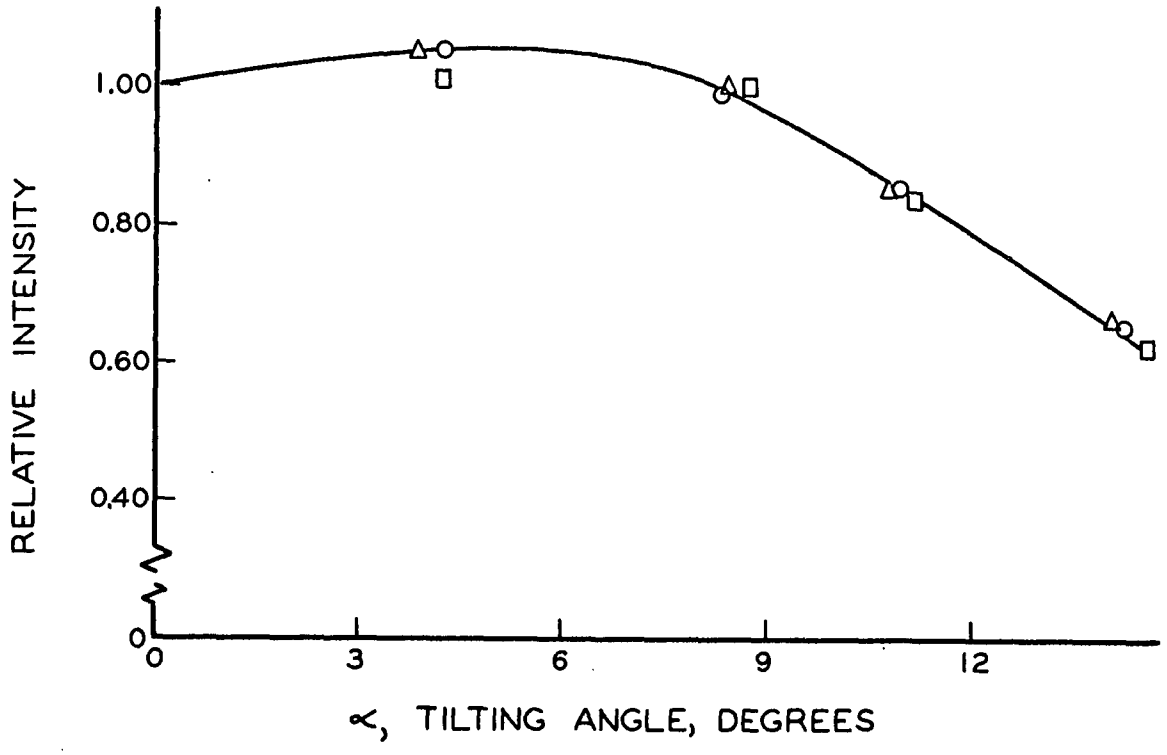

Figure 21. Orientation Measurement
Machine and Angle Measuring Variables

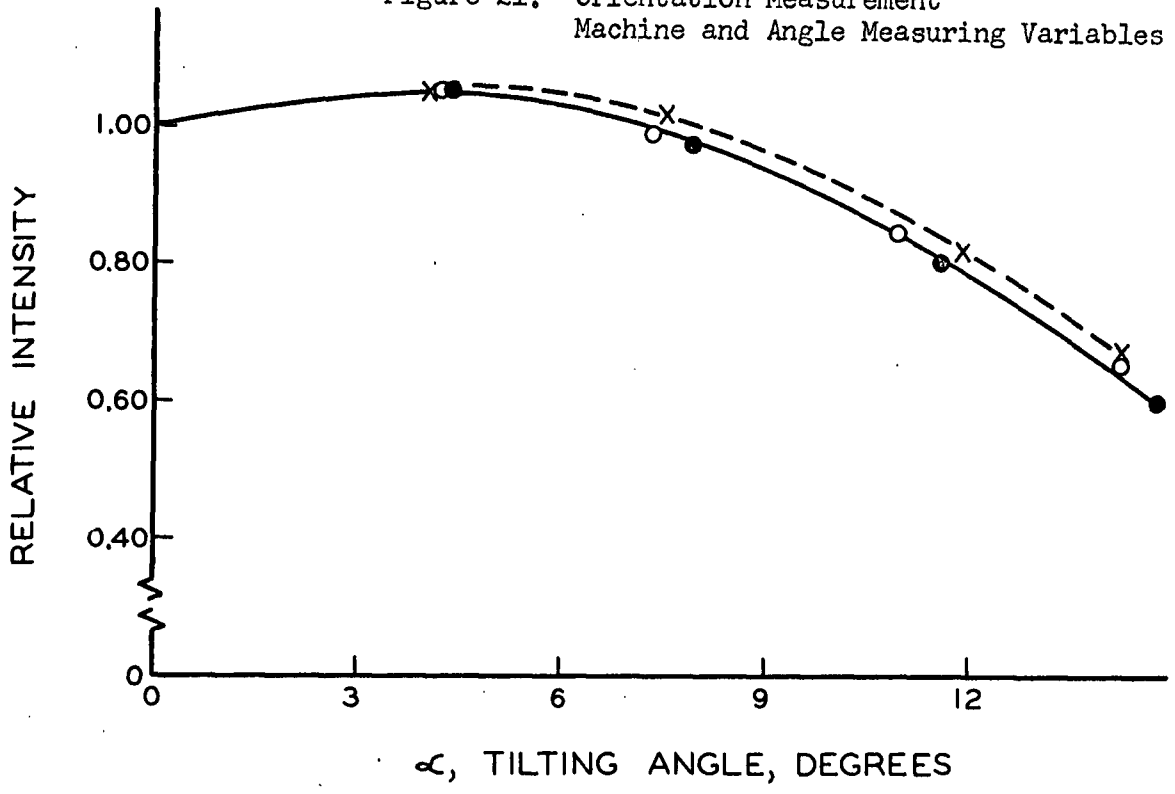

Figure 22. Orientation Measurement
Sample Mounting Reproducibility

in the diffractometer. A set of duplicate measurements was obtained over the range of α from 0 to 15°. Without removing the specimen from the diffractometer, the angle α was set back to zero and the measurements were repeated. This was done a third time. With the exception of one point, all the measurements fall on the same curve. One may conclude that these variables do not have a significant effect upon reproducibility. The pertinent data are recorded in Table XIII, Appendix.

Mounting and Specimen Positioning Variables

Upon completion of the above, the coating was removed from the specimen holder by dissolving the cement in ethyl acetate. The sample was remounted on the holder, positioned in the diffractometer and another set of measurements was made. This was done once more to obtain three independent mounting, positioning, and measuring variability estimates on the same sample. The results are shown in Figure 22 and are recorded in Table XIX, Appendix. This experiment demonstrates that the variability introduced into the test by mounting and positioning variables is slight. The slight lateral displacement of one of the curves is probably due to a slight wrinkle or curvature in the sample surface or to a misalignment of the specimen holder in the diffractometer (81).

Sample Variability

In the later stages of the development of this method, it became evident that the chief difficulty in obtaining reproducibity was the result of a wide range of particle orientations existing within a given coating sample. Figure 23 shows four orientation profiles obtained

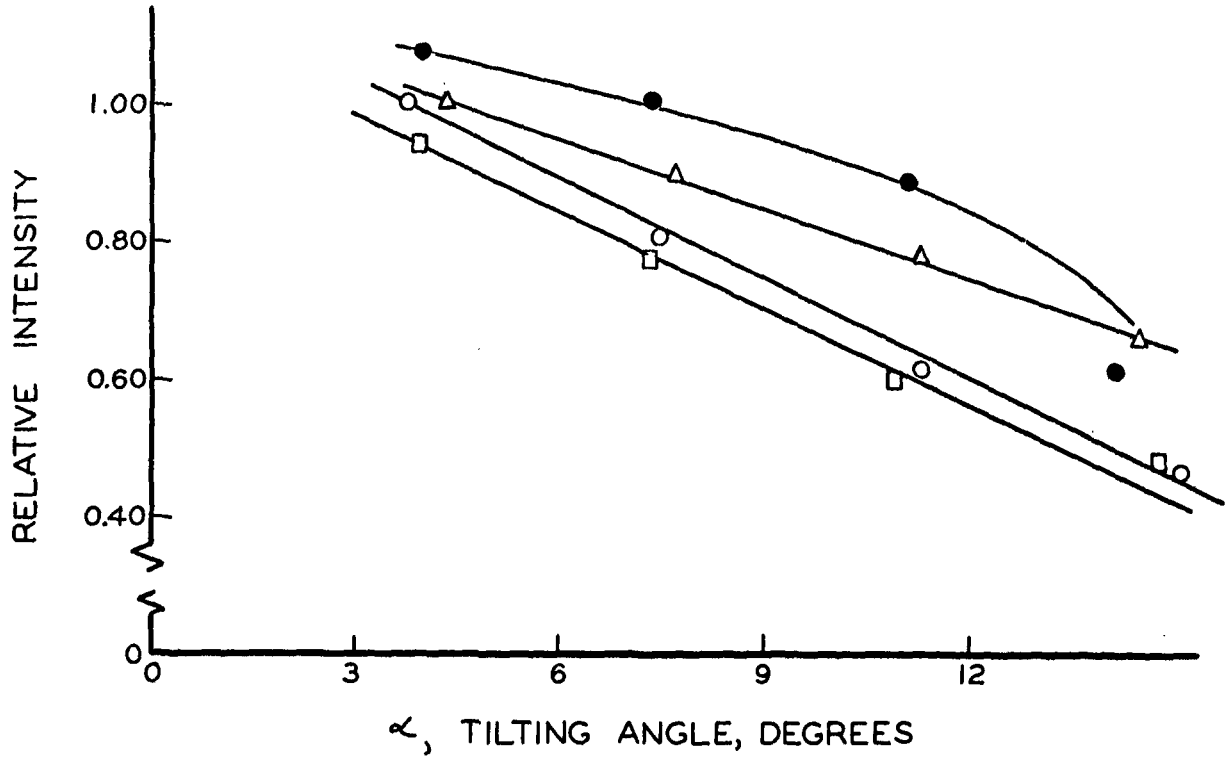

Figure 23. Orientation Measurement Sample Variability

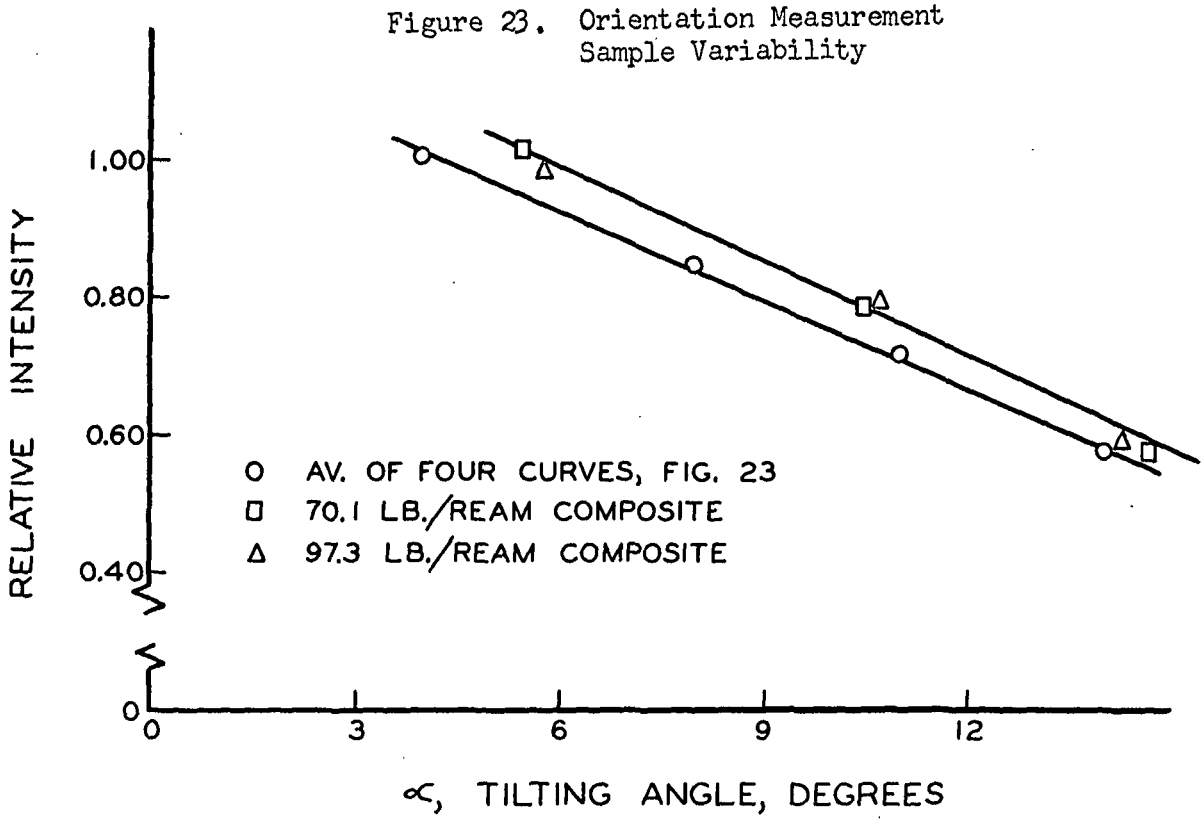

Figure 24. Orientation Measurement Composite Samples

from four single samples of a 27-lb. coating. The time required to obtain these profiles was 10 hours. It is obvious that the time required to obtain a valid average profile would be excessive. To avoid this difficulty, a composite sample was used. In this method, up to seven pieces of coating are examined at the same time (page 69). The effect is to produce an average profile which is weighted in favor of the coating samples near the top of the stack.

Figure 24 presents the average of the four profile curves shown in Figure 23 and the two profiles obtained by the composite method. The agreement between the curves is satisfactory. The experimental data are recorded in Table XX, Appendix.

General Discussion

The majority of the orientation work in this study was performed with a symmetrical slit system in the x-ray diffractometer. In a symmetrical slit system, the divergent and scattering slits (see Figure 13) have the same angular value. A receiving slit was also used and was placed at the theoretical focal point of the diffracted beam. The use of such a system markedly increases the resolving power of the diffractometer (81).

During the course of the analysis of orientation in photographic film, it developed that the results obtained with a symmetrical slit system differed from the results obtained when the receiving and scattering slits were removed from the diffractometer. Orientation profiles obtained with Cronar ortho A litho film using 3 different slit systems in the diffractometer are presented in Figure 25. In the case of the examination made

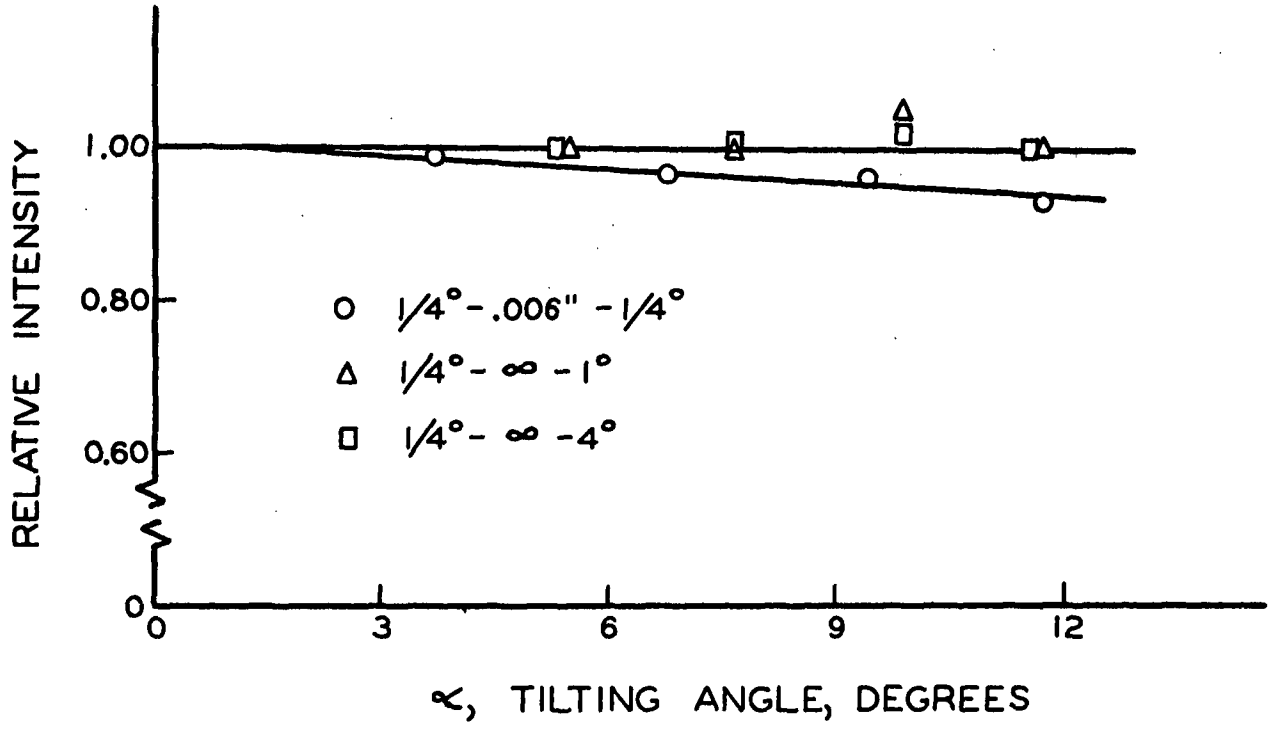

Figure 25. The Effect of the Diffractometer Slit System On Orientation Measurements

using the symmetrical slit system, the profile has a definite slope. Where the receiving slit was removed and the scattering slit enlarged, the data points fell about a straight line of zero slope.[1] The experimental data are recorded in Table XXX, Appendix.

It can be shown that the difference in the orientation profiles noted in Figure 25 arises from defocusing of the diffracted x-ray beam when the sample is tilted as it is in this method. Chernock and Beck (81) have presented a discussion, similar to the one which follows, of errors in the Schulz (79) method for the determination of preferred orientation in thick samples. Their analysis was for a system totally different from the method used in the present study but some of the comments apply.

It is apparent from Figure 26 that the area of the sample covered by the incident x-ray beam is dependent upon the divergent slit (b) width. In true parafocusing (56), the specimen is curved so that all portions of the incident beam strike the specimen at the same angle. When a flat specimen is employed, as in the present case, only the center of the x-ray beam strikes the specimen surface at the indicated angle. The edges of the beam strike the sample at some slightly divergent angle;

[1] The data presented in Figure 25 were obtained by use of the entire photographic film rather than the emulsion layer alone. The fact that the profiles obtained show random orientation indicates that the silver halide particles behave as though they were uniformly distributed throughout the entire film, including the cellulose acetate support. Although this interesting situation was not further investigated, it is felt that this can only occur in systems where the value of μt for the layer of interest and the value of μt for all layers are quite close.

the difference between these angles and the center angle being greater as the divergent slit width is increased.

If the center of the incident x-ray beam is at the correct angle to diffract from a given crystal plane, the edge portions of the beam cannot be. These edge beams can, however, diffract from crystal planes which are tilted away from the plane of the specimen surface. This results in a slightly unfocused diffracted x-ray beam. Depending upon the width of the divergent (b), receiving (c), and scatter (e) slits (Figure 26), a certain amount of this divergent radiation is received by the Geiger counter. The result is an increase in measured intensity over that which is received from those planes which are oriented exactly in the plane of the specimen surface. In other words, the diffracted intensity measured at $\alpha = 0$ is that received from crystal planes oriented at $\alpha = 0 \pm 0.125°$ (for a 1/4° divergent slit) less a portion of radiation which may be blocked by the receiving and scatter slits.

In the case where the sample is tilted to an angle α to its normal position, the situation described continues to exist and further defocusing of the diffracted x-ray beam is caused by the movement of the irradiated edges of the specimen farther from the focusing circle of the goniometer (see Figure 27). If the same slit system is used throughout an analysis, the measured intensity at finite values of α, due to this additional defocusing, is considerably lower than it should be.

From Figures 26 and 27, it may be reasoned that the distortion of the experimental data due to these focusing difficulties is a function

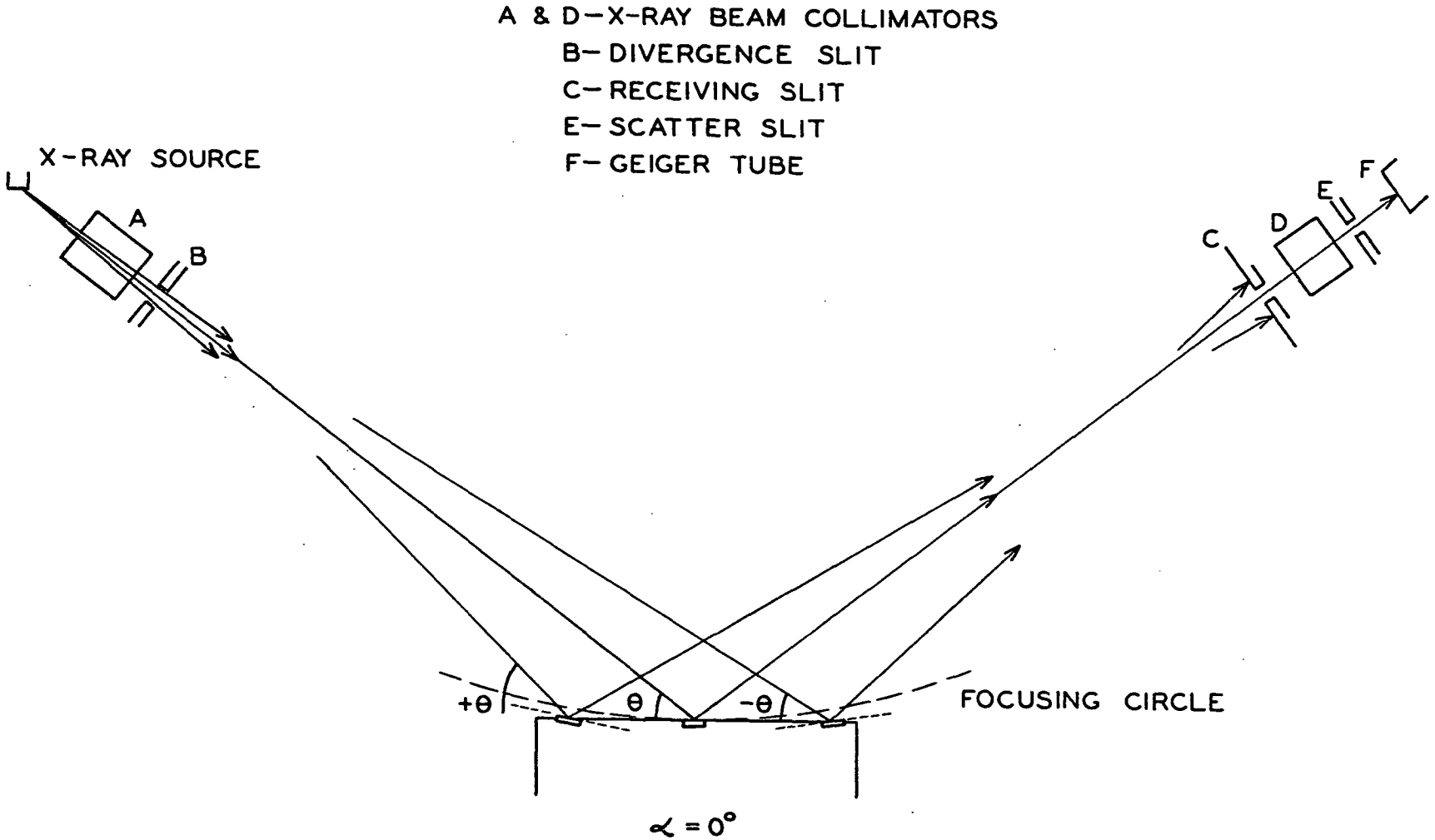

Figure 26. Goniometer Geometry

of α alone if θ and the slit system used are held constant. [It is conceivable that specimen thickness may contribute to this defocusing problem. The geometric analysis of the effect of sample thickness is obscured by the effects of x-ray absorption in the sample. However, the samples used are so thin that significant effects of thickness are unlikely.] Since this was done throughout the work with coating specimens, the results obtained are valid and comparable but they do contain a small, constant error.

The magnitude of the error introduced into the orientation determination by defocusing effects is shown graphically in Figure 28. Five coating samples (including 3 different degrees of orientation and 4 sample thicknesses) were examined using the slit system which was used throughout the study of coatings: 1/4° divergence slit, 0.006-in. receiving slit, and 1/4° scatter slit. The specimens were also analyzed using the following slit system to avoid defocusing errors: 1/4° divergence slit, no receiving slit, and a 4° scatter slit. The experimental data are recorded in Table XXII, Appendix.

The data points for all the specimens are scattered about one line. There is no significant trend revealing effects of sample thickness or orientation. It seems reasonable to conclude that the error introduced into the determination is constant and, therefore, the results reported in this work, although not absolute, are comparable.

It is recommended that future work with this method be carried out using the 1/4 - ∞ - 4° slit system wherever resolution considerations permit.

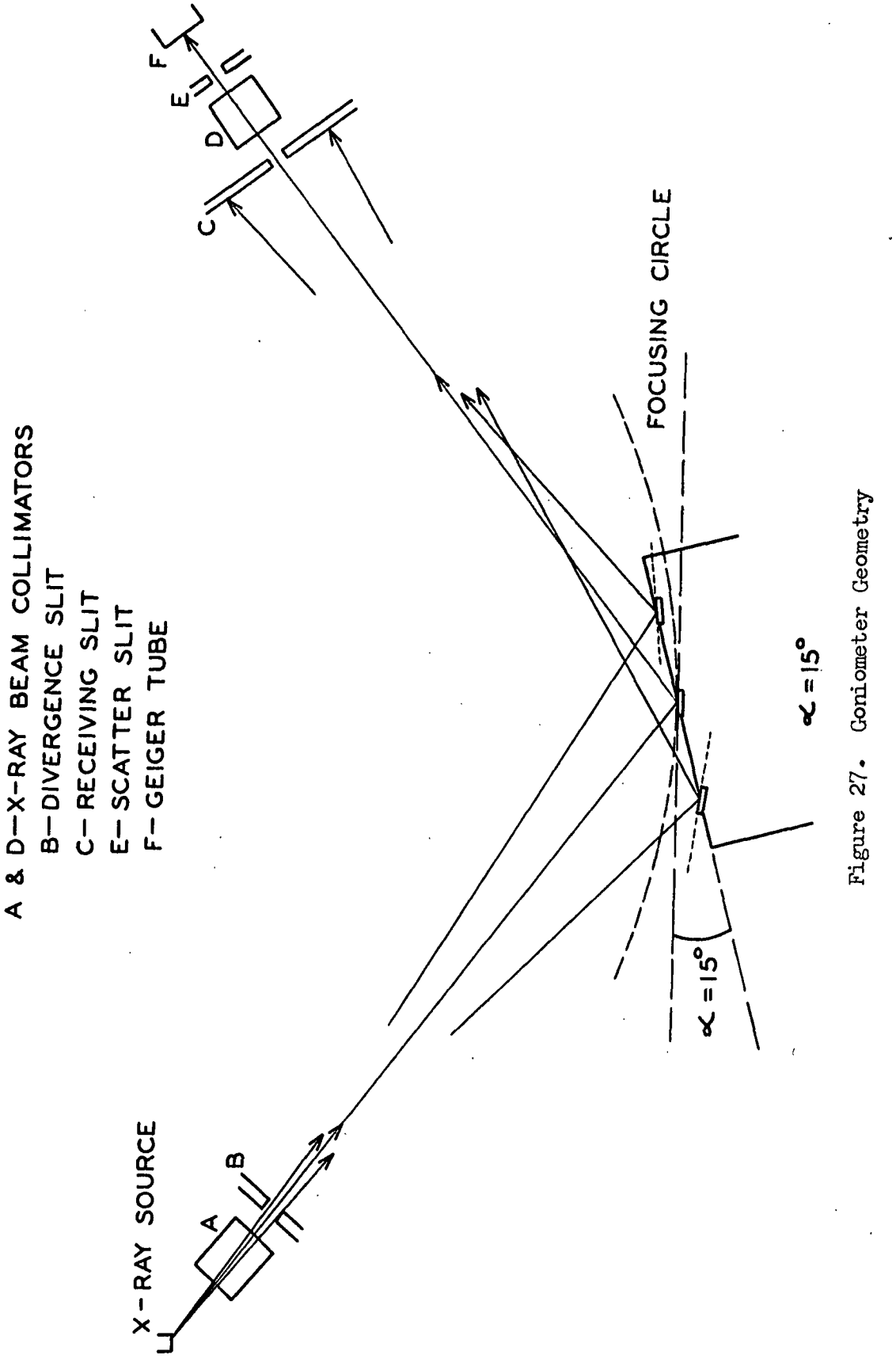

Figure 27. Goniometer Geometry

There is a second minor criticism of this method: measured intensity values are corrected using a precise value of θ in Equation (13); the intensity measurements are made over a range of θ values which may include 0.75° in some cases. The error introduced into the calculated correction factor is about 0.1% in extreme cases.

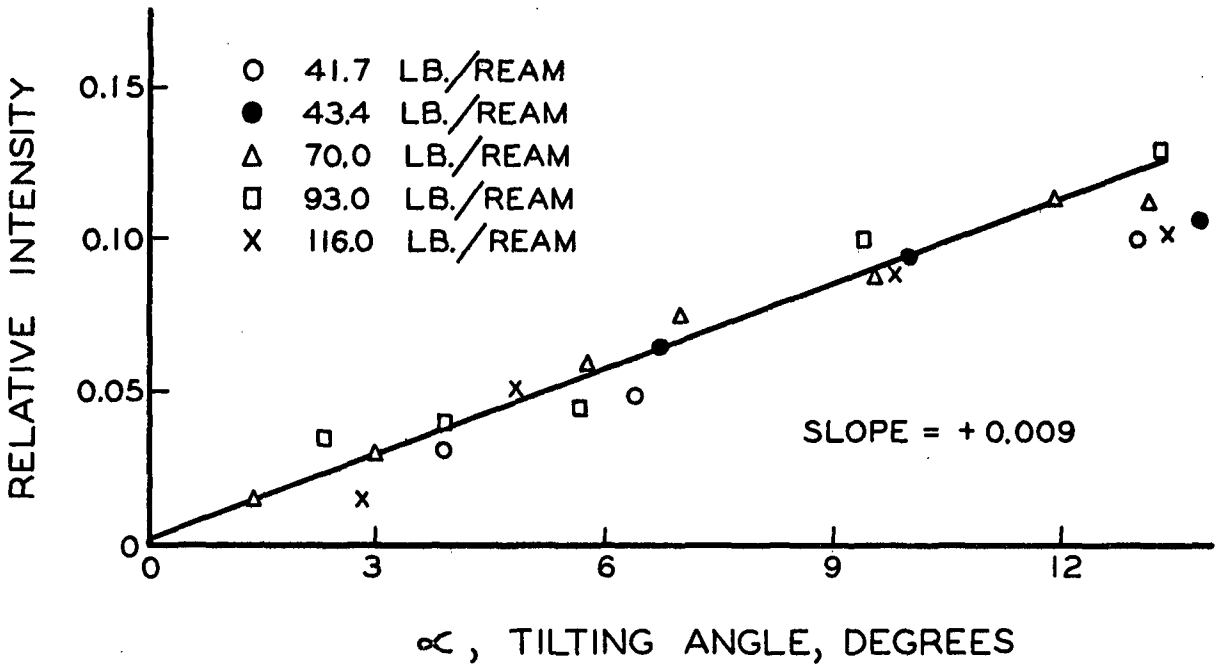

Figure 28. Defocusing Error Magnitude

INVESTIGATIONS OF COATING STRUCTURE

This portion of the study is directed primarily at demonstrating the usefulness and capabilities of the structure analysis techniques which have been described in the previous section. Of no less importance is the secondary objective, that of gaining an insight into coating structure and the way in which it is altered by several selected independent variables.

The scope of this work is far too narrow to allow a complete evaluation of coating structure variables or even more than a cursory examination of the independent variables which have been selected for study. However, the information established here, in spite of its limitations in scope, provides for the first time quantitative values of a basic nature which are useful in understanding the end-use properties of coated papers. It is not within the scope of the present work to develop relations between structural characteristics of clay coatings and their end-use properties.

COATING REPLICATION

It has been shown that the techniques used to evaluate structure in pigment coatings have satisfactory precision and reproducibility. In order to demonstrate that the coatings may be prepared in a reproducible manner, two coatings containing the 0.5 - 1.0 mu clay fraction and Stayco M starch in a 12:100 ratio were prepared independently. In so far as possible, all coating conditions were made equal. The results of the

analysis of these coatings are listed in Table IV. The experimental data are recorded in Tables XXIII through XXV, Appendix.

TABLE IV

COATING REPLICATION

	Coating Number	
	B	J
Clay particle size, mu	0.5-1.0	0.5-1.0
Starch:clay ratio	12:100	12:100
Color solids, %	55	55
Rawstock pore size, mu	0.45	0.45
Coat weight, lb./ream	21.1	21.2
B.E.T. surface area, $M^2/g.$	5.9	6.2
Pore distribution		
Volume av. radius, mu	0.054	0.057
Distribution peak, mu	0.052	0.053
Range, 90%, mu	0.034-0.098	0.036-0.093
Void volume, N_2 adsorp., ml./g.	0.171	0.177
Orientation, slope, ΔR.I./°	-0.062[a]	-0.062[a]

[a] The orientation values reported in the remainder of this work have not been corrected for the constant defocusing error discussed on pages 81 to 88.

The pore distributions are presented graphically in Figure 29. Coating J appears to have a sharper peak in the distribution curve than does coating B but in other respects the two curves are essentially the same. The differences apparent in Figure 29 appear to be just a little greater

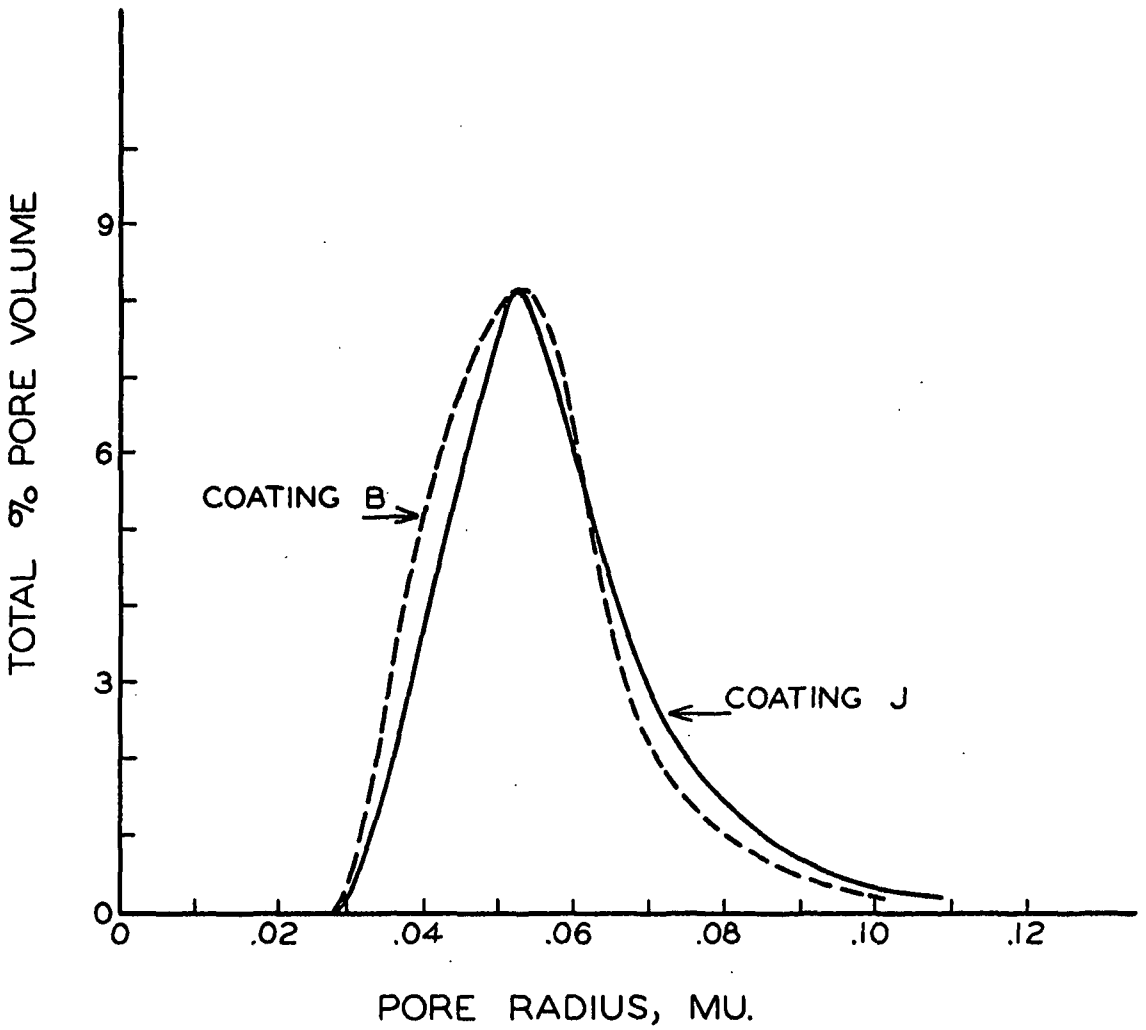

Figure 29. Pore Distributions
Coatings B and J

than the estimated precision of the nitrogen adsorption method in the region of pore radii from 0.028 to 0.060 mu.

The surface area and the void volume of coating B are slightly lower than the corresponding values for coating J. The magnitude of these variations is sufficiently great that "control" or reference coatings should be prepared in each experiment.

THE EFFECT OF CLAY PARTICLE SIZE ON COATING STRUCTURE

Three coatings, each containing a different particle size clay fraction but otherwise identical, were prepared, air dried at 73°F. and 50% R.H., isolated and analyzed according to the procedures described. The coating conditions and the results of the analysis are listed in Table V. The pertinent data are recorded in Tables XXVI, XXVII, and XXVIII, Appendix.

Although clay particle size is the only independent variable employed in this first segment of the study of coating structure, other properties of the clay may vary among the three clay fractions. No account has been made of variations in such clay properties as crystal perfection, the presence of small amounts of nonkaolin impurities and ion substitution.

The B.E.T. surface area, or unbonded area, of these coatings decreases substantially as the particle size of the clay used in the coating is increased. The pore distributions of these three coatings,

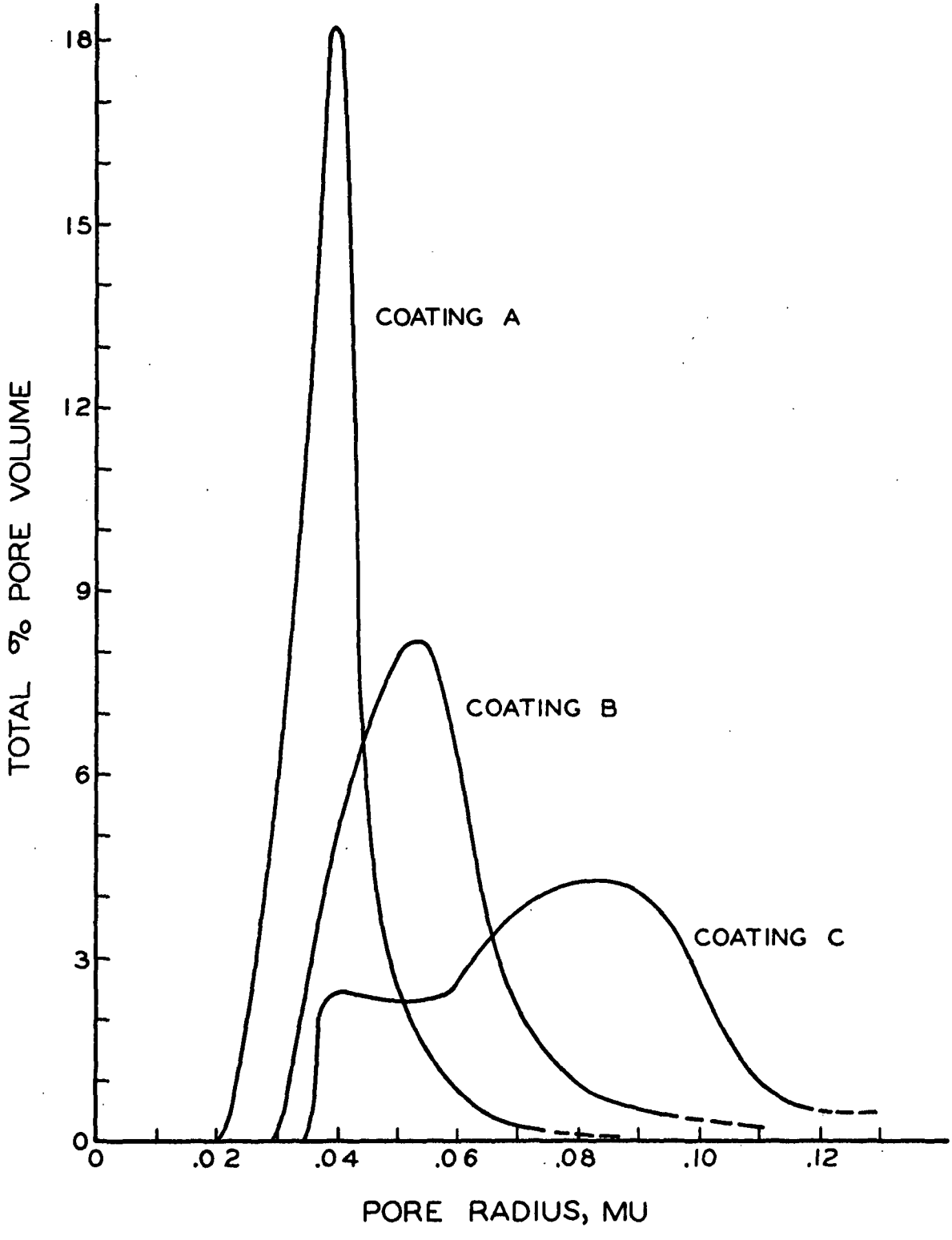

Figure 30. Pore Distributions
Coatings A, B, and C

TABLE V

THE EFFECT OF CLAY PARTICLE SIZE ON COATING STRUCTURE

	Coating		
	A	B	C
Clay particle size, mu	0.0-0.5	0.5-1.0	1.0-2.0
Starch-clay ratio	12:100	12:100	12:100
Color solids, %	55	55	55
Rawstock pore size, mu	0.45	0.45	0.45
Coat weight, lb./ream	22.6	21.1	21.5
B.E.T. surface area, $M^2/g.$	8.4	5.9	3.8 (6.1)[a]
Pore distribution			
Volume av. radius, mu	0.039	0.054	0.079
Distribution peak, mu	0.039	0.053	0.040 and 0.085
Range, mu, 90%	0.023-0.057	0.034-0.098	0.035-0.120
Void volume, N_2 ads., ml./g.	0.187	0.171	0.215
Orientation, slope ΔR.I./°	-0.060	-0.062	-0.045

[a] Surface area calculated from pore distribution.

Figure 30, offer an obvious explanation for this occurrence; it is evident that the pore distributions become increasingly coarser as the clay particle size of the coating is increased while the internal void volume is not sufficiently increased to offset the effect of pore size.

One further observation can be made with respect to the surface area values for coatings A, B, and C. If the assumption is made that most of the starch in the coating color is, at some time during the drying of the

coating, deposited uniformly over the surface of the clay particles, it is possible to calculate a new "total area" of the clay-starch combination. The increased area stems from the increased dimensions of the clay particles due to the "adsorbed" starch film. The details of this calculation are given in Appendix II. If this new "total area" is then used in calculations of the per cent bonded area of the coatings listed in Table V, it develops that the percentage bonded area is essentially identical for all three coatings at about 60%. Superficially, this appears to be in contradiction to what might be expected from a consideration of the role of surface tension in drying operations (33). There is no basis for further discussion of this point since information on vehicle and adhesive migration, rate of drying and so forth was not obtained. The assumptions involved in this calculation are rather gross but the interesting result of these data manipulations indicates that further investigation might be informative.

One of the most interesting aspects of the pore-distribution data is the range of pore sizes present in these coatings. Previous work by Carson (1) had indicated that the average pore radius of a single coated book paper was 0.3 mu. The present data show that the vast majority of the coating pores are between 0.025 and 0.1 mu in radius. The discrepancy between these values and the larger value found by Carson is probably due to the sensitivity of the air permeability method used by the latter to very large pores or pinholes. These pinholes are inherently more likely to occur when coatings are deposited upon a rough surface such as that of a paper rawstock. It should be recalled that, although the nitrogen

adsorption method can detect pores with radii of 0.5mu, this method is not suited to the quantitative evaluation of pores of this size. Pores with radii this large are, in many cases, as large as the clay particles themselves and are more aptly classified as pinholes.

A second interesting aspect of the pore data appears when the B.E.T. area of the coatings is compared to the surface area calculated from the pore distributions. Although in all coatings examined in this study the calculated pore area and volume was larger than the measured values, only in the case of coating C was this difference considered significant. Ries and co-workers (70) state that this phenomenon is due to the presence of constricted pores in the absorbent. If the Pierce method for the computation of pore distributions is modified to handle various pore shapes, the only shape capable of fitting the measured and calculated pore volume and area data is the constricted pore. Admittedly, this is not proof of the existence of such pores in this coating since a portion of the area difference noted could also be due to the cross-section shape of the pores. The evidence is such, however, that it seems wise to regard the pore distribution in coating C as pore volumes controlled by pore openings of the size indicated.

The nitrogen adsorption method cannot indicate the size of the pores which open to either surface of the coating. This deficiency is not important in the case of coatings A and B since the range of pore radii included in these two coatings is quite narrow. Since the pore openings at one surface must also have a distribution, it is unlikely that there

is a substantial difference in the pore openings of the two surfaces. In the case of coating A, 86% of the pore volume is in pores with radii between .025 and .050 mu; in coating B, 84% of the void volume is in pores with radii between .032 and .075 mu. [The remaining pore volume is made up of pores sufficiently large and, therefore, few in number to be considered as a type of surface depression.] It is reasonable to assume, then, that the pore distribution through the thickness of these two coatings is essentially uniform.

There is no basis for a similar conclusion in the case of coating C. Figure 30 shows that the pore distribution in this large clay particle size coating may have two maxima: a small peak in the curve at .040 mu. and a broad maximum in the range 0.065 to 0.10 mu. This same coating showed evidence of being composed, in part, of constricted pores. Based on these two items, the following idealized diagram of a possible coating pore structure is presented.

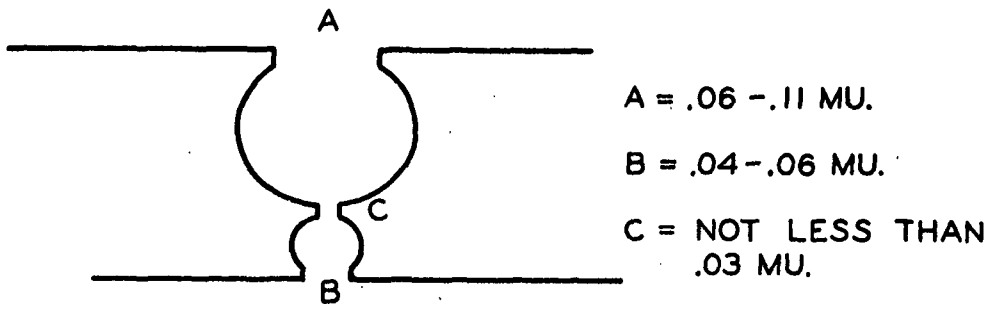

Figure 31. Pore Type, Coating C

The nitrogen adsorption method can give no indication whether pore openings A and B are distributed between the two coating surfaces or whether the larger opening may exist preferentially in one surface of the coating. Further investigation of the pore structure of this coating might prove interesting.

The clay particle orientation in these three coatings is of interest. Hemstock (47) felt that the large particle size clays orient to a greater degree than do smaller particles. X-ray examination of these coatings showed that the largest clay fraction (1.0-2.0) actually had the poorest particle orientation. Conceivably, this could result from the rapid flow of vehicle from the comparatively large interparticle spaces which should exist in this coating. The clay particles would not have the time required to align themselves in the plane of the rawstock surface before they became immobilized. The comparatively large mass of these particles would offer additional resistance to alignment by fluid friction forces during the vehicle migration stage.

The degree of particle orientation in the two smaller particle coatings is nearly identical although the values are consistently lower in the case of the 0.0-0.5mu coating when compared to the 0.5-1.0mu coating. This may be due to the fact that the 0.0-0.5 mu clay fraction particles are quite "chunky" when compared to the clay particles of the larger size fraction. An additional factor is the possibility of the presence of small amounts of nonkaolin impurities in the smallest size clay fraction although x-ray examination of this fraction indicated no significant

content of impurities. A third possibility capable of explaining this observation is that of small clay particles tipping into the pores of the rawstock. The majority of the clay particles in the 0.0-0.5 mu fraction are actually smaller than the pores in type HA-MF rawstock. To examine this possibility, the same coating color used in preparing coating A was also used to prepare 20-lb./ream coatings on type VC and type AA-MF rawstock (0.10 mu and 0.80 mu pore diameter). These coatings were isolated and analyzed for particle orientation. The results are listed in Table VI; the data are recorded in Table XXIX, Appendix.

TABLE VI

THE EFFECT OF RAWSTOCK PORE SIZE ON CLAY PARTICLE ORIENTATION

	Coating		
	F	A	G
Clay particle size, mu	0.0-0.5	0.0-0.5	0.0-0.5
Color solids, %	55	55	55
Starch:clay ratio	12:100	12:100	12:100
Rawstock pore size, mu	.10	.45	.80
Coat weight, lb./ream	21.2	22.6	19.8
Orientation, slope, ΔR.I./°	-0.060	-0.060	-0.057

All of these rawstocks are extremely smooth so that the surface roughness differences should have only minor effects upon particle orientation. From the data in Table VI, it is apparent that the tipping of clay particles into the pores of the rawstock is not a significant effect

until the rawstock pore radius is considerably greater than the largest diameter of the clay particles.

There appears to be a relationship between the degree of particle orientation and the internal void volume of coatings A, B, and C. That such a relationship should exist is reasonable since poorly packed particles have large interparticle spaces. The data presented are not sufficient to clearly establish this correlation; adhesive retention, rawstock roughness, etc. must also affect void volume and particle orientation.

THE EFFECT OF COAT WEIGHT UPON COATING STRUCTURE

Three coatings, 10, 20, and 30 lb./ream, were laid down upon type HA-MF rawstock from the same coating color. The coatings were air-dried at 73°F. and 50% R.H. and then isolated and analyzed. The results of the analysis are listed in Table VII. The analytical data are recorded in Tables XXX, XXXI, and XXXII, Appendix.

The most striking point illustrated by these data is the similarity between these three coatings. Coating D (10.8 lb./ream) appears to have a slightly coarser pore structure than the two heavier coatings (Figure 32). This is reflected in the lower B.E.T. surface area of this coating. Figure 32 indicates rather exaggerated differences in the pore structure of these three coatings due to pronounced differences in their weight/unit area. If the actual volume of pores, per unit area of coated surface, is plotted against pore radius, Figure 33, it becomes evident that the

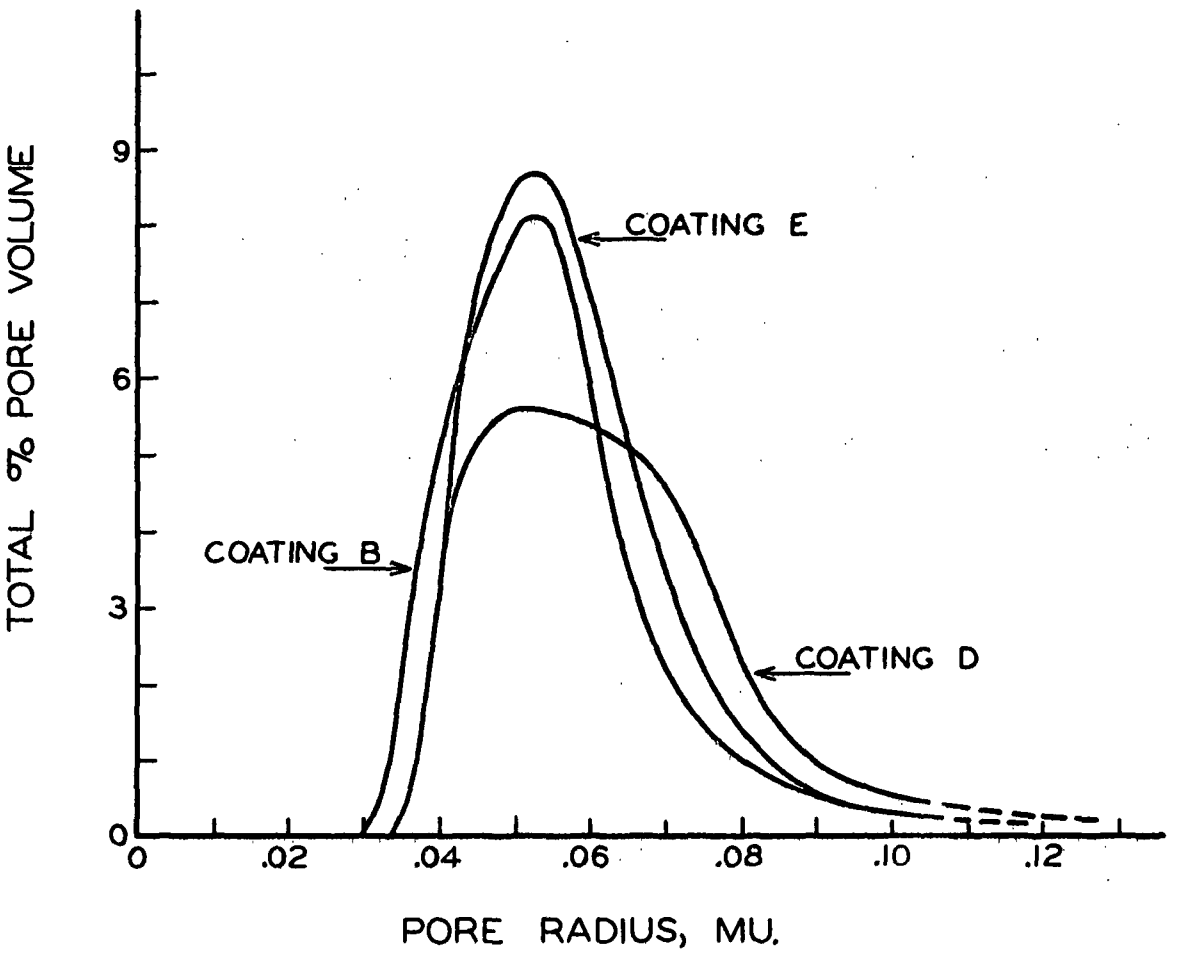

Figure 32. Pore Distributions
Coatings D, B, and E

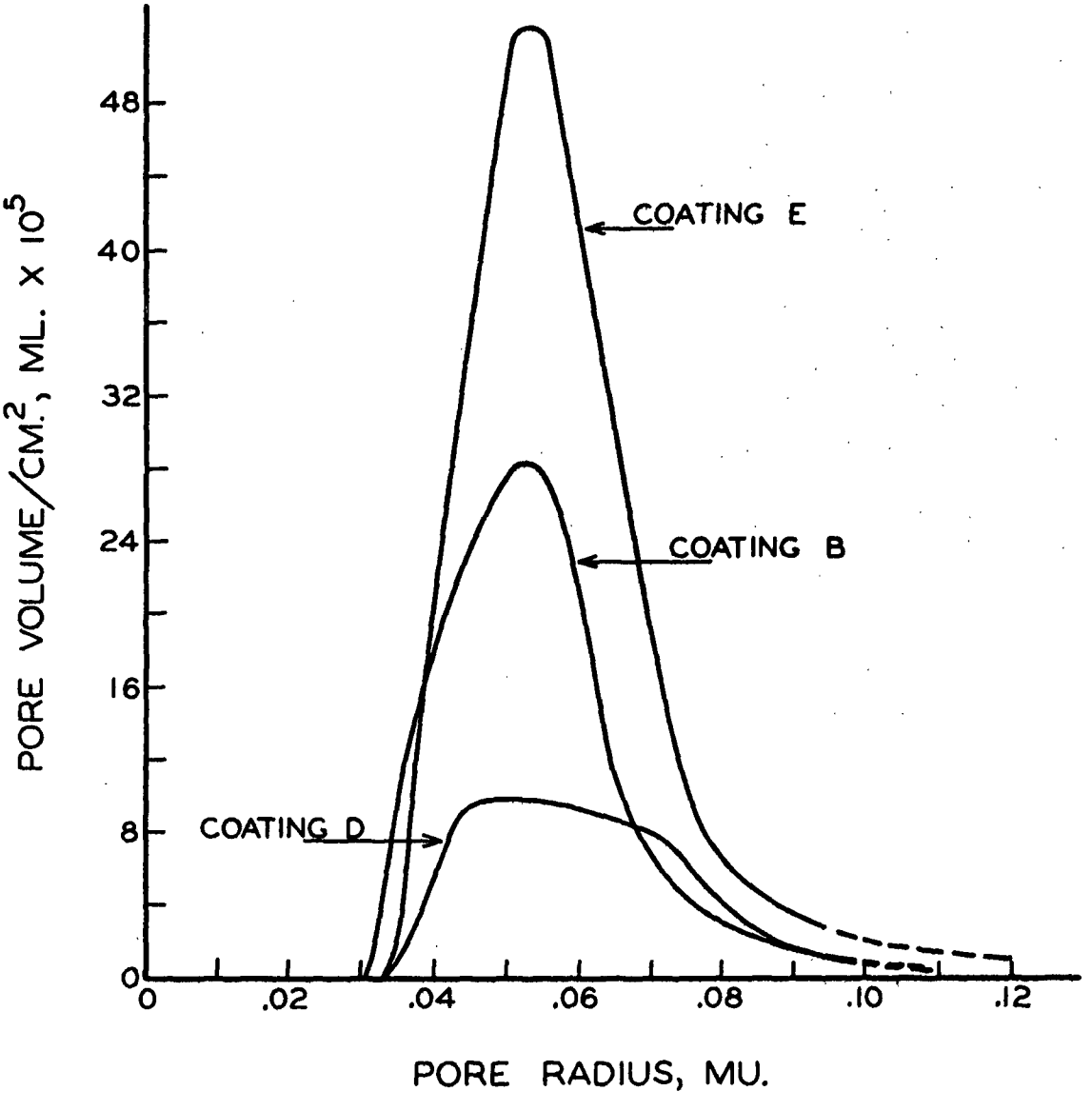

Figure 33. Pore Distributions - Volume Basis
Coatings D, B, and E

TABLE VII

THE EFFECT OF COAT WEIGHT UPON COATING STRUCTURE

	Coating		
	D	B	E
Clay particle size, mu	0.5-1.0	0.5-1.0	0.5-1.0
Starch:clay ratio	12:100	12:100	12:100
Color solids, %	55	55	55
Rawstock pore size, mu	0.45	0.45	0.45
Coat weight, lb./ream	10.8	21.1	33.2
B.E.T. surface area, $M^2/g.$	5.4	5.9	5.8
Pore distribution			
Volume av. pore radius, mu	0.063	0.053	0.056
Distribution peak, mu	0.050	0.053	0.053
Range, mu 90%	0.037-.105	0.034-0.098	0.035-0.093
Void volume, N_2 ads., ml./g.	0.171	0.171	0.176
Orientation, slope, ΔR.I./°	-0.061	-0.062	-0.062

additional coat weight merely serves to increase the volume of pores whose radii lie between 0.030 and 0.085mu. Unfortunately, the nitrogen adsorption method lacks precision in the range of pore radii above 0.085 mu so that the differences in the three curves in this region cannot be considered significant.

Eames (83) has found evidence that lightweight coatings lose proportionately less adhesive to the rawstock during the migration stage of drying than do heavier weight coatings. This information, coupled with the observation that the 10.8-lb. coating set, or lost its watery sheen,

more rapidly than the 20- and 30-lb./ream coatings, indicates that the slight increase in the coarseness of the pore structure of the 10.8-lb./ream coating may be due to the following:

1. The vehicle drains from the lightweight coating into the rawstock rapidly and immobilizes the clay particles before they orient as well as in the heavier coatings. (This decrease in orientation shows up in the values reported for particle orientation although, statistically, the three orientation values are identical.) The less well-oriented clay particles provide the basis for a coarse pore structure.
2. The proportionately larger amount of adhesive retained in the lightweight coating is sufficient to fill in or establish bonds across the smaller interparticle spaces to the extent that the surface area remaining is slightly lower than in the heavier weight coatings.

It is unlikely that this indicates a stratification of the pore structure of heavier coatings; that is, a zone near the rawstock-coating interface which has a coarser pore structure than the remainder of the coating. Such a structure would probably require a break in the tiny water columns which exist in the wet coating. Conceivably, some stratification of pore structure could arise from variations in adhesive migration from certain zones of the coating but such effects would be small.

TABLE VIII

THE EFFECT OF SUPERCALENDERING UPON COATING STRUCTURE

	Coating		
	J	K	L
Clay particle size, mu	0.5-1.0	0.5-1.0	0.5-1.0
Starch:clay ratio	12:100	12:100	12:100
Color solids, %	55	55	55
Rawstock pore size, mu	0.45	0.45	0.45
Coat weight, lb./ream	21.2	20.8	20.6
Supercalender nips	0	1	3-4
Gloss, B & L, %	58.5	70.0	72.5
Opacity, R_o/R_∞, % 450 μ	86.1	89.5	91.5
B.E.T. surface area, $M^2/g.$	6.2	6.4	6.6
Pore distribution			
Volume av. pore radius, mu	0.057	--	0.059
Distribution peak, mu	0.052	--	0.059
Range, 90%, mu	0.032-0.093	--	0.027-0.081
Void volume, N_2 ads., ml./g.	0.177	--	0.177
Orientation, slope, ΔR.I./°	-0.062	-0.065	-0.069

THE EFFECT OF SUPERCALENDERING UPON COATING STRUCTURE

Twenty-four 4 x 5-in. sheets of type HA-MF rawstock were coated with the same coating color and then air-dried at 73°F. and 50% R.H. These coated sheets were divided into three groups of eight sheets each. One of these groups was not calendered; a second group was passed through one

nip of a laboratory supercalender at a pressure of approximately 800 pounds per linear inch; the third group of sheets was passed through 3-4 nips of the supercalender at the same pressure. The specular gloss (75°) of the coated sheets was measured using the Bausch and Lomb glossmeter. The coatings were isolated and the printing opacity of the isolated coatings was measured with the General Electric Recording Spectrophotometer using a modified sample aperture.[1] The coatings were then analyzed according to the procedures described. The results of this analysis are listed in Table VIII. The pertinent experimental data are recorded in Tables XXXIII, XXXIV, and XXXV, Appendix.

Before discussing these data, it should be noted that there exists an unexplored possibility that the MF rawstock and a paper rawstock may behave entirely differently in the supercalendering operation. Superficially, at least, the MF rawstock-coated sheets responded to supercalendering as does coated paper. The caliper of the coated sheets was reduced from 6.2 mils to 3.0 mils and the sheets became visibly less opaque. The gloss measurements listed in Table VIII show that the surface of the coating was smoothed considerably.

A continuous increase in the degree of pigment particle orientation is evident as the amount of supercalendering is increased. This increase in particle orientation would, perhaps, have been more pronounced

[1] The sample aperture of the spectrophotometer was reduced from 1.25-in. diameter to 0.5-in. diameter in order to accomodate the small coating samples. A blank reading was obtained to correct for reflection from the annulus of the aperture-reducing device. This blank was then substracted from both the R_o and the R_∞ readings.

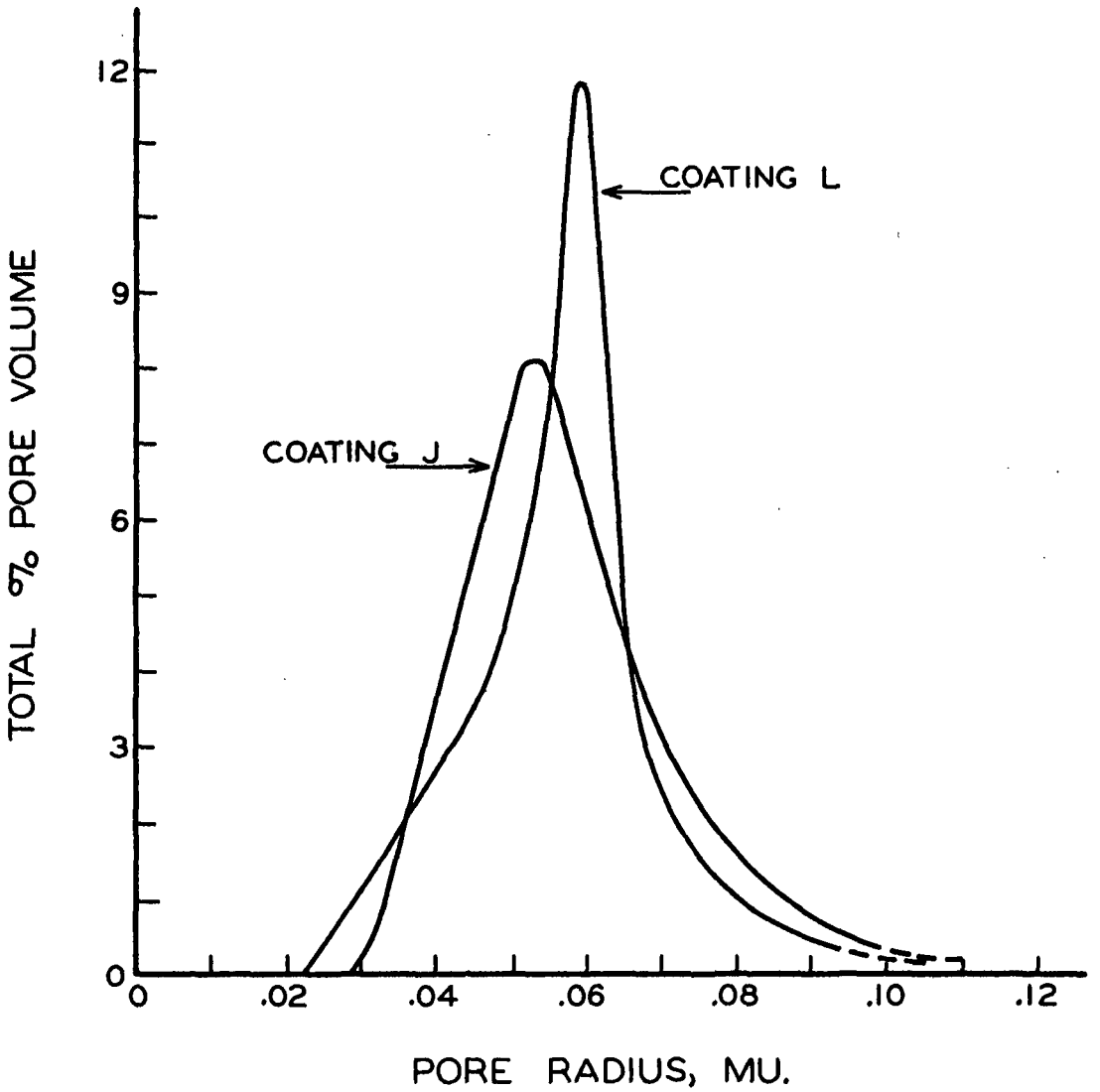

Figure 34. Pore Distributions
Coatings J and L

if the surface of the MF rawstock had been roughened before the coating was laid upon it.

The realignment of pigment particles is accompanied by an increase in the unbonded surface area of the coatings. This is to be expected since it is unlikely that significant realignment of pigment particles could occur without the rupture of pigment-adhesive or adhesive-adhesive bonds. That rupture of bonds occurs in the coating during the supercalendering operation has previously been suggested (47).

More interesting is the change in the pore distributions of these coatings occasioned by supercalendering. From Figure 34 it is apparent that supercalendering causes both a compression of large pores and an expansion of some of the smaller pores. Both could occur as a result of mechanical rupture of pigment-adhesive and/or adhesive-adhesive bonds. It is equally interesting that this shift in the pore distribution of the coating occurred without a simultaneous change in the internal void volume. This indicates that the coating possesses certain properties of an elastic solid since any compression of the coating must have been reversible in spite of the fact that the distortion produced in the coating was sufficient to cause the rupture of bonds.

It has been a common observation that coated papers suffer a loss in opacity during the supercalendering operation. The information presented here indicates that the loss in opacity probably occurs solely in the rawstock since the opacity of the isolated coating actually was increased by the supercalendering operation. This concurs with Tollenaar's

(2) finding that supercalendering produced only a compression of some "inner layer" of coated papers.

THE EFFECT OF RAWSTOCK SURFACE ROUGHNESS AND COLOR DISPERSION ON COATING STRUCTURE

In order to demonstrate that mechanical color dispersion and rawstock surface roughness can affect coating structure, a coating color was prepared as described on pages 30 and 31 with the exception that the color was not passed through the dispersion mill. A 20-lb./ream coating was deposited on type HA-MF rawstock and allowed to air dry at 73°F. and 50% R.H. This coating was isolated and analyzed. The results of the analysis are listed in Table IX.

A second coating was deposited upon sheets of type HA-MF rawstock whose surface had been slightly roughened. The surface of the MF rawstock was roughened by pressing it against a sandblasted brass plate at 20 p.s.i. for one minute. The position of the rawstock against the plate was changed by 180° and the pressing was repeated. This treatment reduces the caliper of the rawstock by only 2%. The analysis of this coating is also presented in Table IX. The analytical data for both coatings are recorded in Tables XXXVI and XXXVII, Appendix.

It is interesting that the pigment particle orientations in coatings B-J and H are identical and yet the surface area of coating H is significantly larger than that of coating B-J. This indicates that the action of mechanical dispersion is not that of dispersing pigment particle agglomerates but dispersion or mixing of the adhesive throughout

TABLE IX

THE EFFECT OF COLOR DISPERSION AND RAWSTOCK SURFACE CONDITION ON COATING STRUCTURE

	Coating		
	(B + J)/2[a]	H	I
Clay particle size, mu	0.5-1.0	0.5-1.0	0.5-1.0
Starch:clay ratio	12:100	12:100	12:100
Color solids, %	55	55	55
Rawstock pore size, mu	0.45	0.45	0.45
Coat weight, lb./ream	21.1	21.8	18.8
Dispersion treatment	dispersed	none	none
Rawstock surface treatment	none	none	roughened
B.E.T. surface area, $M^2/g.$	6.05	6.8	6.9
Orientation, slope ΔR.I./°	-0.062	-0.062	-0.052

[a] Since a reference coating was not directly available for coatings H and I, the average values of coatings B and J are reported.

the color to allow more uniform and complete bonding of the pigment particles. It is reasonable that the orientation was not improved by mechanical dispersion since the pigment had already been chemically dispersed.

In the case of coating I in which a nondispersed coating color was spread upon a slightly roughened rawstock, it is evident that the clay particle orientation suffers considerably when compared to the same coating laid upon a smooth rawstock (coating H). This indicates that the

surface roughness of the rawstock is transmitted through much of the coating otherwise the effect upon particle orientation would be less. The surface areas of coatings H and I are identical, which implies that the coating color and rawstock pore systems reacted in the same way regardless of the surface condition of the latter.

No pore distribution data were obtained for coatings H and I.

SUMMARY AND OBSERVATIONS

This investigation has been directed at the development of methods useful for the evaluation of the physical structure of clay coatings. The coatings examined in this work were prepared by the deposition of aqueous clay-starch coating colors upon a porous rawstock. The rawstock used, Millipore filter, had a smooth surface, pores whose long axes were perpendicular to the plane of the sheet and a structure not destroyed by water. This material is best considered as an idealized coating rawstock. The differences between this material and paper rawstocks must qualify comparisons of the coatings analyzed here and coatings laid on paper rawstocks.

During the course of this work a method was developed for the isolation of clay-starch coatings from Millipore filter in pieces of convenient size. By dissolution of the rawstock in several baths of ethyl acetate, coatings as light as 4 lb./ream were isolated. Evidence was presented to show that the isolation treatment did not affect the strength, the clay particle orientation, the surface area, the void volume and the pore distribution of coatings. Traces of "trapped" ethyl acetate remained in the coating after the isolation treatment. During the coating isolation procedure a film which stained blue with iodine solution was observed to break loose from the surface of the coating which had been in the coating-rawstock interface. This material was assumed to be that portion of the starch adhesive which had migrated into the rawstock.

It was shown in this investigation that low temperature nitrogen

adsorption measurements are sufficiently flexible to describe the surface area, the internal void volume and the pore distribution of isolated coatings. Particular care was required in the determination of the nitrogen desorption isotherm since the samples available were small and most of the useful data were obtained at values of relative pressure greater than 0.96. It was necessary to start the desorption isotherm from the point of complete saturation of the sample in order to assure proper location of the curve. The nitrogen adsorption technique lacks precision in the very high relative pressure region (above 0.99) thus preventing the accurate description of pores larger than 0.2 mu in diameter. In the case of most of the coatings examined in this work this was not a significant limitation.

An established x-ray diffraction method was modified to measure the extent of preferred orientation, with respect to the plane of the coating surface, of pigment particles in coating films. The method requires only that the pigment particles have a regular shape with a particle surface in constant relation to a crystal plane of the pigment. The original method was based on established principles and was designed to evaluate the degree of preferred crystal orientation in samples which were infinitely thick to x-rays. The present modification allowed the method to be used on films which were not infinitely thick to x-rays. Experimental confirmation of derived absorption correction factors was obtained. Within sample variation in the test results was shown to be quite large but was counteracted by the use of composite samples. It was shown that the results presented in this report contain a constant

error that resulted from defocusing of the diffracted x-ray beam. The magnitude of this error was established and a suggestion for avoiding it was presented for systems where fine resolution of the diffracted x-ray beam is not important.

It was shown that a mercury displacement method for the measurement of the void volume of isolated coatings was sensitive to the surface conditions of the coating to the extent that the method had only restricted usefulness.

With certain selected experiments it was demonstrated that the methods described herein were capable of detecting differences in coating structure arising from variations in coating composition, coating conditions and subsequent treatment of the dried coated sheets. The scope of this study was not sufficiently broad to permit conclusions based on the results of these experiments. However, the following observations were recorded.

1. The pore sizes of the clay coatings examined in this work were considerably smaller than had been indicated by previous work in this field. Pore radii of 0.3 mu for single-coated book paper and 0.2 mu for double-coated book paper were obtained by an air permeability technique (1). The present work indicates that few of the pores in the coatings analyzed had radii larger than 0.1 mu. The majority of the pores had radii between 0.025 and 0.075 mu. The discrepancy noted was attributed to the use of a smooth rawstock in the present work and to the sensitivity of

the air permeability method to very large pores and pinholes.

2. The pore structure of the coatings examined varied significantly when three different particle size fractions of a clay were used in the coating. The pore structure became finer and encompassed a narrower range as the average clay particle size was decreased. As would be expected, the free surface area of the coatings increased as the particle size of the clays used in these coatings was decreased.

3. The pore structure of clay coatings was essentially uniform through their thickness in the case of two coatings containing small (under 1 mu) particle size clays. A coating containing a larger particle size clay fraction had a pore distribution which was indicative of nonuniform transverse pore structure.

4. The degree of preferred orientation of clay particles in coatings was found to be dependent upon the average particle size of the clay used in the coating. The large (1.0-2.0mu) particle size clay fraction coating had the least orientation. The small (0.0-0.5 mu) clay fraction yielded coatings whose orientation values were only slightly lower than those of the 0.5-1.0 mu clay fraction coatings. Reasons for this behavior pattern were not developed. It was suggested that the degree of particle orientation was a function of particle size, shape and mass and the rate of vehicle migration into the rawstock. Rawstock pore size was shown to have no effect upon clay particle orientation until the pores of the rawstock were considerably larger than

the greatest dimension of the clay particles. This indicated that the suface pores of the rawstock were plugged by agglomerates of clay particles. In those coatings containing various particle size clays there appeared to be a relationship between the clay particle orientation and the void volume of the coating. This relationship was not investigated further.

5. Coating weight differences (10-20-30 lb./ream) did not appear to have large-scale effects upon coating structure in the case of three coatings which contained the 0.5-1.0 mμ particle size clay. The lightweight coating (10.8 lb./ream) did have a slightly coarser pore structure than did the heavier coatings. The free, or unbonded, surface area of the light coating was slightly less than that of the heavier coatings. This was attributed, tentatively, to rapid immobilization of the pigment particles in the coating color when the color was laid on the rawstock and to lower percentage adhesive loss to the rawstock. Clay particle orientation and internal void volume appeared to be independent of coat weight.

6. Supercalendering of coated Millipore filter sheets produced some realignment of clay particles, rupture of pigment-adhesive and/or adhesive-adhesive bonds, and a shift in the pore structure of the coating. The most interesting effect of supercalendering was the simultaneous compression of some large pores and the enlarging of some small pores. The void volume of the coating was not altered by supercalendering in spite of the fact that

the distortion of the coating was sufficient to cause rupture of bonds. The opacity of the isolated coating was increased by supercalendering.

7. Mechanical treatment (passage through a dispersion mill) of a coating color increased the bonding occurring in the coating but had no effect upon the degree of particle orientation. This indicates that the chief benefit derived from this treatment, neglecting rheological effects, was more intimate and uniform mixing of the pigment and adhesive. The coating concerned was prepared from a chemically well-dispersed clay slip.
8. Roughening the surface of the Millipore filter rawstock had a comparatively large effect upon the pigment particle orientation in the coating but did not affect the free surface area. The surface roughness of the rawstock was evidently transmitted a considerable distance into the coating.

As a general conclusion it may be stated that this work has established and demonstrated a system for the study of the physical structure of clay-starch coating films. Extension of this work to the evaluation of variations in the structure and the end-use properties of coatings which are related to structure will make possible a more fundamental understanding of the properties of coated papers of interest to both the producer and the consumer.

SUGGESTIONS FOR FUTURE WORK

A peculiarity of this study lies in the fact that much of its value is dependent upon the use made, in the future, of the system described herein for the analysis of coating structure. In an effort to stimulate interest in work with this method the following suggestions are presented:

1. Perhaps the most important phase of the future work is a continuation of the study of the effects of component and process variables on coating structure. Studies of the effects of such variables as pigment mixtures, color solids, rawstock pore size, adhesive ratio, coating method, moisture content in supercalendering, etc., should lead to a more fundamental understanding of the coating process. Coupled with these studies should be an evaluation of certain end-use properties of coatings.
2. Certain relationships between various ink receptivity tests and the pore distributions of coatings are logical. The influence of such factors as the pressure applied during the testing of ink receptivity could be evaluated.
3. Interesting relationships between the optical properties of coatings and their free surface area and pore distributions might be developed.
4. The strength of coatings might well be related to the free surface area and the extent of pigment particle orientation. The free surface area of the coating may be construed as a measure of the efficiency with which the adhesive present in

the coating was used; the pigment orientation may limit the efficiency with which a given amount of adhesive can bond particles.

Certain refinements of the system developed in this work represent a promising field for future work.

1. There exists a possibility that the orientation of coatings laid on paper may be examined without isolating the coating. If the value of (μt) of the coating layer can be calculated or measured, it might develop that the distortion of the analytical results introduced by the rawstock would be small. Development and verification of such a technique would extend the usefulness of this method for the study of preferred orientation in coating.
2. The extension of the work on pore distributions of coatings to a measurement of those pores which are continuous (in a direct way) through the coating would be informative. The gas permeation method described by Corte (57) would be of value here.

LITERATURE CITED

1. Carson, F. T., J. Research Natl. Bur. Standards 24, no. 24:435-42 (April, 1940).

2. Tollenaar, D., Intern. Bull. Printing and Allied Trades no. 73: 76-9(Jan., 1956).

3. Comer, J. J., and Lyons, S. C., Tappi 39, no. 9:614-17(Sept., 1956).

4. Comer, J. J., Stetson, H. W., and Lyons, S. C., Tappi 38, no. 10: 620-4(Oct., 1955).

5. Casey, J. P. Pulp and paper. Vol. II. 1st ed. New York, Interscience Publishers Inc., 1952.

6. Tollenaar, D., Intern. Bull. Printing and Allied Trades no. 67:16-18 (Jan., 1954).

7. Roderick, H. F., and Hughes, A. E., Paper Trade J. 110, no. 8:104-8 (Feb. 22, 1940).

8. Lyons, S. C. Paper coating clays. TAPPI Monograph Series no. 7: 37-79(1948).

9. Masterman, F. E., Tappi 35, no. 9:420-5(Sept., 1952).

10. McCarron, R. D., and Rowland, B. W., Paper Trade J. 96, no. 2:36-9 (June 1, 1933).

11. Woodward, L. A., and Lyons, S. C., Tappi 34, no. 10:438(Oct., 1951).

12. Brooks, A. M. Calcium carbonate. TAPPI Monograph Series no. 7:17-32 (1948).

13. Hemstock, G. A., and Swanson, J. W., Tappi 40, no. 10:794-801(Oct., 1957).

14. Cobb, R. M. K., Tappi 41, no. 10:581-7(Oct., 1958).

15. Lukens, A. R., Landis, C. G., and Rochow, T. G., Paper Trade J. 112, no. 8:31-8(April 10, 1941).

16. Hall, G. E., McIntosh, C. D., Liggett, L. M., and Hagemeyer, R. W., Tappi 35, no. 4:223-8(April, 1955).

17. Swanson, J. W., and Hemstock, G. A., Tappi 39, no. 1:30-5(Jan., 1956).

18. Rice, J. C., Tappi 39, no. 1:43-6(Jan., 1956).

19. Albert, C. G., Tappi 34, no. 10:453-8(Oct., 1951).

20. Hemstock, G. A., and Swanson, J. W., Tappi 40, no. 10:833-8(Oct., 1957).

21. Hemstock, G. A., and Swanson, J. W., Tappi 39, no. 1:35-9(Jan., 1956).

22. Rowland, B. W., Paper Trade J. 112, no. 26:75-7(June 26, 1941).

23. Casey, J. P., and Libby, C. E., Tech. Assoc. Papers 31:172-85 (1948).

24. Clarke, A. W., Robinson, A., and Ainsworth-Harrison, H., The Papermaker 110, no. 1:TS4-7(July, 1945).

25. Sears, G. R., Beckman, N. J., Thompson, J. O., and Yurkowitz, I. L., Tech. Assoc. Graphic Arts, Proc. 4:59-68(May, 1952).

26. Zettlemoyer, A. C., Walker, W. C., Fetsko, J. M., and Meyers, R. R., Intern. Bull. Printing and Allied Trades, no. 73:60-3(Jan., 1956).

27. Washburn, E. W., Phys. Rev. 17:273-83(1921).

28. Norton, F. H., J. Am. Ceramic Soc. 31, no. 8:236-40(Aug., 1948).

29. Cobb, R. M. K., and Lowe, D. V., J. Rheology 1, no. 2:158-66(Jan., 1930).

30. Cobb, R. M. K., Tech. Assoc. Papers 21:110-19(1938).

31. Voet, A., and Brand, J. S., Paper Trade J. 122, no. 24:34-9(June 13, 1946).

32. Dappen, J. W. Distribution of starch in clay coatings, Doctor's Dissertation. Appleton, Wis., The Institute of Paper Chemistry, 1950.

33. Campbell, W. B. Cellulose-water relationships in papermaking. Forest Service Bull. 84. Canada, Dep't Interior, 1933.

34. Cobb, R. M. K., Tappi 41, no. 10:587-600(Oct., 1958).

35. Davidson, G., Tech. Assoc. Papers 23:58(1940).

36. McCready, W., Tech. Assoc. Papers 23:58(1940).

37. Schoch, T. J., Tappi 35, no. 7:22-38A(July, 1952).

38. Frost, F. H., Tappi 35, no. 7:16-22A(July, 1952).

39. Black, W. C., Tappi 35, no. 7:44-52A(July, 1952).

40. Rowland, B. W., Tech. Assoc. Papers 23:203-9(1940).

41. Singleterry, C. R., Paper Trade J. 113, no. 18:37-40(Oct. 30, 1941).

42. The Institute of Paper Chemistry, Unpublished work, 1956.

43. Thompson, R. N. Preparation of paper coating colors. TAPPI Monograph Series no. 11. 1954.

44. Hull, H. H., Am. Inkmaker 29, no. 9:33-5, 70(Sept., 1951).

45. Van den Akker, J. A., Paper Ind. 28, no. 1:57-9(April, 1946).

46. Thomas, E. E., Paper Trade J. 122, no. 22:33-5(May 30, 1946).

47. The Institute of Paper Chemistry, Unpublished work, 1956.

48. Drexel, R. Personal communication, June 17, 1957.

49. Glasstone, S. Textbook of physical chemistry. New York, D. Van Nostrand Company, Inc., 1946.

50. Müller, H., Kolloidchem. Beih. 27:223-50(1928).

51. Cushing, M. L. Personal communication, May, 1957.

52. Merchant, M. V. A study of certain phenomena of the liquid exchange of water-swollen cellulose fibers and their subsequent drying from hydrocarbons. Doctor's Dissertation. Appleton, Wis., The Institute of Paper Chemistry, 1957.

53. Haselton, W. R. An investigation of the adsorption of gases by wood and its components. Doctor's Dissertation. Appleton, Wis., The Institute of Paper Chemistry, 1953.

54. Brunauer, S., Emmett, P. H., and Teller, E., J. Am. Chem. Soc. 60, no. 2:309-19(Feb., 1938).

55. Drake, L. C., Ind. Eng. Chem. 41, no. 4:780-5(April, 1949).

56. Adams, C. R., and Milligan, W. O., J. Phys. Chem. 58, no. 3:219-22 (March, 1954).

57. Corte, H. The porous structure of paper--its measurement and its modification by beating. In Fundamentals of papermaking fibres. p. 307. Surrey, England. Tech. Sec. Brit. Paper and Boardmakers Assoc., 1958.

58. Milligan, W. O., and Adams, C. R., J. Phys. Chem. 58, no. 10:891-3(Oct., 1954).

59. Joyner, L. G., Barrett, E. P., and Skold, R., J. Am. Chem. Soc. 73, no. 7:3155-8(July, 1951).

60. Juhola, A. J., and Wiig, E. O., J. Am. Chem. Soc. 71, no. 6:2069-77, 2078-80(June, 1949).

61. Cohan, L. H., J. Am. Chem. Soc. 60, no. 2:433-5(Feb., 1938).

62. Cohan, L. H., J. Am. Chem. Soc. 66, no. 1:98-105(Jan., 1944).

63. Carman, P. C., J. Phys. Chem. 57, no. 1:56-64(Jan., 1953).

64. Shull, C. G., J. Am. Chem. Soc. 70, no. 4:1405-10(April, 1948).

65. Wheeler, A., Presentations at the catalysis symposia, Gibson Island A.A.A.S. Conferences, 1945 and 1946. (reported in references 64 and 66).

66. Barrett, E. P., Joyner, L. G., and Halenda, P. P., J. Am. Chem. Soc. 73, no. 1:373-80(Jan., 1951).

67. Pierce, C., J. Phys. Chem. 57, no. 2:149-52(Feb., 1953).

68. Barrett, E. P., and Joyner, L. G., Anal. Chem. 23, no. 5:791-2(May, 1951).

69. Ries, H. E., Johnson, M. F. L., and Melik, J. S., J. Phys. Coll. Chem. 53:638-61(1949).

70. Ries, H. F., Johnson, M. F. L., Van Nordstrand, R. A., and Bauermeister, H. O., J. Am. Chem. Soc. 67, no. 8:1242-5(Aug., 1945).

71. Lange, N. A. Handbook of chemistry. 8th ed. Sandusky, Ohio, Handbook Publishers Inc., 1952.

72. Talvenheimo, G., and White, J. L., Anal. Chem. 24, no. 11:1784-9 (Nov., 1952).

73. Hathaway, J. C., Clay Minerals Bull. 3, no. 15:8-13(Oct., 1956).

74. Cano-Ruiz, J., and MacEwan, D. M. C., Clay Minerals Bull. 3, no. 15: 40-3(Oct., 1956).

75. Nagelschmidt, G., J. Sci. Instr. 18, no. 5:100-1(May, 1941).

76. Brindley, G. W. X-ray identification and crystal structure of clay minerals. London, The Mineralogical Soc., 1951.

77. Klug, H. P., and Alexander, L. E. X-ray diffraction procedures. New York, J. Wiley and Sons, Inc., 1954.

78. Decker, B. F., Asp, E. T., and Harker, D., J. Appl. Phys. 19, no. 4: 388-92(April, 1948).

79. Schulz, L. G., J. Appl. Phys. 20, no. 11:1030-3(Nov., 1949).

80. Field, M., and Merchant, M. E., J. Appl. Phys. 20, no. 8:741-5(Aug., 1949).

81. Chernock, W. P., and Beck, P. A., J. Appl. Phys. 23, no. 3:341-5 (March, 1952).

82. Parrish, W., Philips Tech. Rev. 17, no. 7-8:206-21(Jan., Feb., 1956).

83. Eames, A. C. Personal communication, Nov., 1958.

84. Norton, F. H., and Johnson, A. L., J. Am. Ceramic Soc. 27, no. 3: 77-80(1944).

APPENDIX I

TABULATION OF EXPERIMENTAL DATA

TABLE X

CLAY SURFACE AREA

Clay	P, mm.	P/P_o	V[ml. (STP.)/g.]	$P/V(P_o-P)$
0.0-0.5 mu	64.7	0.0851	4.478	0.0208
	107.9	0.1419	4.972	0.0333
	158.7	0.2088	5.594	0.0472
	203.3	0.2075	6.142	0.0595
	Vm = 4.61 ml.		Area = 20.15 $M^2/g.$	
0.5-1.0 mu	79.2	0.1041	3.371	0.0345
	119.4	0.1568	3.701	0.0503
	168.3	0.2211	4.049	0.0701
	Vm = 3.22 ml.		Area = 14.04 $M^2/g.$	
1.0-2.0 mu	72.4	0.0954	2.403	0.0439
	117.3	0.1545	2.668	0.0685
	158.3	0.2088	2.887	0.0913
	193.6	0.2554	2.107	0.1102
	Vm = 2.36 ml.		Area = 10.30 $M^2/g.$	

TABLE XI

THE EFFECT OF ETHYL ACETATE ON THE BONDING STRENGTH OF COATED PAPER

	VVP-Control	VVP-Ethyl Acetate Treated
	13.70	13.88
	12.44	13.99
	11.65	13.42
	11.34	12.21
	9.93	12.89
	15.12	11.81
	15.12	12.89
	15.37	15.81
	9.43	14.43
	11.88	15.81
	15.28	10.37
	14.03	12.89
	14.70	
	14.94	
	11.93	
Average	13.11	Average 13.37

TABLE XII

THE EFFECT OF ETHYL ACETATE ON ORIENTATION IN CLAY COATING

θ = 18.8°, 1/4° -.006" -1/4° slits

Control: 108 lb./ream, 12:100 starch:clay ratio

α, degrees	Measured[a] Intensity	Correction Factor	Corrected[a] Intensity	Relative[a] Intensity
0.00	7780	1.00	7780	1.00
3.45	5420	0.822	6600	0.849
6.55	3410	0.667	5110	0.656
9.90	1800	0.493	3650	0.470
13.65	624	0.292	2140	0.275
Ethyl-Acetate Treated: 108 lb./ream, 12:100 starch:clay ratio				
0.00	7580	1.00	7580	1.00
3.25	5380	0.830	6490	0.855
6.55	3260	0.667	4890	0.645
9.90	1704	0.493	3460	0.456
13.95	516	0.274	1885	0.249

[a] Intensity units represent counts indicated by the Geiger tube in the area under the diffraction peak.

TABLE XIII

THE EFFECT OF ETHYL ACETATE ON COATING SURFACE AREA

Control: Isolated from Aluminum Foil

P, mm.	P/P_o	V[ml.(STP)/g.]	$P/V(P_o-P)$
67.3	0.0884	1.964	0.0494
128.1	0.1683	2.249	0.0900
193.7	0.2545	2.502	0.1364
77.5	0.1006	2.009	0.0557
131.8	0.1709	2.231	0.0924
191.3	0.2481	2.440	0.1352

Vm = 1.875, Area = 8.16 $M^2/g.$

Ethyl-Acetate Treated

90.0	0.1158	1.918	0.0683
138.1	0.1777	2.141	0.1009
190.5	0.2451	2.364	0.1373
224.2	0.2885	2.516	0.1611
71.9	0.0941	1.821	0.0570
113.1	0.1480	2.024	0.0858
176.2	0.2305	2.313	0.1295

Vm = 1.862, Area = 8.12 $M^2/g.$

TABLE XIV

THE EFFECT OF ETHYL ACETATE IN NITROGEN ADSORPTION DETERMINATION

P, mm.	P/P_o	V[ml.(STP)/g.]
	Control	
307.5	0.4041	3.026
406.8	0.5345	3.490
428.2	0.6941	4.226
653.5	0.8587	5.633
733.6	0.9682	16.731
	Desorption	
764.6	1.00	223.228
758.0	1.00	164.937
746.2	0.9838	120.962
748.5	0.9821	98.691
754.0	0.9798	77.033
741.9	0.9765	46.802
737.8	0.9698	23.515
521.2	0.6848	3.959
	Ethyl-Acetate Treated	
374.1	0.4813	3.178
520.4	0.6695	3.984
675.6	0.8690	5.684
752.6	0.9668	13.721
	Desorption	
766.9	1.00	187.507
764.6	1.00	148.243
756.5	0.9856	129.540
751.0	0.9820	108.181
753.6	0.9805	90.356
748.0	0.9777	57.173
743.6	0.9715	29.993
738.2	0.9643	15.320
457.0	0.5969	1.769

TABLE XIV (continued)

THE EFFECT OF ETHYL ACETATE IN NITROGEN ADSORPTION DETERMINATION

Control Duplicate

P, mm.	P/P_o	V[ml.(STP.)/g.]
746.8	0.9786	31.744
	Desorption	
768.3	1.00	174.047
766.4	1.00	146.779
754.2	0.9846	131.645
752.3	0.9819	104.833
750.7	0.9792	67.831
746.0	0.9747	39.433
739.9	0.9675	19.094
459.4	0.6007	3.631

TABLE XV

THE LINEAR X-RAY ABSORPTION COEFFICIENT FOR CLAY-STARCH COATINGS

Cu-K_α x-rays; 12:100 starch:clay ratio

Sample	Coat Weight, lb./ream	Incident Angle, degrees	I^a	$I_o{}^a$	μ
1	30.8	90	38300	43500	66.8
2	23.7	90	38000	41700	63.8
3	28.9	90	38300	43500	71.6
4	35.4	11.5	24900	51600	65.2
5	35.4	12.1	24150	50600	67.5
6	35.4	12.4	24300	50100	68.5
7	35.4	13.3	25700	49800	67.5

[a] Counts per minute registered.

TABLE XVI

COMPARISON OF VOID VOLUME MEASUREMENTS

Coating	Coat Weight, lb./ream	Void Volume, ml./g. Hg displ., 15 p.s.i.a.	Hg displ., 30 p.s.i.a.	Nitrogen Absorption
F	10.8	0.264	--	0.171
B	21.1	0.242	--	0.171
G	33.2	0.216	--	0.176
	Gloss %			
J	58.5	0.246	0.225	0.177
K	70.0	0.225	0.209	--
L	72.5	0.421	0.204	0.177

TABLE XVII

EQUATION (13) PROOF
CRONAR ORTHO A LITHO EMULSION (2 layers)

$\mu t = .219$, $\theta = 16.0°$

α, degrees	Measured Intensity	Correction Factor	Corrected Intensity	Relative Intensity
0.0	29300	1.00	29300	1.00
3.40	23700	0.810	29300	1.00
5.30	21000	0.710	29600	1.01
7.10	18000	0.614	29300	1.00
8.90	15150	0.513	29600	1.01
10.80	12100	0.398	30300	1.032
12.20	8640	0.303	28500	0.974
14.30	4220	0.140	30100	1.029

ROYAL PAN EMULSION

$\mu t = .292$, $\theta = 15.5°$

0.0	23500	1.00	23500	1.00
3.85	18100	0.771	23500	1.00
6.90	14300	0.594	24100	1.025
9.30	10560	0.451	23400	0.995
12.20	5530	0.248	22400	0.953

TABLE XVIII

ORIENTATION REPRODUCIBILITY

Machine, Angle and Measuring Variables
$\theta = 18.8°$, 1° -.066" -1° slits
22.6 lb./ream coating

α, degrees	Measured Intensity	Correction Factor	Corrected Intensity	Relative Intensity
0.0	16512	1.00	16512	1.00
4.19	14400	0.830	17350	1.050
7.30	11520	0.703	16400	0.990
10.90	8112	0.577	14050	0.850
14.20	4608	0.425	10830	0.655
0.0	16224	1.00	16224	1.00
3.80	14208	0.837	17000	1.048
7.35	11424	0.700	16310	1.005
10.70	7968	0.579	13770	0.848
14.05	4704	0.435	10830	0.667
0.0	16224	1.00	16224	1.00
4.20	13632	0.830	16420	1.010
7.70	11136	0.685	16250	1.000
11.15	7680	0.562	13630	0.840
14.55	4128	0.406	10140	0.625

TABLE XIX

SPECIMEN MOUNTING REPRODUCIBILITY

θ 18.8°, 1° -.006" -1° slits
22.6 lb./ream

α, degrees	Measured Intensity	Correction Factor	Corrected Intensity	Relative Intensity
0.00	16512	1.00	16512	1.00
4.19	14400	0.830	17350	1.050
7.30	11520	0.703	16400	0.990
10.90	8112	0.577	14050	0.850
14.20	4608	0.425	10830	0.655
0.0	16032	1.00	16032	1.00
4.10	14016	0.831	16890	1.050
7.50	11424	0.699	16370	1.020
11.85	7104	0.540	13160	0.820
14.20	4608	0.426	10820	0.675
0.0	16320	1.00	16320	1.00
4.25	14208	0.832	17100	1.050
7.90	10760	0.677	15890	0.973
11.55	7152	0.548	13090	0.803
14.75	3936	0.400	9830	0.601

TABLE XX

COATING ORIENTATION VARIABILITY

θ = 18.8°, 1° -.006" -1° slits
1.0-2.0 mu clay fraction, 12:100 starch:clay ratio

Sample Wt., lb./ream	α, degrees	Measured Intensity	Correction Factor	Corrected Intensity	Relative Intensity
27.9	0.0	17280	1.00	17496	1.00
	3.80	14496	0.825	17550	1.00
	7.50	9600	0.682	14080	0.305
	11.30	5760	0.540	10660	0.610
	15.10	2832	0.348	8720	0.464
26.5	0.0	18816	1.00	18816	1.00
	4.35	15264	0.808	18860	1.00
	7.70	11520	0.683	16900	0.897
	11.30	8064	0.549	14700	0.780
	14.50	4944	0.401	12320	0.655
35.8	0.0	19862	1.00	19862	1.00
	3.95	15360	0.822	18200	0.941
	7.35	10464	0.683	15300	0.770
	10.90	6336	0.539	11820	0.596
	14.80	3216	0.340	9450	0.475
34.3	0.0	21600	1.00	21600	1.00
	4.00	18816	0.814	23100	1.070
	7.40	14784	0.680	21700	1.000
	11.10	10176	0.534	19000	0.880
	14.15	4992	0.382	13000	0.603
Average of four previous samples	0	--	--	--	1.00
	4	--	--	--	1.00
	8	--	--	--	0.849
	11	--	--	--	0.722
	14	--	--	--	0.578
70.1	0.0	28992	1.00	28992	1.00
	5.50	21696	0.736	29500	1.020
	10.55	11424	0.501	22800	0.786
	14.65	4968	0.304	16300	0.562
97.3	0.0	33200	1.00	33200	1.00
	5.80	23300	0.716	32500	0.979
	10.75	12384	0.469	26400	0.796
	14.25	5424	0.269	19500	0.588

TABLE XXI

THE EFFECT OF A SYMMETRICAL SLIT SYSTEM ON ORIENTATION DATA

CRONAR ORTHO A LITHO PHOTOGRAPHIC FILM

μt = .185, θ = 16°

Slit System 1/4° -.006" -1/4°

α, degrees	Measured Intensity	Correction Factor	Corrected Intensity	Relative Intensity
0.0	2470	1.00	2470	1.00
3.70	1950	0.795	2450	0.990
6.75	1550	0.652	2380	0.962
8.90	1214	0.508	2390	0.963
11.70	828	0.360	2300	0.932

Slit System 1/4° -∞ -1°

0.0	4950	1.00	4950	1.000
5.45	3550	0.721	4910	0.995
7.65	2970	0.606	4900	0.994
9.85	2500	0.482	5190	1.050
11.65	1820	0.367	4960	1.005

Slit System 1/4° -∞ -4°

0.0	15180	1.00	15180	1.00
5.45	10940	0.721	15180	1.000
7.65	9310	0.606	15350	1.010
9.85	7490	0.482	15520	1.025
11.65	5560	0.367	15150	1.000

TABLE XXII

DEFOCUSING ERROR

Slit System 1/4° -.006" -1/4°

Sample Wt., lb./ream	α, degrees	Measured Intensity	Correction Factor	Corrected Intensity	Relative Intensity
No. 1	0.0	6050	1.00	6050	1.00
43.4	4.90	3820	0.779	4900	0.810
	6.70	2980	0.703	4220	0.698
	10.00	1610	0.565	2850	0.471
	11.20	1080	0.513	2100	0.348
	13.80	486	0.379	1281	0.212
Slit System 1/4° -∞ -4°					
No. 1	0.0	86600	1.00	86600	1.00
43.4	4.10	62600	0.815	76800	0.887
	6.70	46300	0.703	65900	0.762
	10.00	27600	0.565	49000	0.565
	12.70	14040	0.440	31900	0.368
	13.80	10390	0.379	27400	0.316
	14.40	9040	0.344	26100	0.301
Slit System 1/4° -.006" -1/4°					
No. 2					
41.7	0.0	5560	1.00	5560	1.00
	3.90	4010	0.821	4870	0.875
	6.40	2960	0.713	4150	0.746
	10.10	1640	0.565	2900	0.521
	13.00	936	0.428	2184	0.392
Slit System 1/4° -∞ -4°					
No. 2					
41.7	0.0	84500	1.00	84500	1.00
	3.90	63200	0.821	76400	0.905
	6.40	47800	0.713	67000	0.793
	10.10	29200	0.565	51600	0.610
	13.00	17700	0.428	41300	0.488
Slit System 1/4° -.006" -1/4°					

TABLE XXII (continued)

Sample Wt., lb./ream	α, degrees	Measured Intensity	Correction Factor	Corrected Intensity	Relative Intensity
No. 3 70	0.0	3720	1.00	3720	1.00
	1.40	3410	0.835	3660	0.985
	3.00	3020	0.930	3540	0.950
	4.80	2560	0.769	3330	0.895
	7.00	2040	0.671	3040	0.816
	9.60	1415	0.548	2590	0.697
	11.90	921	0.431	2140	0.575
	13.2	634	0.361	1784	0.480
Slit System 1/4° -∞ -4°					
No. 3 70	0.0	59500	1.00	59500	1.00
	1.40	55500	0.835	59600	1.00
	3.00	49900	0.930	58400	0.980
	4.80	43600	0.769	56800	0.955
	7.00	35500	0.671	53000	0.891
	9.60	25500	0.548	46600	0.784
	11.90	17700	0.431	40900	0.687
	13.20	12700	0.361	35100	0.591
Slit System 1/4° -.006" -1/4°					
No. 4 93	0.0	3600	1.00	3600	1.00
	2.30	3070	0.885	3470	0.964
	3.90	2620	0.809	3240	0.900
	5.70	2210	0.723	3060	0.850
	9.40	1297	0.542	2390	0.665
	13.30	586	0.335	1748	0.485
Slit System 1/4° -∞ -4°					
No. 4 93	0.0	65200	1.00	65200	1.00
	2.30	57800	0.885	65200	1.00
	3.90	49600	0.809	61200	0.940
	5.70	41300	0.723	58300	0.893
	9.40	2700	0.542	49900	0.765
	13.30	1346	0.335	40100	0.615
Slit System, 1/4° -.006" -1/4°					
No. 5 116	0.0	3650	1.00	3650	1.00
	2.80	3022	0.860	3520	0.964
	4.80	2450	0.764	3200	0.876
	9.60	1258	0.522	2410	0.660 (660)

TABLE XXII (continued)

Slit System 1/4° -∞-4°

	α, degrees	Measured Intensity	Correction Factor	Corrected Intensity	Relative Intensity
No. 5	0.0	65300	1.00	65300	1.00
116	2.80	54700	0.860	63700	0.977
	4.80	46200	0.764	60500	0.926
	9.60	25400	0.522	48600	0.745
	13.40	11720	0.317	36900	0.565

TABLE XXIII

B.E.T. SURFACE AREA

Coatings B, J

Coating	P, mm.	P/P_o	V[ml.(STP.)/g.]	$P/V(P_o-P)$
B	66.2	0.0874	1.382	0.0693
	127.6	0.1685	1.608	0.1260
	180.8	0.2388	1.760	0.1782
	232.2	0.3067	1.911	0.2315
B	85.8	0.1131	1.444	0.0883
	133.5	0.1759	1.587	0.1345
	193.4	0.2549	1.781	0.1921
	Vm = 1.35, Area = 5.9 $M^2/g.$			
J	73.0	0.0952	1.510	0.0697
	109.5	0.1428	1.650	0.1009
	149.9	0.1955	1.751	0.1388
	210.6	0.2747	1.949	0.1943
J	91.6	0.1194	1.600	0.0849
	128.7	0.1677	1.719	0.1173
	184.2	0.2402	1.893	0.1670
	Vm = 1.42, Area = 6.2 $M^2/g.$			

TABLE XXIV

CLAY PARTICLE ORIENTATIONS

Coatings B, J
$\theta = 18.8°$, 1/4° -.006"-1/4° slits

Coating B

Sample Wt., lb./ream	α, degrees	Measured Intensity	Correction Factor	Corrected Intensity	Relative Intensity
118.1	0.0	8400	1.00	8400	1.00
	5.45	4460	0.729	6130	0.730
	9.70	1930	0.513	3760	0.448
	13.40	600	0.316	1900	0.226
110.4	0.0	8100	1.00	8100	1.00
	3.70	6030	0.743	7340	0.906
	6.55	3910	0.676	5790	0.714
	10.25	2110	0.489	4310	0.532
	12.95	970	0.343	2830	0.349
	0.0	7380	1.00	7380	1.00
	3.60	5520	0.835	6610	0.895
	7.05	2920	0.651	4490	0.608
	10.05	1750	0.503	3480	0.472
	13.10	732	0.339	2160	0.292

Coating J

90.9	0.0	7800	1.00	7800	1.00
	4.30	4850	0.792	6120	0.785
	6.70	3360	0.675	4980	0.637
	9.90	1690	0.516	3270	0.419
	13.10	672	0.349	1930	0.246
90.4	0.0	7100	1.00	7100	1.00
	1.35	6120	0.933	6060	0.924
	2.60	5600	0.871	6420	0.903
	6.00	3340	0.712	4680	0.658
	9.35	1690	0.546	3090	0.435
	13.30	456	0.336	1355	0.191
89.3	0.0	5550	1.00	5550	1.00
	3.15	3860	0.848	4590	0.830
	6.30	2500	0.699	3580	0.645
	9.50	1416	0.540	2620	0.472
	12.80	576	0.373	1538	0.278

TABLE XXV

NITROGEN ADSORPTION DATA

Coatings B, J

Coating J			J, duplicate		
P, mm.	P/P_o	V[ml.(STP.)/g.]	P, mm.	P/P_o	V[ml.(STP.)/g.]
331.7	0.4327	2.352	333.7	0.4349	2.377
447.8	0.5841	2.759			
605.8	0.7905	3.611			
718.3	0.9374	5.704			
753.8	0.9830	25.950			
	Desorption			Desorption	
769.3	1.0016	185.15	762.1	1.0004	142.88
767.8	1.0013	126.11	754.6	0.9941	111.60
753.0	0.9879	101.79	749.0	0.9861	92.36
750.8	0.9835	77.23	748.2	0.9829	68.84
748.2	0.9804	52.31	742.2	0.9772	27.13
747.0	0.9782	35.32			
736.8	0.9663	10.58			
407.1	0.5330	3.026			
Coating B					
337.1	0.4451	2.123			
487.1	0.6432	2.606	396.3	0.5228	2.292
633.5	0.8365	3.530	726.0	0.9568	7.177
736.2	0.9721	12.855	745.3	0.9823	33.120
	Desorption			Desorption	
757.6	1.0001	193.15	754.7	0.9998	166.88
758.1	1.0002	158.81	750.8	0.9939	105.32
758.2	1.0001	118.54	742.6	0.9831	81.43
747.0	0.9857	91.98	740.4	0.9805	59.46
744.2	0.9818	68.43	737.8	0.9770	37.05
742.7	0.9790	47.35	730.7	0.9698	14.16
739.4	0.9755	24.41			
728.3	0.9611	9.23			
534.7	0.7056	2.994			

TABLE XXVI

B.E.T. SURFACE AREAS - COATINGS A, B, C

Coating	P, mm.	P/P_o	V[ml.(STP.)/g.]	$P/V(P_o-P)$
A	76.6	0.1006	2.018	0.0555
	123.4	0.1622	2.237	0.0865
	195.5	0.2306	2.493	0.1203
	228.9	0.3008	2.697	0.1595
A	91.0	0.1209	2.090	0.0658
	132.7	0.1763	2.393	0.0934
	181.1	0.2407	2.481	0.1279
	238.9	0.3173	2.742	0.1695
	Vm = 1.93, Area = 8.4 $M^2/g.$			
B	66.2	0.0874	1.382	0.0693
	127.6	0.1685	1.608	0.1260
	180.8	0.2388	1.760	0.1782
	232.2	0.3067	1.911	0.2315
B	85.8	0.1131	1.444	0.0883
	133.5	0.1759	1.587	0.1345
	193.4	0.2549	1.781	0.1921
	Vm = 1.35, Area = 5.9 $M^2/g.$			
C	80.2	0.1053	0.896	0.1313
	128.7	0.1691	1.052	0.1934
	182.3	0.2396	1.142	0.2758
	230.3	0.3026	1.210	0.3586
C	74.2	0.0992	0.991	0.1119
	137.0	0.1832	1.151	0.1948
	191.6	0.2562	1.209	0.2846
	249.2	0.3333	1.328	0.3763
	Vm = 0.871, Area = 3.80 $M^2/g.$			

TABLE XXVII

CLAY PARTICLE ORIENTATION

Coatings A, B, and C
θ = 18.8°, 1/4 -.006" -1/4° slits

Coating A

Sample Wt., lb./ream	α, degrees	Measured Intensity	Correction Factor	Corrected Intensity	Relative Intensity
108.3	0.0	8590	1.00	8590	1.00
	3.40	6050		7250	0.845
	6.70	3540		5310	0.620
	9.90	1848		3650	0.426
	13.00	870		2540	0.296
110.6	0.0	7590	1.00	7590	1.00
	4.30	5060		6410	0.845
	8.60	2420		4240	0.559
	13.50	684		2020	0.266
115.1	0.0	8610	1.00	8610	1.00
	4.50	5110		6560	0.762
	8.90	2315		4170	0.485
	13.15	6840		2080	0.242
Coating B					
118.1	0.0	8400	1.00	8400	1.00
	5.45	4460	0.729	6130	0.730
	9.70	1930	0.513	3760	0.448
	13.40	600	0.316	1900	0.226
110.4	0.0	8100	1.00	8100	1.00
	3.70	6030	0.743	7340	0.906
	6.55	3910	0.676	3790	0.714
	10.25	2110	0.489	4310	0.532
	12.95	970	0.343	2830	0.349
108.0	0.0	7380	1.00	7380	1.00
	3.60	5520	0.835	6610	0.895
	7.05	2920	0.651	4450	0.608
	10.05	1750	0.503	3480	0.472
	13.10	732	0.339	2160	0.292

TABLE XXVII (continued)

Coating C

Sample Wt., lb./ream	α, degrees	Measured Intensity	Correction Factor	Corrected Intensity	Relative Intensity
116.1	0.0	4310	1.00	4310	1.00
	3.60	2900	0.826	3510	0.812
	6.90	1870	0.659	2840	0.659
	10.10	1128	0.305	2230	0.516
	13.15	576	0.328	1760	0.408
117.4	0.0	4010	1.00	4010	1.00
	4.30	2660	0.783	3400	0.847
	8.00	1610	0.595	2710	0.675
	13.00	648	0.338	1913	0.478
117.5	0.0	4030	1.00	4030	1.00
	5.10	2470	0.752	3290	0.815
	9.00	1360	0.550	2470	0.612
	13.25	557	0.325	1715	0.425

TABLE XXVIII

NITROGEN ADSORPTION DATA

Coatings A, B, C

Coating A			A, duplicate		
P, mm.	P/P_o	V[ml.(STP.)/g.]	P, mm.	P/P_o	V[ml.(STP.)/g.]
352.8	0.4672	3.211			
452.2	0.5981	3.641			
521.5	0.6894	4.094			
645.8	0.8535	5.346			
738.8	0.9801	21.296	728.4	0.9561	11.580
	Desorption			Desorption	
765.6	1.0006	218.87	766.0	1.0003	204.45
765.3	1.0000	152.06	766.0	1.0003	144.88
764.9	0.9998	124.48	762.2	0.9970	118.90
743.5	0.9739	81.86	747.2	0.9776	102.17
741.1	0.9720	56.72	743.5	0.9730	70.38
736.2	0.9670	33.50	740.2	0.9701	47.68
716.2	0.9394	11.65	731.5	0.9602	21.94
356.8	0.4679	3.479	390.6	0.5127	3.505
Coating B			B, duplicate		
337.1	0.4451	2.123			
487.1	0.6432	2.606	396.3	0.5228	2.292
633.5	0.8365	3.530	726.0	0.9568	7.177
736.2	0.9721	12.855	745.3	0.9823	33.120
	Desorption			Desorption	
757.6	1.0001	193.15	754.7	0.9998	166.88
758.1	1.0002	158.81	750.8	0.9939	105.32
758.2	1.0001	118.54	742.6	0.9831	81.43
747.0	0.9857	91.98	740.4	0.9805	59.46
744.2	0.9818	68.43	737.8	0.9770	37.05
742.7	0.9790	47.35	730.7	0.9698	14.16
739.4	0.9755	24.41			
728.3	0.9611	9.23			
534.7	0.7056	2.994			

TABLE XXVIII (continued)

Coatings A, B, C

Coating C			C, duplicate		
P, mm.	P/P_o	V[ml. (STP.)/g.]	P, mm.	P/P_o	V[ml.(STP.)/g.]
249.2	0.3333	1.328			
368.4	0.4927	1.547			
485.5	0.6493	1.823			
579.8	0.7754	2.089			
733.0	0.9789	8.513	66.94	0.8875	2.865
	Desorption			Desorption	
				Saturation	
753.5	1.0004	199.94			
752.4	0.9995	144.12	758.5	0.9949	132.54
745.6	0.9902	118.81	752.3	0.9894	106.55
744.8	0.9886	95.54	750.9	0.9864	59.70
743.2	0.9870	73.39	748.1	0.9815	36.15
740.4	0.9835	46.84	742.3	0.9735	15.41
734.6	0.9761	26.30	224.0	0.2937	1.191
708.2	0.9410	6.67			

TABLE XXIX

CLAY PARTICLE ORIENTATION

θ = 18.8°, 1/4° -.006" -1/4° slits

Coatings D and E

Coating D

Sample Wt., lb./ream	α, degrees	Measured Intensity	Correction Factor	Corrected Intensity	Relative Intensity
66.6	0.0	7100	1.00	7100	1.00
	3.45	4770	0.835	5710	0.806
	6.70	2740	0.676	4050	0.570
	10.10	1488	0.533	2790	0.393
	13.15	606	0.369	1640	0.231
60.9	0.0	6910	1.00	6910	1.00
	3.60	4720	0.828	5700	0.821
	6.85	2660	0.686	3880	0.562
	10.25	1415	0.530	2670	0.386
	13.50	540	0.362	1490	0.215

Coating E

107.6	0.0	6650	1.00	6650	1.00
	3.40	4940	0.835	5910	0.861
	6.90	2730	0.656	4160	0.626
	10.25	1620	0.491	3300	0.497
	13.40	648	0.319	2030	0.305
100.2	0.0	6240	1.00	6240	1.00
	3.10	3690	0.750	4920	0.789
	9.50	1728	0.533	3240	0.520
	13.40	642	0.326	1969	0.315
104.8	0.0	6940	1.00	6940	1.00
	4.90	4340	0.761	5700	0.822
	9.90	1728	0.506	3410	0.491
	13.50	624	0.316	1970	0.284

TABLE XXX

B.E.T. SURFACE AREA DATA

Coatings F and G

Coating	P, mm.	P/P_o	V[ml.(STP.)/g.]	$P/V(P_o-P)$
F	52.2	0.0691	1.269	0.0505
	114.3	0.1513	1.484	0.1201
	175.5	0.2323	1.643	0.1839
	213.0	0.2820	1.749	0.2246
	93.2	0.1222	1.457	0.0956
	146.4	0.1920	1.617	0.1470
	214.5	0.2813	1.766	0.2217
	237.2	0.3111	1.805	0.2502
	79.6	0.1044	1.393	0.1362
	130.3	0.1709	1.513	0.1362
	181.4	0.2379	1.640	0.1904
	232.6	0.3050	1.783	0.3035
	Vm = 1.337, Area = 5.80 $M^2/g.$			
G	72.5	0.0957	1.367	0.0775
	123.5	0.1631	1.547	0.1260
	173.2	0.2313	1.700	0.1771
	229.4	0.3029	1.823	0.2384
	69.7	0.0920	1.428	0.0710
	125.4	0.1655	1.572	0.1262
	184.0	0.2429	1.729	0.1835
	Vm = 1.337, Area = 5.8 $M^2/g.$			

TABLE XXXI

CLAY PARTICLE ORIENTATION

θ = 18.8° 1/4° -.006" -1/4° slits

Coatings F and G

Coating F

Sample Wt., lb./ream	α, degrees	Measured Intensity	Correction Factor	Corrected Intensity	Relative Intensity
67.5	0.0	7920	1.00	7920	1.00
	3.45	5420	0.837	6490	0.819
	6.90	3430	0.676	3080	0.641
	10.10	1690	0.529	3200	0.404
	13.35	624	0.358	1740	0.220
76.7	0.0	7000	1.00	7000	1.00
	3.55	4940	0.826	5980	0.855
	6.70	2976	0.680	4370	0.625
	10.25	1428	0.511	2790	0.399
	13.50	612	0.340	1800	0.257
80.2	0.0	6760	1.00	6760	1.00
	4.70	4030	0.771	5230	0.774
	9.90	1632	0.529	3090	0.456
	13.15	670	0.356	1880	0.278

Coating G

140.1	0.0	8500	1.00	8500	1.00
	3.60	5760	0.823	7010	0.825
	6.50	3380	0.679	4970	0.585
	9.90	1680	0.498	3370	0.397
	13.15	616	0.323	1910	0.225
139.1	0.0	8720	1.00	8720	1.00
	3.40	6000	0.831	7210	0.826
	6.75	3600	0.669	5390	0.617
	9.90	1692	0.496	3410	0.391
	13.75	528	0.289	1825	0.209
127.0	0.0	8550	1.00	8530	1.00
	3.60	5360	0.824	6510	0.762
	6.90	2970	0.655	4540	0.530
	10.25	1270	0.485	2620	0.307
	13.45	432	0.314	1375	0.161

TABLE XXXII

NITROGEN ADSORPTION DATA

Coatings F, G

Coating F

P, mm.	P/P_o	V[ml.(STP.)/g.]	P, mm.	P/P_o	V[ml.(STP.)/g.]
335.0	0.4434	2.088			
459.0	0.6075	2.482			
609.3	0.8063	3.164			
720.6	0.9534	6.322			
741.7	0.9815	25.093			
	Desorption			Desorption	
				Saturated	
757.1	1.0001	217.45			
758.2	1.0001	181.77	766.9	0.9980	107.78
758.3	0.9996	126.43	756.4	0.9868	86.26
751.3	0.9909	101.05	754.9	0.9840	60.62
745.9	0.9839	80.89	750.0	0.9782	31.17
746.9	0.9831	59.08			
745.3	0.9798	37.94			
741.9	0.9749	16.95			
645.9	0.8485	3.417			

Coating G

				G, duplicate	
310.1	0.4094	2.048			
434.3	0.5734	2.401			
553.0	0.7298	2.822			
794.6	0.9299	4.966			
74.53	0.9830	21.755	62.40	0.8161	3.418
	Desorption			Desorption	
759.3	1.0004	146.43	767.2	1.0001	153.42
750.9	0.9888	105.84	765.0	1.0001	130.51
747.0	0.9840	82.72	759.5	0.9932	111.76
745.4	0.9815	64.26	752.8	0.9857	96.81
743.9	0.9792	43.06	749.2	0.9801	50.78
741.2	0.9759	22.38	738.3	0.9659	15.71
629.2	0.8285	3.912	251.0	0.3283	2.123

TABLE XXXIII

B.E.T. SURFACE AREA

Coatings J, K, L

Coating	P, mm.	P/P_o	V[ml.(STP.)/g.]	$P/V(P_o-P)$
J	73.0	0.0952	1.510	0.0697
	109.5	0.1428	1.650	0.1009
	149.9	0.1955	1.751	0.1388
	210.6	0.2747	1.949	0.1943
	91.6	0.1194	1.600	0.0849
	128.7	0.1677	1.719	0.1173
	184.2	0.2402	1.893	0.1670
	Vm = 1.42, Area = 6.2 $M^2/g.$			
K	68.9	0.947	1.546	0.0643
	105.3	0.1383	1.679	0.0955
	148.5	0.1949	1.824	0.1328
	201.2	0.2642	2.032	0.1767
	85.9	0.1126	1.627	0.0780
	136.2	0.1785	1.781	0.1220
	sample ruined			
	Vm = 1.47, Area = 6.4 $M^2/g.$			
L	75.8	0.1003	1.559	0.0745
	128.3	0.1698	1.751	0.1168
	173.6	0.2297	1.890	0.1579
	203.0	0.2687	1.942	0.1892
	82.7	0.1083	1.583	0.0773
	129.1	0.1691	1.750	0.1163
	176.4	0.2311	1.926	0.1560
	Vm = 1.52, Area = 6.6 $M^2/g.$			

TABLE XXXIV

CLAY PARTICLE ORIENTATION

θ = 18.8°, 1/4° -.006" -1/4° slits

Coatings J, K, L

Coating J

Sample Wt., lb./ream	α, degrees	Measured Intensity	Correction Factor	Corrected Intensity	Relative Intensity
90.9	0.0	7800	1.00	7800	1.00
	4.30	4850	0.792	6120	0.785
	6.70	3360	0.675	4980	0.637
	9.90	1690	0.516	3270	0.419
	13.10	672	0.349	1930	0.246
90.4	0.0	7100	1.00	7100	1.00
	1.35	6120	0.933	6060	0.924
	2.60	5600	0.871	6420	0.903
	6.00	3340	0.712	4680	0.658
	9.35	1690	0.546	3090	0.435
	13.30	456	0.336	1355	0.191
89.3	0.0	5550	1.00	5550	1.00
	3.15	3860	0.848	4590	0.830
	6.30	2500	0.699	3580	0.645
	9.50	1416	0.540	2620	0.472
	12.80	576	0.373	1538	0.278

Coating K

89.5	0.0	8010	1.00	8010	1.00
	3.0	5610	0.854	6570	0.820
	6.55	3160	0.687	4610	0.575
	9.35	1390	0.548	2540	0.317
	13.00	576	0.354	1630	0.203
89.5	0.0	6190	1.00	6190	1.00
	3.25	4220	0.840	5030	0.812
	6.00	2980	0.714	4170	0.674
	8.20	1970	0.605	3250	0.525
	11.50	874	0.438	2000	0.322

TABLE XXIV (continued)

Sample Wt., lb./ream	α, degrees	Measured Intensity	Correction Factor	Corrected Intensity	Relative Intensity
88.0	0.0	8510	1.00	8510	1.00
	2.90	6530	0.857	7630	0.894
	6.10	4010	0.706	5660	0.665
	9.35	2230	0.548	4070	0.476
	12.60	874	0.378	2310	0.270
Coating L					
88.6	0.0	6990	1.00	6990	1.00
	3.60	4610	0.822	5600	0.802
	6.50	2710	0.688	3440	0.565
	9.90	1320	0.518	2540	0.367
	13.10	394	0.352	1120	0.160
90.1	0.0	7610	1.00	7610	1.00
	3.25	5180	0.840	6180	0.812
	6.35	2900	0.694	4190	0.550
	9.50	1370	0.537	2540	0.330
	12.50	505	0.381	1320	0.174
84.5	0.0	7500	1.00	7500	1.00
	3.40	5020	0.834	6000	0.802
	6.70	2880	0.681	4210	0.563
	9.90	1472	0.524	2810	0.374
	12.80	514	0.369	1248	0.186

TABLE XXXV

NITROGEN ADSORPTION DATA

Coatings J, L

Coating J			J, duplicate		
P, mm.	P/P_o	V[ml.(STP.)/g.]	P, mm.	P/P_o	V[ml.(STP.)/g.]
331.7	0.4327	2.352	333.7	0.4349	2.377
447.8	0.5841	2.759			
605.8	0.7905	3.611			
718.3	0.9374	5.704			
753.8	0.9830	25.95			
	Desorption			Desorption	
769.3	1.0016	185.15	763.1	1.0004	142.88
767.8	1.0012	126.11	754.6	0.9941	111.60
753.0	0.9879	101.79	749.0	0.9861	92.36
750.8	0.9835	77.23	748.2	0.9829	68.84
748.2	0.9804	52.31	742.2	0.9772	27.13
747.0	0.9782	35.32			
736.8	0.9663	10.58			
407.1	0.5330	3.026			
Coating L			L, duplicate		
321.3	0.4252	2.354	707.3	0.9265	5.521
472.1	0.6249	2.931	745.4	0.9764	20.979
709.7	0.9393	6.082			
743.1	0.9842	32.755			
	Desorption			Desorption	
753.5	1.0005	159.18	764.4	1.0001	125.49
752.4	1.0003	115.03	759.0	0.9918	110.77
744.2	0.9870	103.84	753.3	0.9845	91.95
742.1	0.9836	81.34	751.6	0.9821	61.98
739.5	0.9805	44.00	748.3	0.9778	32.94
735.5	0.9753	23.97			
729.4	0.9668	12.49			
415.2	0.5504	3.105			

TABLE XXXVI

B.E.T. SURFACE AREA

Coatings H and I

Coating	P, mm.	P/P_o	V[ml.(STP.)/g.]	$P/V(P_o-P)$
H	29.2	0.0382	1.305	0.0303
	81.5	0.1066	1.626	0.0732
	138.0	0.1805	1.836	0.1194
	201.1	0.2627	2.016	0.1757
	71.4	0.0938	1.580	0.0655
	125.0	0.1642	1.814	0.1062
	183.4	0.2409	2.015	0.1574
	236.9	0.3111	0.204	0.2049
	Vm = 1.55, Area = 6.8 $M^2/g.$			
I	42.0	0.0553	1.455	0.0403
	109.6	0.1443	1.776	0.0949
	161.4	0.2126	1.970	0.1370
	204.1	0.2688	2.098	0.1752
	55.2	0.0727	1.418	0.0553
	112.6	0.1484	1.800	0.0968
	172.1	0.2268	2.018	0.1457
	221.6	0.2921	2.205	0.1871
	Vm = 1.58, Area = 6.9 $M^2/g.$			

TABLE XXXVII

CLAY PARTICLE ORIENTATION

$\theta = 18.8°$, 1/4° -.006" -1/4° slits

Coating H and I

Coating H

Sample Wt., lb./ream	α, degrees	Measured Intensity	Correction Factor	Corrected Intensity	Relative Intensity
112.2	0.0	8350	1.00	8350	1.00
	4.85	6720	0.765	8790	1.050
	7.80	4270	0.611	7000	0.839
	11.10	2280	0.439	5200	0.623
	14.40	951	0.259	3670	0.439
119.9	0.0	9000	1.00	9000	1.00
	5.40	6560	0.734	8950	0.994
	8.70	3960	0.567	6980	0.776
	12.10	2110	0.387	5450	0.606
	15.10	846	0.225	3760	0.418
117.5	0.0	8450	1.00	8450	1.00
	5.25	5230	0.740	7060	0.835
	8.15	3190	0.591	5400	0.640
	11.30	1680	0.426	3940	0.466
	14.00	672	0.281	2390	0.283

Coating I

102	0.0	6550	1.00	6550	1.00
	5.04	5090	0.751	6760	1.030
	10.55	2380	0.379	4970	0.759
	14.65	865	0.251	3440	0.525
100.3	0.0	7200	1.00	7200	1.00
	4.35	6040	0.788	7660	1.060
	9.10	3260	0.559	5840	0.811
	14.40	1130	0.269	4200	0.584
103.6	0.0	8160	1.00	8160	1.00
	5.20	5190	0.748	6940	0.850
	10.35	2210	0.488	4540	0.556
	15.00	600	0.225	2660	0.326

APPENDIX II

THE CALCULATION OF PER CENT BONDED AREA IN COATINGS

The potential bonding area of a coating may be considered to be the total area of the clay platelets when each of the platelets is surrounded by a film of starch. The areas of the clays used in this study were given in Table I. The weight average equivalent spherical diameter of the clay fractions was obtained from the distributions presented in Figure 1. Through the use of the Müller equation the equivalent spherical diameter of the clays and the surface areas of the clays, it was possible to calculate the approximate dimensions of the various clay fractions. The ratios of the greatest diameters of the clay particles to their thickness was reported in Table I. The calculated dimensions for each of the fractions are given in Table XXXVIII. It is noted that the Müller equation was intended for use with monodisperse fractions only.

$$R = \frac{8}{3} \frac{a\left[(1-(b/a)^2\right]}{\left[\frac{3-2(b/a)^2}{1-(b/a)^2}\right]\left[\frac{1}{2}\left(\frac{\pi}{2} - \arcsin b/a\right)\right]}$$

where (a) and (b) are the semidiameter and the semithickness of a disc which falls in a viscous medium with the same velocity as a sphere of radius (R).

TABLE XXXVIII

CLAY PARTICLE DIMENSIONS

Clay Fraction	Clay Area, $M^2/g.$	Disc Radius Mx 10^7	Disc Thickness, Mx 10^8	No. of Particles per g.
0.0-0.5	20.15	1.48	4.9	1.14×10^{14}
0.5-1.0	14.04	2.53	6.6	2.90×10^{13}
1.0-2.0	10.30	4.70	9.4	5.90×10^{12}

The quantity of starch added to the clay is known. Since both the area of the clay and the density of the starch are available, it was possible to calculate the thickness of the starch film which was assumed to form around each clay particle. The starch film increases the dimensions of the particles and, therefore, their area. It is possible, then, to calculate the new "total area" of the clay-starch combination. The following tabulation shows the effect of the starch film upon the area of the clay-starch combination.

TABLE XXXIX

THE TOTAL AREA OF THE CLAY-STARCH COMBINATION

Clay Fraction	Clay Area, $M^2/g.$	Starch Film Thickness, A.	"Total Area" $M^2/g.$[a]	Coating Area, $M^2/g.$	Bonded Area, %
0.0-0.5	20.15	40	21.2	8.4	60.4
0.5-1.0	14.04	60	14.7	5.9	59.8
1.0-2.0	10.30	80	9.55	3.8	60.2

[a] this value represents the area per gram of clay-starch combination: not per gram of clay

The percent bonded area is calculated from the free surface area of the coating and the "total area" of the clay-starch combination.